Microfluidics Separation and Analysis of Biological Particles

Beech, Jason

2011

MICROFLUIDICS SEPARATION AND ANALYSIS OF BIOLOGICAL PARTICLES

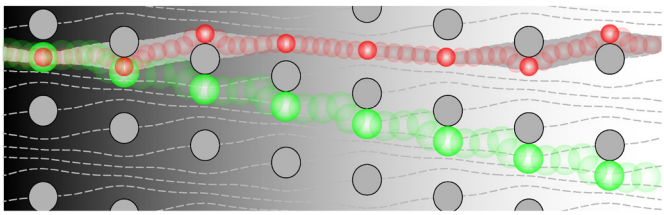

Jason P. Beech

Solid State Physics
Lund Institute of Technology
Lund University

MICROFLUIDICS
SEPARATION AND ANALYSIS OF BIOLOGICAL PARTICLES

Doctoral Thesis

Jason P. Beech

Supervisor:
Jonas Tegenfeldt

Faculty Opponent:
Prof. Shuichi Takayama
University of Michigan

LUNDS UNIVERSITET

Division of Solid State Physics
Department of Physics
Lund University

Division of Solid State Physics
Department of Physics
Lund University
P. O. Box 118
S-221 00 Lund

ISBN 978-91-7473-195-8
Printed in Sweden by Media-Tryck, Lund
October 2011

“It’ll sort!”

Colin R. Beech to Susan M. Beech, frequently.

Abstract

In the last decade, powerful communication and information technology in the form of the mobile phone has been put into the hands of more than 50% of the global population. In stark contrast, a lack of access to medical diagnostic technology with which to diagnose both communicable and non-communicable diseases will mean that many of these people will die of easily treatable conditions. Small, portable, effective and affordable devices able to give relevant information about the health of an individual, even in resource poor environments, could potentially help to change this. And the developing world is not the only resource poor environment; areas struck by natural disaster or by outbreaks of infectious disease or on the battlefield or even at the frontiers of exploration we find environments in which a mobile phone-sized laboratory would have a profound impact, not only on medical, but environmental diagnostics. There are also less dramatic examples. Compared to a well-equipped hospital most environments are resource poor, including the home. Blood sugar measuring devices for example put important information immediately into the hands of the diabetes sufferer in their own home, allowing them to make informed, life-saving decisions about food intake and medication without recourse to medical doctors.

These diagnostic devices will be based on technologies that go under the collective names of micro-total-analysis systems, μTAS, or Lab-on-a-Chip. One of the uniting, integral features of all these technologies is the need to manipulate small volumes of fluids, often containing cells or other particles, from which the diagnostic information is to be wrung. The manipulation of such small volumes of fluids is known as microfluidics.

This doctoral thesis is concerned with particle separation science. More specifically it is concerned with the development of tools for the separation of biologically relevant particles, an important step in almost any analysis, using techniques that have been made possible through the advent of microfluidics. A technique based on the flow of fluid through arrays of micrometre-sized obstacles, Deterministic Lateral Displacement (DLD), is promising because of its exceptional resolution, its suitability for biological separations, the wide range of sizes across which it works and not least because of the promise it holds as a candidate for integration within a lab-on-a-chip. The first devices utilizing the principle were limited to use in the separation of particles by size only. However, there are many physical properties other than size holding a wealth of information

about particles, for example cancer and infection with malaria or HIV have been shown to change the deformability of cells and so measuring deformability could provide a means of diagnosing these conditions.

The central tenet of this work is that DLD can be used to separate particles by highly relevant physical properties other than size, for example shape, deformability or electrical properties and that devices that can do this in a cheap and simple way will constitute powerful particle separation tools, useful for diagnostic applications and well suited for integration in a Lab-on-a-Chip.

The aim of this thesis is to present four research papers, documenting the development of new methods that improve the existing DLD technique. Paper I describes how the elastomeric properties of polydimethylsiloxane can be utilized to achieve tuneable separation in DLD devices, making it easier to take advantage of the high resolution inherent in the method. Paper II presents the use of dielectrophoresis to achieve tuneability, improve dynamic range and open up for the separation of particles with regard to factors other than size. Paper III describes how control of particle orientation can be used to separate particles based on their shape and how this can be used to separate blood-borne parasites from blood. Finally Paper IV deals with the size, shape and deformability of cells and how DLD devices can be used, both to measure these properties, and to perform separations based on them.

The hope is that these methods might ultimately play a small part in helping diagnostics technology to become as ubiquitous as information technology has become in the last ten years and that this will have a profound impact on global health.

Keywords: Separation science, Deterministic Lateral Displacement, Microfluidics, Lab-on-a-Chip, Point-of-Care, morphology, deformability.

List of Publications

This thesis is based on the following papers, which will be referred to by their roman numerals in the text. All material from papers I, II and III is reproduced by permission of The Royal Society of Chemistry.

I. **Tuneable Separation in Elastomeric Microfluidic Devices**
Jason P. Beech and Jonas O. Tegenfeldt
Lab Chip, 8, 657-659 (2008)
I designed and built the setup, fabricated devices, performed the experiments, analysed the data and wrote the paper.

II. **Tipping the Balance with Dielectrophoresis – Electrical Deterministic Lateral Displacement Devices**
Jason P. Beech, Peter Jönsson and Jonas O. Tegenfeldt
Lab Chip, 9, 2698-2706 (2009)
I designed devices, planned and performed all of the experiments, and wrote most of the paper excluding those parts relating to simulation and modelling which where written together with Peter. Modelling and simulations where performed by Peter who also wrote the particle tracking software.

III. **Separation of Parasites from Human Blood using Deterministic Lateral Displacement**
Stefan H. Holm*, Jason P. Beech*, Michael P. Barrett and Jonas O. Tegenfeldt
Lab Chip, 11, 1326-1332 (2011)
Design and fabrication of devices, performance of experiments, analysis and the writing of the paper were a joint effort between myself and Stefan, who I was supervising as a diploma student at the time. Stefan developed the particle tracking software used in the analysis. *authors contributed equally

IV. **Sorting Cells by size, shape and deformability**
Jason P. Beech, Stefan Holm, Kalle Adolfsson and Jonas O. Tegenfeldt
Manuscript (2011)
I designed and performed all experiments, analysis of results and wrote the paper. Kalle developed protocols for changing the morphology of blood cells. The devices and particle tracker were same as those used in Paper III.

Related Publications

The following related publications by the author do not constitute an integral part of this thesis and are therefore not included.

I. Use of PLL-g-PEG in Microfluidic Devices for Localising Selective and Specific Protein Binding

Rodolphe Marie, Jason P. Beech, Janos Vörös, Jonas O. Tegenfeldt, and Fredrik Höök
Langmuir, **22**, 24, 10103-10108 (2006)

II. Nanoconfinement-enhanced Conformational Response of Single DNA Molecules to Changes in Ionic Environment

Walter Reisner, Jason P. Beech, Niels B. Larsen, Henrik Flyvbjerg, Anders Kristensen, and Jonas O. Tegenfeldt
Physical Review Letters, **99**, 5, 058302 (2007)

III. Multidirectional Sorting Modes in Deterministic Lateral Displacement Devices

Brian R. Long, Martin Heller, Jason P. Beech, Heiner Linke, Henrik Bruus and Jonas O. Tegenfeldt.
Physical Review E, Stat Nonlin Soft Matter Phys**,** **78**, 11, 146304 (2008)

IV. Shear-Driven Motion of Supported Lipid Bilayers in Microfluidic Channels

Peter Jönsson, Jason P. Beech, Jonas O. Tegenfeldt, and Fredrik Höök
J. Am. Chem. Soc. **131**, 14, 5294-5297 (2009)

V. The Mechanical Behavior of a Supported Lipid Bilayer under External Shear Forces

Peter Jönsson, Jason P. Beech, Jonas O. Tegenfeldt, and Fredrik Höök
Langmuir, **25**, 11, 6279-6286 (2009)

VI. Nano-engineered Living Bacteria Motors for Active Microfluidic Mixing

M. Al-Fandi, M. A. K. Jaradat, K. Fandi, Jason P. Beech, J. O. Tegenfeldt, and T. C. Yih
IET. Nanobiotechnology, **4**, 3, 61-71 (2010)

VII. Arrays of oxide nanotubes with integrated microfluidic connections

H. Persson, Jason P. Beech, L. Samuelson, S. Oredsson, C. N. Prinz and J. O. Tegenfeldt
Submitted to Nano Research, under review (2011)

Preface and Acknowledgments

In the spring of 2004 I took Jonas Tegenfeldt's course in experimental biophysics and I have never looked back. At some time in the autumn of the same year, shortly after I began work on my diploma project with Jonas as my supervisor, we were sitting on a train bound for the Danish Technical University and a meeting with some European Union project partners. Jonas had recently returned from post-doctoral studies at Princeton in the group of Robert Austin and wanted me to do something with a new particle separation method that his lab mates had been working on, but we weren't exactly sure what. Spurred on by the imminent meeting, the discussion was a lively one and by the time we arrived in Denmark we had envisioned much of the work presented in this thesis. That it has taken this long to bring the projects to fruition is no reflection of any lack of enthusiasm on my part or on that of Jonas, but it is rather testament to the opportunities Jonas has always given me to pursue interesting projects (as the list of related publications I think bears witness). Thank you Jonas for the belief you have always shown in me, for the opportunities you have given me and for bringing me this far.

I would also like to thank Fredrik Höök, who was my first supervisor, on paper at least, for helping me to get the PhD position in the first place and for wise words when I was starting out.

During the course of this PhD project I have worked with many people. I would like to thank Magnus, Rodolphe, Brian, Andreas, Anders, Lisa, Lars-Henrik, Christelle, Aline, Waldemar, Dmitry and Gudrun who populated the labs and biogroup meetings for the first couple of years. More recently Henrik, Cassie, Mercy, Johanna, Martina, Farnaz, Greger and Heiner who have all at some point brought some kind of cake to our Friday meetings, it has really been a pleasure and an honour to work with you.

I would like to extend special thanks to Peter Jönsson without whom Paper II would never have got finished, to Kalle Adolfsson for figuring out how to change the shape of red blood cells that I used in Paper IV, to Mike Barrett for supplying us with the parasites we used in Paper III and to Stefan Holm who worked with me ceaselessly on Paper III and whose devices and particle tracker made Paper IV possible.

Others have also helped me in specific ways. Bo Baldertorp helped with FACS measurements, Fredrik Johansson with critical point drying and SEM measurements, Lars Wallman helped with mask fabrication, Thomas Laurell lent me his high-speed camera and Per Augustsson helped me to get said camera working. Discussions with Kevin Loutherback about fluid flow in very shallow devices were also very useful.

I have also been lucky to have had the opportunity to travel during the last five years and for this I would like to thank the Royal Physiographical Society in Lund for their generous travel grants and Niklas Sköld and Fredrik Persson who have on separate occasions had to put up with me in shared hotel rooms.

There are many others at the Solid State Physics department whose help I would like to acknowledge or whom I would like to thank for some small favour or other, from those that toil to keep the money rolling in to those that keep the important machines, such as the coffee machine, working, but you are far too numerous to mention by name and so I thank you collectively. There are a few people though that I have bothered slightly more than all the others and whom I would like to thank personally, Mariusz Graczyk, Bengt Bengtsson, Anders Kvennefors, Lena Timby and Mona Hammar.

If I have forgotten anyone in the above then I am sincerely sorry, remind me the first chance you get.

On the off chance that any of you ever see this thesis I'd better also say cheers to my expat friends for moral support and the odd pint over the years and to all the Ahlgrens, my in-laws, for making me part of the family.

Lastly there are a few people for whom thanks really don't seem enough. Mum and Dad, I don't know if you ever secretly regret leaving England, I hope not. For me, cresting the hill between Santiago and Masca for the first time on the back of the truck, balanced on our packing cases and looking in awe down into the valley that would become home is one of the most powerful memories of my life. I didn't appreciate then what you were doing or why but I look back at that day as a second beginning and I know now that I owe you everything. Last but not least, my wife Nelly, and my children Jonatan and Freja, I promise, this is the last PhD I'll ever do.

List of acronyms and notation

a ..... acceleration
α ..... correction factor in calculation of effective size
A ..... area
β ..... width of lamina at P_1
BSA ..... bovine serum albumin
CTC ..... circulating tumour cell
d ..... gap between posts in lateral direction
D ..... diffusion coefficient
D_c ..... critical diameter
D_{eff} ..... effective particle diameter
DEP ..... dielectrophoresis
nDEP ..... negative dielectrophoresis
pDEP ..... positive dielectrophoresis
I-DEP ..... insulator-based dielectrophoresis
DR ..... dynamic range
Device ..... a lab-on-a-chip or μTAS system, in our case fabricated in glass and silicone rubber
D_H ..... hydraulic diameter
DLD ..... deterministic lateral displacement
D_{part} ..... particle diameter
Δp ..... pressure difference (across device)
ε ..... permittivity, strain
E ..... Young's modulus
E_{RMS} ..... root mean square electric field
EDTA ..... Ethylenediaminetetraacetic acid
ϕ ..... volumetric flow rate
ϕ_{gap} ..... volumetric flow rate through one array gap
f ..... force
f_{CM} ..... Clausius Mossotti factor
F_{DEP} ..... dielectrophoretic force
F_{drag} ..... viscous drag force
$F_{inertial}$ ..... inertial forces

F_n ..... normal force
F_p ..... fraction of 99% pure sample collected
$F_{viscous}$ ..... viscous forces
γ ..... Poisson's ratio
η ..... dynamic viscosity
j ..... $\sqrt{-1}$
k_B ..... Boltzmann constant
l ..... length
L ..... characteristic length, channel length
LOC ..... lab-on-a-chip
λ ..... centre-to-centre post spacing
m ..... mass
μTAS ..... micro total analysis systems
P ..... electric polarization
P_i ..... position number for lamina flow stream between posts
p ..... pressure
PDMS ..... polydimethylsiloxane
Pe ..... Péclet number
PLL-g-PEG ..... poly(L-lysine) grafted to poly(ethylene glycol)
POC ..... point-of-care
a, r ..... radius
R_c ..... critical radius
R_{eff} ..... effective particle radius
Re ..... Reynolds number
$Re( )$ ..... real part
RBC ..... red blood cell
R_H ..... hydraulic resistance
ρ ..... density
σ ..... conductivity, stress
SDS ..... sodium dodecylsulphate
SS ..... sodium salicylate
u,v ..... velocity vector
V ..... characteristic velocity
W_{DEP} ..... dielectrophoretic energy
WBC ..... white blood cell (leukocyte)
ω ..... angular frequency
x, y, z ..... rectilinear spatial coordinates

Contents

1 Introduction

As particle-laden fluids are forced to flow through channels containing ordered arrays of micrometer-sized obstacles the particles follow paths through the arrays that are highly dependent on both the geometry of the array and on the size and shape of the particles themselves. The principle is simple; it is based on the displacement of the particles in a deterministic manner in the lateral direction as compared to the flow direction – in short: Deterministic Lateral Displacement (DLD). Huang *et al* used the effect to separate particles by size [6]. Huang showed how the resolution in these devices (or their ability to detect small size differences), could be much greater than in conventional size-based separation techniques, reporting a resolution of 10 nm when separating micrometre-sized polymer beads, an order of magnitude improvement compared to other methods. Subsequent work, by Huang and others, has shown how DLD can be used for the separation and analysis of a wide range of biological particles [6-15] in devices no more than a centimetre or two in size.

This introductory chapter will deal with some of the concepts introduced in the above paragraph. We will begin, in general terms, by considering what biological particles are, why one might want to separate them from one another, how the methods for doing this vary and why performing particle-particle separations in miniaturized devices is so attractive and the focus of much current research.

1.1 Particles

The word particle probably conjures up a variety of images for you depending on your background. You might think of an elementary particle, such as a proton, or something more tangible, like a particle of sand. The word particle comes from the Latin, *particula* meaning 'little part' and is therefore equally suited to protons, atoms, molecules and pieces of sand despite a span in mass of 20 orders of magnitude. Much of the work performed in research laboratories and in industrial processes involves the breaking down of complex mixtures into their constituent parts (or particles) and the subsequent separation of these particles from one another. Whether it is the breaking down of a sample of soil into size sorted particular fractions or the breaking down of just one of these soil particles into its

constituent atoms the processes used come under the rubric, separation science [16].

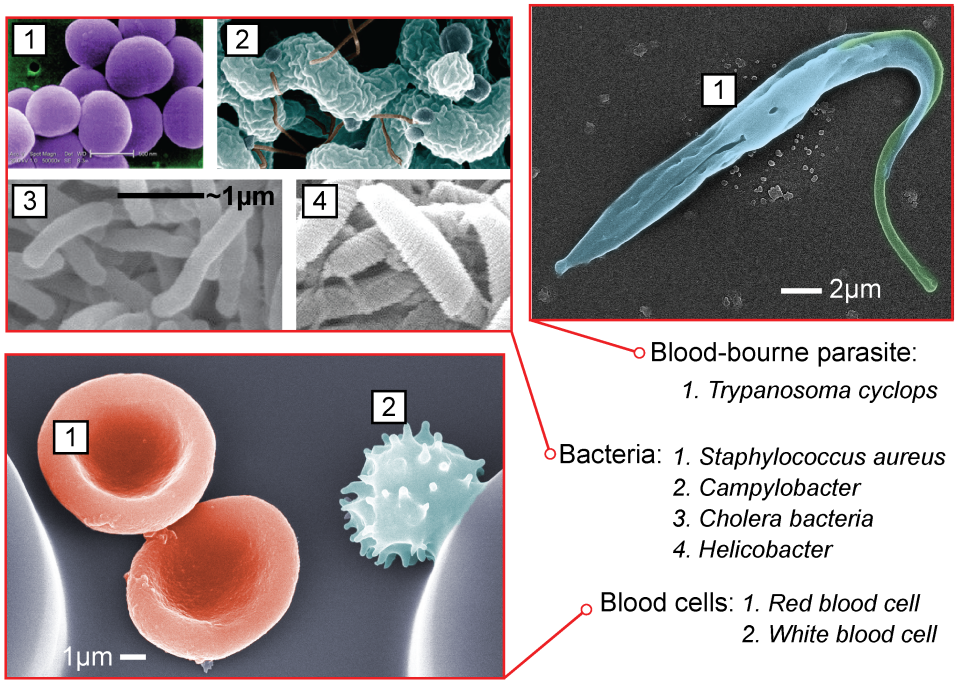

Figure 1 Some examples of biological particles, the separation of which is often part of laboratory analyses. These particles present a wide range of sizes, shapes and other properties. Blood cells are for example highly deformable and the parasite, T. cyclops, is motile with the flagella shown in green beating many times a second. (Images of bacteria from Wikimedia Commons [1-4].)

1.1.1 Biological particles

We are interested first and foremost in particles with biological relevance. Particles that most obviously fall into the category 'relevant' are those that make up living systems and these range in size and complexity from individual molecules such as proteins and DNA to single cells and even entire (micro)-organisms. The products of biotechnological processes are also of great interest. Table 1 gives an overview of some of the particles that are commonly the focus of separation.

Human blood is probably the most widely used source of diagnostic information. In Papers III and IV we are concerned with separating blood into its component parts. Not only those components that make up healthy blood but also foreign bodies that can infect blood and cause sickness need to be counted and characterised and often separation is an important step in this process. The table in Appendix 1 gives an overview of the concentrations, shapes and sizes of cells

found in healthy human blood and a few examples of other bodies that we are interested in for diagnostic purposes. In addition to this, polystyrene beads of various sizes can be invaluable as models for biological particles and are widely used when developing separation systems.

The principles of DLD and the improvements to DLD that we have developed are applicable to these and all manner of other particles. Provided there is a difference in the innate properties of two particles, be it in size, shape, deformability or electrical properties for example then we can use our methods to prize the particles apart. In the remainder of this thesis 'particle' is used to denote these biologically relevant entities.

Table 1 An overview of bioparticles that are commonly the subject of separations.

Particle	Diameter [μm]
Whole cells:	
Bacterial	0.5 – 5.0
Yeast	2.0 – 10
Fungi and algae	40 – 70
Mammalian cells	5 – 40
Plant cells	50 – 100
Cell debris:	
Bacterial	0.05 – 3.0
Yeast	0.05 – 8.0
Inclusion bodies†	0.05 – 1.2
Crystals	1.0 – 100
Virus and virus-like particles‡	0.02 – 0.2

† Aggregates, usually of proteins that are the result of viral activity

‡ VLP:s are virus capsids without nucleic acid contents.

1.1.2 Characteristics of particles

The particles mentioned above have many different physical characteristics that distinguish them from one another. Size and density are examples of properties that have long been used to identify and separate cells. Recently the deformability of cells has received much attention due to the realisation that it can reveal much about the state of the cell even in the absence of size or density differences. Infection with malaria [17, 18], cancer [19] and HIV [20] are examples where the deformability of cells is known to change and deformability is therefore a factor that can be used in diagnostic devices to identify cell type and/or cell health.

While Table 1 (and Appendix 1) give some examples of the sizes of biological particles, Figure 1 highlights the danger of thinking of biological particles in the simplistic terms of a diameter only; many biological particles have complex shapes. The shape of a red blood cell for example is affected by a variety of factors

from genetic conditions [21], disease states [22], drugs [23, 24], ex vivo storage conditions [25, 26] and pregnancy [27]. Living cells are in some cases motile and motility is achieved by rapid changes in shape. Motility is often a direct indicator of sperm cell health for example [28]. Cell cycle has also been shown to affect the morphology and elasticity of cells [29].

Electrical properties are specific to particle types. Particles have a surface charge and an electrical polarizabilty. Magnetic properties, acoustic impedance and optical properties such as index of refraction also vary between particles.

Cells have small molecules on their surfaces that allow them to adhere to each other and to other surfaces. These molecules and therefore the ability of cells to adhere to surfaces are very specific to cell type.

1.2 Separation

1.2.1 Why separate particles?

It can be important to separate particles for many reasons. Clinical analysis, diagnosis and preparative techniques rely heavily on separation at some stage in the process. Because many biologically relevant samples such as whole blood, saliva and cell lysates are highly complex and because the targets for detection can be present in extremely low concentrations, separation is often an essential part of any analytical process, necessary in order to avoid problems of cross-sensitivity. The problem in these cases is basically analogous to that of the classic needle in a haystack. The job of separation is to remove as much of the hay as possible before one begins hunting for the needle. An example of this is the difficulty of detecting parasites in blood as described in Paper III. Parasites can be present in very low numbers, sometimes lower than 1 per µl (one small droplet of blood) compared to the 5 000 000 or so red blood cells in the same volume [30]. Before parasites can be found, identified and counted the huge background, the hay, must be removed using some manner of particle separation. The problems are the same for other types of rare cells such as circulating tumour cells. Separation or pre-concentration can even be necessary at more than one stage in a process as described by Chen and Cui [31]. For example if cells are being analysed then it might be necessary to first isolate the cells of interest. These cells can then be lysed (broken apart) after which further separation of the proteins or genetic material in the cell lysate can be performed.

Separation is not only about simplifying complex mixtures of particles. In the separation field distinction is made between preparative methods, where separated particles are collected, and analytical methods, where the aim is to count or perform other measurements on particle systems without necessarily collecting

any separated fractions. The ability to separate infers the ability to identify and analyse the components in a complex mixture. A method that can separate particles by a specific property can also be used to measure that specific property and so can also be used to detect any changes in that property. For these reasons separation methods are often synonymous with analytical or diagnostic methods. This is true for our methods also and while we talk primarily of separation in this thesis the methods can be used equally well for analytical purposes as they can for preparative ones.

1.2.2 How is separation achieved?

Separation is achieved by the application of forces to particles. If the forces applied to a mixture of particles result in the movement of the particles relative to one another then they will become separated. This relative displacement of particles based on the application of forces is the underlying mechanism in all separations and the many methods that have been developed to achieve separation differ from one another in the types of forces and in the means by which these forces are applied only.

Any characteristic property of a cell, such as those discussed in chapter 1.1.2, can be selected as a separation parameter by the application of the appropriate forces. Often two forces are used to achieve differential motion of particles. Density and viscous drag are examples of properties that have been used for millennia to separate particles. Throwing grain and chaff into the air on a windy day to separate them is a good example of this. The denser, more streamlined grain falls to the ground while the chaff experiences more air resistance and is carried away be the wind.

Size alone is often used as a parameter in separation. Sieving is the classic example of such separation. Even particles too large to pass through a sieve might conceivably do so if they are soft and are able to deform and so deformability also plays a roll in separations. To continue the same analogy, sticky particles can also stick in a sieve, despite being small enough to pass through the holes and so the ability of cells to adhere to surfaces is also important and widely used for separation.

In the following sections we will argue for the benefits of miniaturized separation systems and the interesting applications they make possible. We focus our discussions therefore on these new methods, examples of the mechanisms that have been used to date and on their relative benefits and limitations. Despite their diminutive sizes, these devices depend on the same underlying physical principles as the more traditional approaches which are much more thoroughly discussed in the seminal work *Unified Separation Science* [16] by Giddings.

1.2.3 Limitations of traditional methods

Flow cytometry is a method that measures properties of particles as they pass, one by one, through a beam of light [32]. Fluorescence Activated Cell Sorters or FACS machines and other flow cytometers ranging in size from desktop to room sized models are standard pieces of equipment at most large hospitals and are used to analyse and separate cells and other biological particles. While flow cytometers can sort cells at rates of up to 100 000[1] per second they are expensive and require extensive infrastructure such as lab space, power, personnel and reagents as discussed by Pappas and Wang [33]. Although information about the size and granularity of particles can be gleaned from scattered light, generally these methods also require the fluorescent labelling of samples. While these requirements are easily met in large hospitals they can be limiting factors in other settings from laboratories to developing-world health clinics. Another drawback of large flow cytometers is that they are not suited to integration with other analysis steps.

FACS machines are examples of technological solutions that have been designed and optimized for use in centralized laboratories, much like the very first computers. Traditionally samples are collected, either from the patient the environment or other system and sent to these centralised labs where analysis takes place. This way of doing things is costly in both time and money. Parallels can be drawn between the benefits of miniaturizing chemical and biological systems and the benefits of miniaturising electronics systems that has put powerful computers in the palms of our hands and lead to the information revolution.

1.3 The advent of μTAS and Lab-on-a-chip

In 1979 Steven Terry used techniques borrowed from the electronics industry[2] to fabricate a gas chromatograph on a silicon wafer that despite being three orders of magnitude smaller than its conventional laboratory predecessors suffered no loss of function [34]. In 1990 Manz proposed the integration of modules with the

[1] For example, Accuri C6 Flow Cytometer® 10 000 detection events s^{-1} and BD FACSAriaTM 70 000 detection events s^{-1}.

[2] The group of techniques developed to fabricate integrated circuits, such as photolithography to define patterns and etching to transfer those patterns into a material, typically silicon, are collectively known as “micromachining”. A comprehensive catalogue of techniques developed to date can be found in Marc Madou’s Fundamentals of Microfabrication and Nanotechnology [Madou, M. J., Fundamentals of Microfabrcation and Nanotechnology 3rd ed. 2009, Boca Raton: CRC Press. 2640 p.]

capabilities of performing all the steps necessary for the chemical analysis of a biological sample on a single chip [35]. In the last 20 years much work has been done on the development of these Micro Total Analysis Systems or μTAS. 'Lab-on-a-chip' is a slightly broader term encompassing the miniaturization of any chemical or biological process to chip scales that has also become widespread and we will use this term throughout the thesis to denote such miniaturized systems. Figure 2 shows an example of a DLD separation device and the small features that make the device function.

The benefits of miniaturization and integration are many including increased automation, parallelization, speed, resolution and portability as described in reviews by Mosadegh [36], Dittrich and Manz [37], Franke and Wixforth [38], Erickson [39], Verpoorte [40], Mark [41], Craighead [42] and Squires [43]. Several other reviews have covered the progress made towards chips that can be used for cell biology [44, 45] and Cellomics research [46]. More specific reviews deal with microfluidics techniques for cell sorting and separation [47-51], cell lysis, cell culture and cell electroporation [52] and also the specific problems related to the analysis of blood in microfluidics devices are covered by Toner *et al* [53].

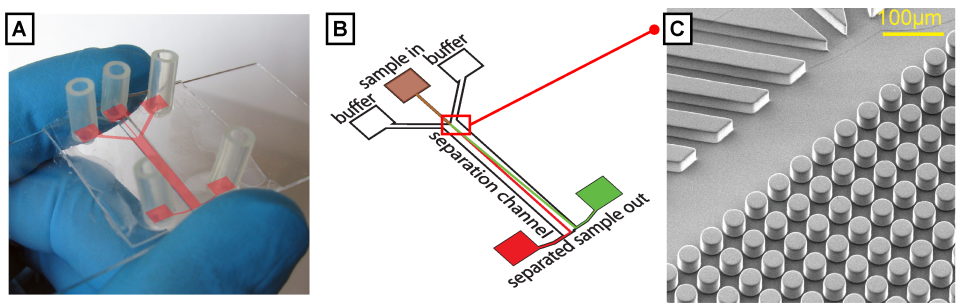

Figure 2 Example of a microfluidics device. (A) The device is fabricated in silicone rubber and glass and is no more than a few cm^2 in size. (B) In this device a sample is separated into two size-based fractions. (C) The micrometre-sized features that give the device its functionality.

1.4 Diagnostics at the Point of Care

The goal for many researchers in the fields of μTAS and Lab-on-a-chip is at present the development of devices that will be able to diagnose a patient on the spot, wherever the patient happens to be, in just a few minutes without the need for extensive laboratory testing [54-56]. Devices that can be used at the point of care, or POC diagnostic devices, it is believed, stand to revolutionize the health care

industry, not least in the developing world as proposed by Yager in Nature [57] due to their low cost and portability, and will help to usher in an era of personalized medicine in which treatments are tailored to the individual based on richer and more frequently collected diagnostic data taken from increasingly smaller samples. This information will make it possible to take into consideration the physiology of the individual patient and not only the expected pathology of the disease. The blood glucose meter that can be used at home to monitor blood sugar levels has had a large impact on the quality of life for sufferers of diabetes and is an excellent example of the power of personalised medicine.

An example of a technology that has, more recently, successfully been taken out of the lab and into field in the developing world is the 'mChip' developed by Sia *et* al [58]. The device uses the ELISA technique to diagnose HIV and syphilis simultaneously from 1µl of unprocessed patient blood and it does this using small disposable plastic cassettes that are read out with a small handheld device no larger than a mobile telephone, taking only a few minutes.

1.5 Strategies for separation in lab-on-a-chip devices

Because separation is sometimes and end in itself and sometimes only one step in a larger process, our aims are to develop particle separation devices that can function both independently and in concert with other components in lab-on-a-chip devices. In many cases the criteria for good separation might be high throughput or high resolution only and in these cases the size and cost of a device and the requirements for peripheral equipment are not limiting factors (these will be covered in chapter 4). Lab-on-a-chip devices for point of care however, specifically if they are to be of use in resource poor environments such as developing world settings or even the average home, must fulfil other criteria such as low cost, portability and ease of use, all of which can be achieved by minimizing bulky, power consuming and complex peripheral equipment [59][3]. Methods that are passive, continuous and label-free make good candidates for components that can be integrated in POC devices. Appendix 2 contains a table that summarizes some of the most common methods that have been used to

[3] At this point, the design and development stage, we use peripheral microscopes, light sources, pumps and pressure controllers etc. All of these components have been miniaturized in recent years and can be integrated into devices.

separate and analyse particles. The table shows the separation mechanism, the particle property that can be measured and in most cases some measure of the resolution and/or throughput of the method.

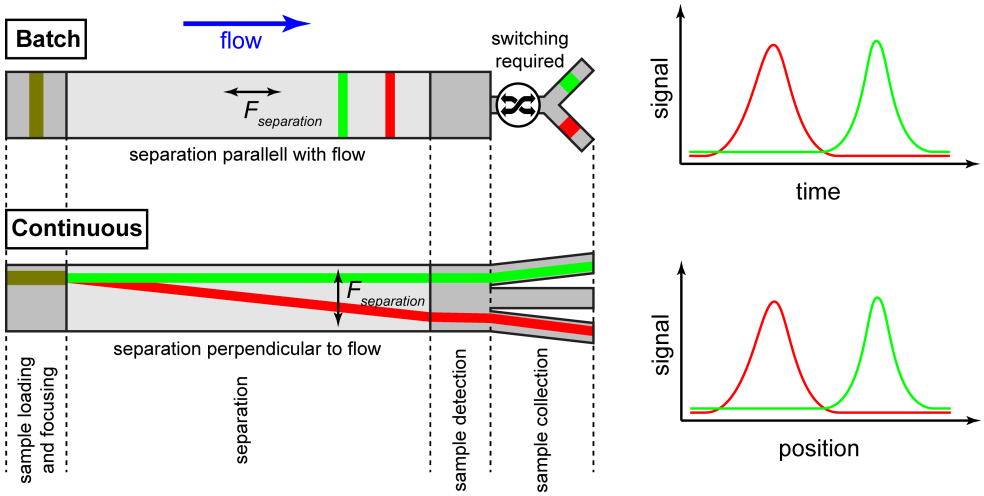

Figure 3 Batch contra continuous separation methods. Batch methods separate finite volumes of sample parallel with the flow direction. The separated sample fractions pass a detector at different times. Collection of the separated fractions can only be achieved with a flow switching mechanism that redirects different components to different outlets. Continuous methods separate perpendicularly to the flow direction. Fractions are identified by their position at the end of the device. Separation in space means that fractions are easily collected at different outlets (adapted from reference 31).

1.5.1 Continuous versus batch methods

When the forces used to separate particles are parallel, or antiparallel, the particles follow the same paths but at different rates and the resulting separation is in time only. This is typical of batch methods, so called because they deal with samples one finite volume or 'batch' at a time. If the forces have components perpendicular to one another then particles instead follow different paths and become separated in space. The differences between these two approaches are summarized in Figure 3.

In order for separation and the closely related pre-concentration techniques to be integrable within a Lab-on-a-chip it is advantageous, as described by Pamme [60], that the process be continuous. Batch methods can be integrated with other analysis steps but require controlled sample injection and flow switching for the collection of separated fractions that greatly increase the complexity of devices. Continuous methods accept the continuous input of a sample at one end, separate the particles in space, and allow for the extraction of any number of fractions at

the other. The continuity of flow through such devices means that they can be more easily integrated with other analysis steps both upstream and downstream.

Continuity is also important in order to fully benefit from tuneability. If separation parameters are changed during continuous separations then the effects of those changes can be observed in real time. This means that feedback can be used to tune and optimize separations. This is important in the context of Papers I and II in which we present tuneable separation devices.

1.5.2 Labelling and label-free methods

The molecules on the surfaces of cells that are specific to cell type can be used in different ways to achieve separation. The attraction of particles to surfaces via surface charge is used in ion exchange columns for the separation of parasites from blood cells for example [61, 62]. The adhesion of cells to tailored surfaces can also be used to trap and concentrate cells [63]. Alternatively surface properties can be used to attach labels to cells, which can then be used for identification and separation. Antibodies for example are very specific and can be used to attach magnetic or fluorescent labels to cells. Magnetic activated cell sorting, MACS, uses magnetic fields to collect cells labelled in this way [64] and FACS, that we mentioned previously, uses fluorescence to identify cells that once identified can be sorted using the application of electric fields [32, 65]. While MACS and FACS can be used to separate cells based on very specific properties the labelling steps necessary in both cases entail extra work and extra costs. The labelling steps might also have a negative effect on the viability of the cells, which could be a concern in some cases, for example if the cells are destined for culturing or therapeutic use. 'Label-free' methods are methods that do not require this additional step and are as such potentially simpler, cheaper and free of the effects of the labels themselves. Gossett *et al* recently reviewed the benefits and limitations of label-free methods [49]. The table in Appendix 2 is an extended version of table 1 in Gossett's review.

1.5.3 Passive or applied fields

Separation methods can be roughly divided into passive and active methods [48]. Passive methods rely on interactions between particles and the forces that occur as the particles and carrier fluids are pushed through the device. Because these methods rely on microfluidic phenomena, other than ensuring control of fluid flow, using a pressure difference for example, no other forces or external fields need be applied. Active devices rely on the application of external fields such as magnetic or electric fields and are therefore generally more complicated both to fabricate and to use than passive devices although there are exceptions; gravity for example can be used as an applied field.

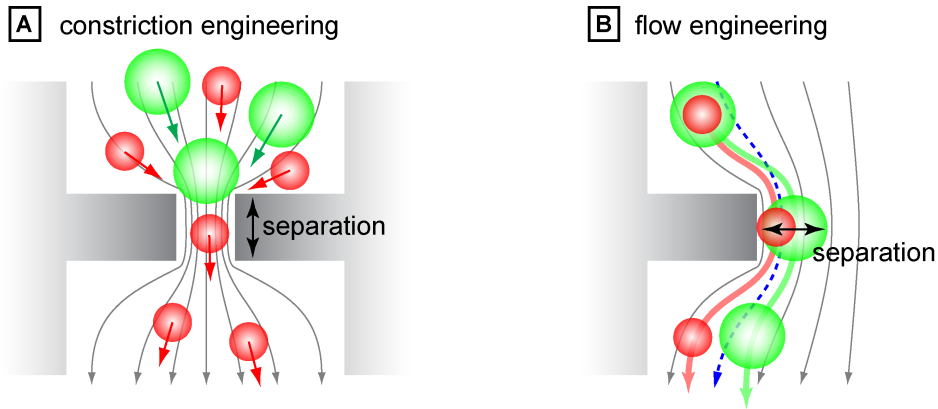

Figure 4 Clogging and non-clogging particle separation geometries. (A) In a sieve-like device constrictions are engineered to selectively trap particles. (B) In non-clogging devices flows are engineered such that particles move through the device but are forced across streamlines to become separated.

1.6 Chip-based separation techniques

Many methods have been developed to date that are capable of separating, concentrating or simply analysing particles in microfluidics systems. Deterministic lateral displacement is a continuous, label-free, passive method and so for the sake of brevity we limit the discussion here to methods that possess these same properties. In Paper II however we apply external electric fields to our device in order to add functionality and so we briefly mention some other separation techniques that rely on applied fields. (see Appendix 2 for further examples).

As we will discuss in the following chapter, inertial effects can almost always be neglected in microfluidic systems. Under some conditions however, as described by Di Carlo and coworkers [66] inertial effects can lead to both secondary flows in fluids, and to the migration of particles perpendicular to the direction that the carrier-fluid is moving in. This secondary effect is dependent on particle size and has been used, in a range of device geometries, to achieve particle separation [3, 67-72]. Recently, and interesting in the context of Paper IV, an inertial microfluidics device was used to separate particles based on a combination of size and deformability [73]. In general devices using inertial effects must be run at low particle concentrations because particle-particle interactions stop separation from occuring, which means that samples such as blood need to be diluted many times (~30 000 times [74]) requiring the use of considerable volumes of carrier fluids. High cell number throughput can still be achieved due to the high volume flow rates used. In reference [74] the throughput was only 22 000 cells/minute but

parallelization could increase this. While this method will undoubtedly find applications, this reliance on buffers for dilution might prove limiting in resource poor settings. Furthermore it is hard to extricate the effects of size and deformability when using this technique as both contribute to particle behaviour. Di Carlo also explored the effects of particle shape [75] and concluded that it had little effect on particle behaviour although more recent work has shown some sensitivity to particle length [76].

A wide variety of devices have been designed based on engineering constrictions in various geometries [77-79] to function like sieves, see Figure 4A. Constrictions have also been used to trap individual cells [80] and droplets containing cultures of cells [81]. These techniques are inherently "clogging", due to the fact that, as is the case with a traditional filter or sieve, particles remain in the sieving structure and will eventually hinder the performance of the separation. Clogging devices are well suited for particle-liquid separation where the removal of all particles is the aim. Inline water filters are a good example of this [82]. They are not however as well suited for particle-particle separations as the effective pore size changes rapidly as soon as particle capture begins. Transit time analysers measure the time it takes for deformable particles to squeeze through constrictions that are smaller than the cells themselves. The time taken to make this passage is dependent on cell size and deformability. The method is a prime example of how a traditional method, membrane filtration, can be improved by miniaturization and was first developed by Austin *et al* [83, 84]. The method has recently been used by Bow *et al* to detect the infection of RBCs by malaria parasites [85]. As with inertial methods transit time techniques require considerable dilution of samples. What is more, while they can continuously analyse particles, they have not yet been shown capable of continuous separations.

Techniques that use steric and other forces from channel walls to force particles to cross streamlines while simultaneously allowing them to flow through the device are in principle non-clogging, see Figure 4B. DLD can be thought of as a non-clogging sieve. Another non-clogging method is that known as Pinched-flow fractionation that was pioneered by Yamada *et al* [86]. Particles are forced against a channel wall and their hydrodynamic centres of mass adopt positions relative to the wall dependent on the particle size. As the flow later diverges due to a widening of the channel the particles follow slightly different flow directions, which depend directly on their size, and they become separated. Pinched-flow has been used for passive size-base separations [87, 88] but also together with added external forces such as optical forces [89] and sedimentation forces [90]. Pinched flow and inertial microfluidics have recently been combined for the extraction of rare cells from blood [91]. Hydrodynamic filtration is a method closely related to pinched-flow and has been recently shown to have some sensitivity to particle shape. Sugaya *et al* where able to separate budding from non-budding yeast, although the size differences where also considerable [92].

Biomimetic separation methods utilize the characteristic flow behaviour of blood cells in the microvasculature to separate different cells types in microfluidic channels. At high cell concentrations such as those found in blood, deformable cells such as red blood cells migrate to the centre of the channel and less deformable cells such as white blood cells [93] or malaria infected red blood cells [94] migrate towards and become concentrated at the channel walls, a phenomena known as margination. Also in a bifurcating channel, red blood cells have a tendency to flow into the channel with the highest flow rate, a phenomena known as the Zweifach-Fung effect, and this can be used to remove cells from plasma [95].

Among the many active methods that have been developed in chip-based configurations are acoustophoresis [96, 97], magnetophoresis [98] and dielectrophoresis [99].

1.7 Deterministic Lateral Displacement

DLD is a method of particle separation that is, in light of the discussions above, well suited for the separation of biologically relevant particles in miniaturized devices. To recapitulate:

- DLD devices are continuous, making them well suited for integration with other components in a lab-on-a-chip.
- DLD is a passive mechanism and devices can therefore be made simple, requiring only a means of generating flow.
- DLD does not rely on stochastic processes like diffusion that need to be given time to work and devices using DLD can therefore be run arbitrarily fast, provided the criteria for low Reynolds number flow are met as will also be discussed in the following chapters. This means that volume flow rates of ~ml/min can be achieved in a single device and even higher throughputs could be achieved by the running of many devices in parallel[4].

[4] We previously presented a method of hot embossing DLD devices in thin films. Many of these thin devices could be stacked in order to achieve increased throughput [J. P. Beech, T. Mäkelä, P. Majander and J. O. Tegenfeldt, *Throughput Through Thin-Film Fluidics,* The 12th International Conference on Miniaturized Systems for Chemistry and Life Sciences, San Diego, USA, 2008, 1492–1494.]

- DLD occurs when particles flow through arrays of obstacles, which means that there is some risk of devices clogging although steps can be taken to minimize this, see chapter 4.
- DLD devices can be made no larger than a postage stamp and are therefore of great interest both as stand-alone separation devices and as integrable components for Lab-on-a-Chip and POC devices.
- DLD can be used to separate particles in the size range relevant for cells, subcellular components and other interesting bio-particles (100 nm to 100 μm). .
- DLD devices can perform separations with high resolution, down to 20 nm in diameter when separating micrometre-sized polystyrene beads [6].
- DLD has proven capable of dealing with biological samples. A review of the literature to date is given in chapter 3.6.
- In the first paper by Huang *et al.* [6], DLD is presented as a purely size-based separation technique. The method however can be adapted to separate by and measure many different relevant particle properties, which is the focus of this thesis.

1.8 Developing and improving DLD devices

This thesis presents my efforts to develop the method of DLD and to add to it new functionality. The benefits conferred by each development are easiest to appreciate after first understanding how the method of DLD functions and so before returning to a summary of the work presented in Papers I to IV in chapter 5 we will look in more detail in chapters 2-4 at the theory of microfluidics, the mechanism of DLD and the design and fabrication of functioning devices.

In brief:

Paper I describes how we have used the elastomeric properties of polydimethylsiloxane to change the geometry of the post array in a DLD device during ongoing separation thereby achieving tuneable, size-based separation.

Paper II describes how forces can be added to DLD in order to achieve tuneability with regards not only to size but also to other particle properties. In the specific case reported in Paper II we use the application of electric fields that give rise to dielectrophoretic forces within the post array to achieve tuneability. These DEP forces are sensitive not only to particle size but also to the dielectric characteristics of particles which can be leveraged to separate cells, for example, live from dead, healthy from sick or cells at different stages of their developmental cycle that might not display any significant differences in size.

In Papers III and IV we control the orientation of non-spherical particles by varying the device depth. This allows us to chose which particle dimension to sort by, for example the length or thickness of a particle and in Paper III we use this to optimize separation of parasites from blood. In Paper IV, as well as orientation, we look at the deformation of cells due to shear forces in our devices. Particle trajectories give us information about how much cells are deformed due to these shear forces, and we can use DLD devices to both measure mechanical properties as well as separate by them.

The remainder of this thesis will be presented in the following way:

Chapter 2 will deal with some of the theory of microfluidics and the behaviour of particles in fluids that underlie the functioning of the DLD devices that we have developed.

Chapter 3 will describe the flow of fluid through post arrays, the functional components of DLD devices and will explain why particles take different paths through post arrays and become separated.

Chapter 4 In order to be separated or otherwise analysed, particles need to be injected into devices through inlets, imaged, and collected through outlets. This chapter will deal with the design and fabrication of functioning devices.

Chapter 5 will present the developments to the method of DLD that we report in Papers I to IV.

Chapter 6 will present an outlook into the future of the methods we have developed. I will take the opportunity here to speculate on how our methods might find uses and on how we might develop them further.

2 Microfluidics theory

Definition of a fluid: *A fluid is a substance that continually deforms under the action of shear stress.*

Microfluidics: *The science and engineering of systems in which fluid behaviour differs from conventional flow theory primarily due to the small length scale of the system* [100].

We are all familiar with fluidics on the macro scale. A jet of water from a garden hose, the bubbling and gurgling of a running stream or the swirling of your morning coffee as you stir in the sugar are everyday examples of fluids behaving under the influence of applied forces. Fluids are caused to move by body forces such as gravity, normal forces such as pressure and shear forces that give rise to viscosity. We learn about these forces and how to balance them when we learn to swim. With the exception of extremely slow moving fluids (see Figure 5A), inertial effects dominate fluid flow on the macro scale (see Figure 5C). The situation is very different for fluids flowing through the micrometre-scale environments encountered within the field of microfluidics. On these scales inertia is almost always negligible and behaviour is dominated by viscous forces, by surface effects such as surface tension and wetting and by diffusion and can sometimes seem counterintuitive or at the least unfamiliar to the uninitiated.

In this chapter we consider the theory that describes both the flow of fluid in microfluidics devices and those phenomena that influence the behaviour of fluid-borne particles. In both cases the focus is on the effects that underlie the workings of Deterministic Lateral Displacement. Phenomena that are most important in the basic description of DLD are laminar flow, the velocity profile and viscous drag on particles. Fluid resistance is also important for the designing of inputs and outputs to our devices. Other phenomena that modify the behaviour of particles in DLD devices are diffusion, which is always present at the microscale and often working against our efforts to separate particles, dielectric forces, which we use in Paper II and the rotation and deformation of particles due to interactions with both the fluid and the solid walls of the devices, which are important in Papers III and IV.

The interested reader is referred to the books by Bruus [101], Hauke [102], Nguyen and Wereley [100] for theoretical details and in-depth discussions of the

physics of microfluidics and also to several review papers that have been written on the subject [43, 103-106].

2.1 Characteristics of flow

Newton's second law relates the force exerted on a mass to the resulting acceleration.

$$m \cdot \mathbf{a} = \mathbf{F} \tag{1}$$

While Newton's second law describes the motion of the centre of mass of an object, a raindrop for example, the detailed behaviour of the liquid within the raindrop requires a description of the fluid as a continuous medium rather than as a discrete mass. Instead of discrete forces and masses fluids are better described in terms of continuous fields such as mass density and force density. The

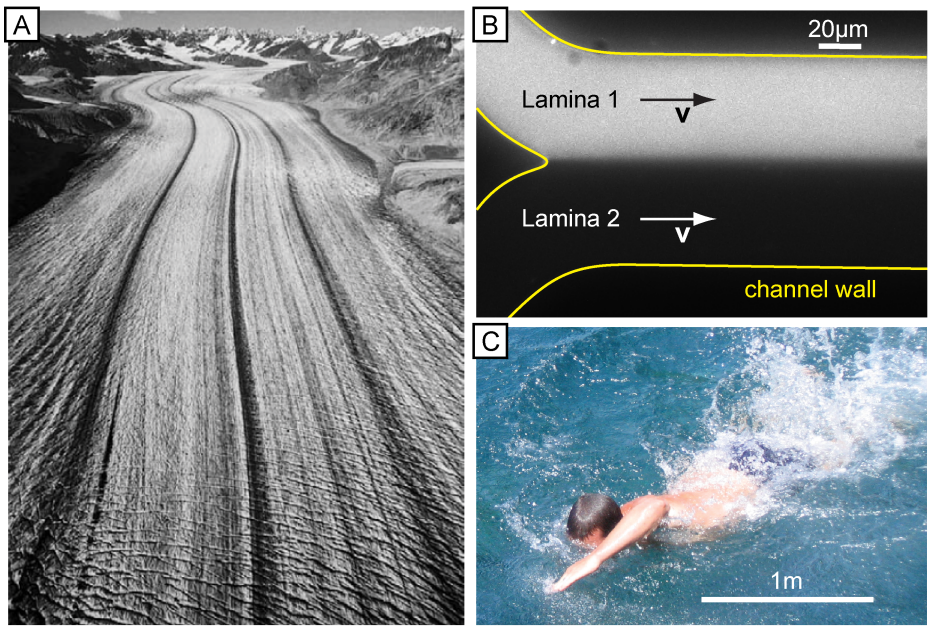

Figure 5 Laminar or turbulent flow? (A) Due to the high viscosity, flow in a glacier is laminar. Streamlines move parallel to one other and turbulence is absent. Copyright Wiley-VCH Verlag GmbH & Co. KGaA. Reproduced with permission [8]. (B) Two streams meet but continue as if still confined by channel walls. These non-mixing streams are referred to as lamina and such flow is called laminar flow. (C) The author investigating inertial effects and turbulence at the macro scale.

Navier-Stokes equation describes the velocity, **v**, and the pressure, p, in a Newtonian fluid[5] with density ρ and dynamic viscosity η.

$$\rho\left[\frac{\partial \mathbf{v}}{\partial t}+(\mathbf{v}\cdot\nabla)\mathbf{v}\right]=-\nabla p+\eta\nabla^2\mathbf{v}+\mathbf{f} \tag{2}$$

$$\nabla\cdot\mathbf{v}=0 \tag{3}$$

Eq. 2 is analogous to Newton's second law with inertial acceleration terms to the left and force terms on the right. The inertial acceleration term on the left consists of 'local' acceleration, $\partial\mathbf{v}/\partial$t, and convective acceleration, $(\mathbf{v}\cdot\nabla)\mathbf{v}$. Local acceleration describes the change in the velocity of a fluid over time at a fixed point in space. An example of this would be the change in the velocity of the water through the nozzle of a hose as the tap is opened and closed. Convective acceleration is the change in velocity as fluid moves from one place to another. This could be likened to the changes in velocity you might experience travelling down a river on a boat as the river narrows and widens and the flow slows down and speeds up accordingly. The force terms consist of $-\nabla p$, the pressure gradient, and $\eta\nabla^2\mathbf{v}$, the viscous effects. **f** represents body forces such as gravity and electrical forces.

Eq. 3 is the continuity equation, arrived at by assuming an incompressible fluid where ρ is constant in both time and space.

2.2 The Reynolds Number and the Stokes Equation

Because of the nonlinear term in the Navier-Stokes equation, $(\mathbf{v}\cdot\nabla)\mathbf{v}$**,** it cannot generally be solved analytically. Luckily, the equation can be greatly simplified under specific conditions such as those found at the small length scales relevant for microfluidic devices. Because it is the inertial term $(\mathbf{v}\cdot\nabla)\mathbf{v}$ that causes the problem we want to know when it can be neglected. The inertial forces are characterised by non-linear terms of the form:

[5] For Newtonian fluids the viscosity η does not vary with shear rate.

$$F_{inertial} \propto \rho \mathbf{v} \frac{\partial \mathbf{v}}{\partial x} \tag{4}$$

A measure of the inertia of the flow can be expressed in terms of a characteristic velocity, V, and length, L:

$$F_{inertial} \to \rho \frac{V^2}{L} \tag{5}$$

The viscous forces are characterised by terms of the form:

$$F_{viscous} \propto \eta \frac{\partial^2 \mathbf{v}}{\partial x^2} \tag{6}$$

Which can similarly be expressed in terms of V and L:

$$F_{viscous} \to \eta \frac{V}{L^2} \tag{7}$$

The ratio between equations 5 and 7 gives the ratio between inertial and viscous forces:

$$\frac{F_{inertial}}{F_{viscous}} = \frac{\rho L V}{\eta} \equiv \mathrm{Re} \tag{8}$$

The characteristic length L is a length scale that characterizes the system[6] and V is often taken to be the average velocity. *Re* is a dimensionless number known as the Reynolds number after Osborne Reynolds. The Reynolds number is ubiquitously used to predict whether and when the Navier-Stokes equation can be simplified. Systems with large spatial dimensions, high densities, large velocities or small viscosities are characterized by large Reynolds numbers (see Figure 5C). It is such flow, known generally as turbulent flow that we are well acquainted with on the macro scale. The flow of coffee around the inside of a cup is dominated by inertia (stop stirring and see what happens) and is therefore in general turbulent, exhibiting eddies and vortices that are characteristic of turbulent flow. The onset of turbulence depends on the geometry of the system and occurs only when inertia totally dominates, becoming increasingly more likely for *Re* >1500. For Reynolds numbers spanning the range on the order 1 to 1000, non-turbulent inertial effects such as Dean flow and non-turbulent vortices may occur [66]. Low Reynolds

[6] The characteristic length is often taken to be the smallest length scale of the system such as the radius for a particle or the smallest width of a channel. The hydraulic diameter D_H for a channel is also commonly used:

$$D_H = \frac{4 \times \text{cross sectional area}}{\text{wetted perimeter}}$$

note: for a channel of circular cross section D_H is equal to twice the radius.

numbers characterize systems with sufficiently small dimensions, low densities, low velocities or high viscosities (see Figure 5A and B). In microfluidic systems with water as the fluid, characteristic channel dimensions in the range 10^{-6} m to 10^{-3} m and characteristic velocities in the range 10^{-6} m s^{-1} to 10^{-3} m s^{-1} *Re* ranges from 10^{-6} to 1 and viscosity dominates. Under such conditions when the inertial terms can be neglected the Navier-Stokes equation simplifies to the linear Stokes equation,

$$0 = -\nabla p + \eta \nabla^2 \mathbf{v} \tag{9}$$

2.2.1 Laminar flow

Laminar flow is essential in order for DLD to function. Laminar is derived from the word lamina, which means "thin layer". In fluidics these thin layers consist of non-mixing parallel flows, often visualised by particles or dye molecules. Such laminae can be seen in the glacier shown in Figure 5A, and Figure 5B shows laminar flow in a microchannel.

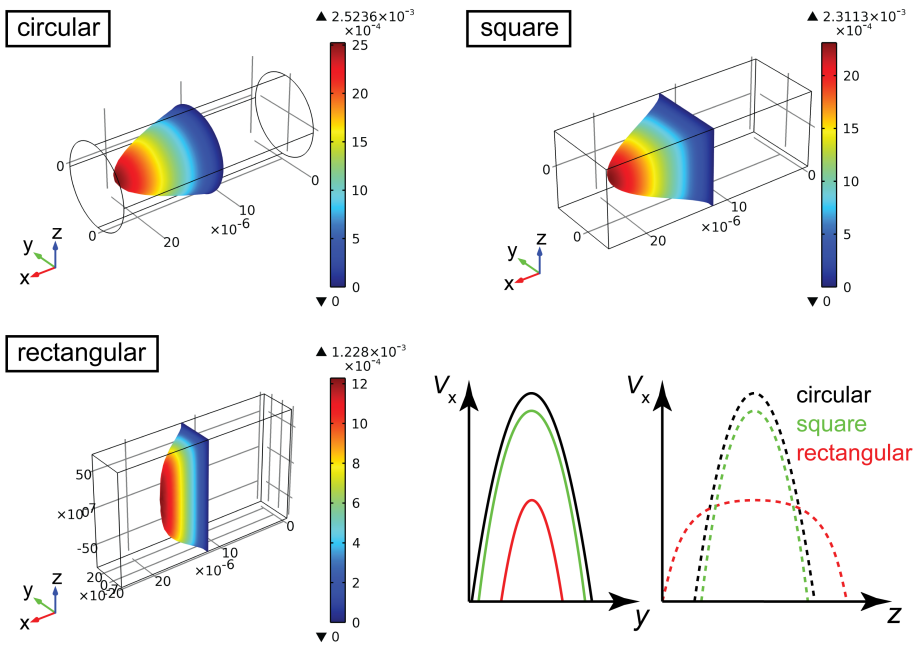

Figure 6 Solutions to the Stokes equation in three example channels. The cross sectional area ($\pi \cdot 5 \cdot 10^{-6}$ m^2) and the length ($25 \cdot 10^{-6}$ m) are the same in each of the three channels and the pressure difference across the channels is 10 Pa. The line profiles (bottom right) show the lateral distributions of velocities (V_x) in each of the channels.

If two fluids are flowing in two channels that meet in a "Y"-shaped geometry, provided the flow is characterised by low *Re,* the two fluids will continue to flow next to each other as if they are still confined by channel walls as can be seen in Figure 5B. In the absence of any applied forces, the only transport between laminae is due to diffusion as will be described in chapter 2.3.3.

Another feature of laminar flow, which will become important later when we look at the theory of DLD, is the velocity profile. Examples of fluid flow in three microfluidic channels are shown in Figure 6, calculated using Comsol™ to solve the linear Stokes equation. Because of the viscous drag from the walls of the channel the flow velocity is zero here, a condition known as the no-slip boundary condition[7]. In the centre of the channel, furthest from the wall, the velocity has its maximum. This effect is analogous to what happens when you push out the middle of a deck of cards with your finger while holding the top and bottom cards still. The fluid laminae slide across each other in a manner similar to the cards. Between two parallel walls the velocity field forms a parabola across the width of the gap. In a circular channel the velocity profile is also parabolic along any line through the centre as can be seen in Figure 6, this is known as Poiseuille flow. In the square channel the flow profiles across the width of the channel, $V_x(y)$, and across the breadth, $V_x(z)$, are also equal and parabolic. For the rectangular channel the situation is somewhat different. In the y direction, the smallest dimension of the channel, the flow profile $V_x(y)$ is parabolic but across the depth of the channel the profile, $V_x(z)$, is parabolic near the wall but flattens out in the centre. We will see in chapter 3.3 that this dependence of the flow profile on the shape of the channel is very important for the behaviour of particles in DLD devices.

2.2.2 Hydraulic resistance

Figure 6 highlights another effect that channel geometry has on the fluid flow. In each of the three channels in Figure 6 the cross sectional area, channel length, and pressure difference across the channel are the same; the resulting flow rate through the channels however are not the same. The volume flow rates are 9.9, 8.7 and 5.2 nl $\cdot$ s^{-1} for the circular, square and rectangular channels respectively. This is because fluid resistance is a function of channel geometry. Because the flow profiles in a given geometry retain the same shape regardless of pressure, provided

[7] Some experimental evidence exists that indicates that fluids may have non-zero velocities relative to channel walls in microfluidic devices [107. Huang, P. and K.S. Breuer, *Direct measurement of slip length in electrolyte solutions.* Physics of Fluids, 2007. **19**(2).] This is measured in slip-length, which is the distance inside the wall that the velocity would reach zero if the velocity gradient where equal to that at the wall (~50nm in reference 105). While a non-zero slip-length would affect the critical separation size in DLD devices this effect would be very small and also equal for all particles therefore not changing the relative behaviour of particles or the devices' ability to separate them. We therefore neglect wall slip in the following discussions.

Re is less than 1, and because pressures can be applied to achieve the desired flow rates, resistances in the separation structures of a DLD device are not critical design parameters. However, devices rely on rectangular input and output channels that require the careful balancing of flow rates in order to inject and collect streams of particles. The flow rate ϕ due to a pressure difference ΔP across a channel with the hydraulic resistance R_h is given by:

$$\phi = \frac{\Delta P}{R_h} \tag{10}$$

There is no known analytical solution to the hydraulic resistance in a rectangular channel but the following Fourier sum representing the solution and the subsequent simplification have been derived by Bruus [101]. Here w is the width of the channel, h is the height and $w>h$. L is the channel length and η is the viscosity of the fluid:

$$R_h = \left(\frac{h^3 w}{12\eta L} \left[1 - \sum_{n,odd}^{\infty} \frac{1}{n^5} \frac{192}{\pi^5} \frac{h}{w} \tan\left(n\pi \frac{w}{2h} \right) \right] \right)^{-1} \tag{11}$$

In many cases the following approximation is good enough:

$$R_h = \left(\frac{h^3 w}{12\eta L} \left[1 - 0.63 \frac{h}{w} \right] \right)^{-1} \tag{12}$$

For example if $w=2h$ then the error is 0.2% and in the worst case, with $w=h$ the error is 13%. Because it is extremely difficult to fabricate perfectly rectangular channels, sidewalls are often not perfectly parallel, corners are rounded to varying degrees and surfaces can have varying amounts of roughness. Also the properties of the fluid might not be exactly known. Taken together these factors mean that use of the exact solution is often not justified.

2.3 Particles in fluids

2.3.1 Viscous drag contra applied forces

A rigid sphere of radius a moving with velocity $\mathbf{v}$[8] relative to an incompressible fluid with viscosity η, as depicted in Figure 7, will at low *Re* experience a viscous drag force given by Eq. 13.

$$\mathbf{F}_{drag} = -6\pi\eta r\mathbf{v} \tag{13}$$

This drag force dominates the behaviour of particles at low Reynolds numbers. Consider for example a neutrally buoyant sphere of 1 μm radius moving under the influence of a constant force at 100 μm s^{-1} in water. When the force is removed the particle will stop within ~0.3 ångström[9]. Due to the dependence of the drag force on the velocity, the particle nears this distance in an exponential manner, which would take an infinitely long time. In reality though the motion becomes dominated by collisions with water molecules and within microseconds the particle will, except for this Brownian motion, come to a standstill. What this means is that, although inertial effects have been used for separation as described in chapter 1.6, in most cases the inertia of the particle can be neglected. There are two important conclusions to draw from this: Firstly in the absence of forces other than viscous drag, particles move at the same velocity as the suspending fluid medium and they will at all times follow streamlines. Secondly, any additional force applied to a particle will cause the particle to accelerate, or to cross

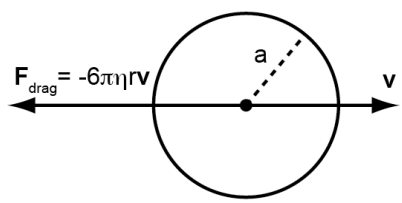

Figure 7 Viscous drag on a spherical particle.

[8] The particle velocity **v** is relative to the velocity of the media at distance d from the centre of the particle where $d \to \infty$. The no slip boundary condition is given by **v**=0 for $d=a$.

[9] $$\Delta x = \frac{v_0 m}{6\pi\eta r}\left(1 - e^{-t\frac{6\pi\eta r}{m}}\right)$$

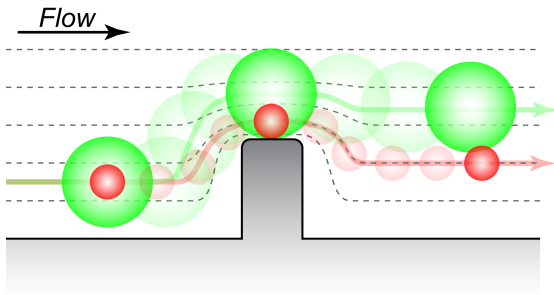

Figure 8 Particles can be forced across lamina by interactions with structures in microfluidics devices. The green and red particles are following the same streamline before they come to the obstacle. Both particles are hindered by the surface of the obstacle and forced to cross streamlines. The hydrodynamic centre of mass of the larger particle is kept further from the surface of the obstacle and the particles leave following different streamlines. Neglecting diffusion, which also moves particles across streamlines, the fate of these different streamlines will now decide the trajectories of the particles.

streamlines, but will quickly be balanced by viscous drag. A constant force will therefore cause a particle to move with constant velocity.

Fluidics-based particle separation techniques are almost exclusively based on the application of selective forces, dependent on specific particle characteristics, that force particles into streamlines that a) move with differing velocities, leading to separation in time, or b) leave a device at differing positions leading to separation in space, as described in chapter 1.5.1.

The forces that cause particles to cross streamlines are numerous and give rise to the wealth of techniques mentioned in the introduction. These forces can be divided into stochastic and deterministic forces. Diffusion is a stochastic process, present to varying degrees in all microfluidics systems. The other forces are deterministic in nature. These are externally applied body forces such as gravity, electrophoretic and dielectrophoretic forces, magnetic forces, acoustic forces and steric forces.

Note about effects that we neglect in the current discussion: *The polystyrene particles used in our measurements have a density marginally greater than that of water (1050kg m^{-3} as opposed to 1000kg m^{-3} for water), giving them negative buoyancy. This means that due to the influence of gravity they will sink over time. While particles may sediment in reservoirs, where they can spend several hours due to the large volumes and low flow rates, most are too small to sediment on the timescales relevant to transit through a typical microfluidic device*[10]*. We also*

[10] J. P. Beech and J. O. Tegenfeldt, *Gravitationally driven deterministic lateral displacement devices*, The 13th International Conference on Miniaturized Systems for Chemistry and Life Sciences, Jeju, Korea, 2009, 779-781.

assume that all effects of DLD discussed in the present work are independent of the position of particles normal to the device plane and we therefore neglect sedimentation. Electrophoresis is due to the action of an electric field on the fixed net charge of a particle. In paper II AC fields are used in which the electric field and thus the electrophoretic force average to zero. Like sedimentation, electrophoresis will not be discussed here.

2.3.2 Steric hindrance

Non-clogging filters use steric forces from channel walls to force particles to cross streamlines while simultaneously allowing them to flow through the device. It is this effect that underlies separation in DLD devices and while the exact way this is achieved will be covered in the following chapters it is worth repeating the basic idea here. Figure 8 shows two different sized particles with their hydrodynamic centres of mass following the same streamline. As the fluid flows past the obstacle the cross sectional area of the flow is decreased, the flow accelerates and the streamlines move closer together. The streamline that the particles are following moves closer to the obstacle than either particle is able to follow and they are both forced to cross streamlines. Neglecting the effect of the particles on the flow, the streamline they are pushed into is the streamline that is one particle radius from the surface of the obstacle at the point at which the particle starts to move radially away from the surface of the obstacle. As the particles move away from the obstacle they follow different streamlines. The fate of the particles will now be decided by what happens to the streamlines. Deterministic lateral displacement, pinched flow fractionation and hydrodynamic filtration all use this effect in different configurations to achieve separation.

2.3.3 Diffusion

For low-Reynolds number flows, mixing is driven by diffusion only. The mean square distance that a particle diffuses in time t is given by:

$$\left\langle r^2 \right\rangle = 2k \cdot Dt \tag{14}$$

where k is the dimensionality of the problem and is equal to 1, 2 and 3 for 1, 2 and 3 dimensional diffusion respectively. D is the diffusion coefficient and is given by the Stokes-Einstein relation.

$$D = \frac{k_B T}{6\pi\eta a} \tag{15}$$

Here k_B is Boltzmann's constant[11], T the temperature and a the particle radius. Diffusion is omnipresent in microfluidic devices at experimental time scales. Although diffusion has been used to separate particles [79] in the context of DLD it both modifies the separation behaviour of devices and reduces the resolution [108, 109] and must always be considered, see chapter 3.5.3 for more details. The Péclet number expresses the relative importance of convection to diffusion. With L and V a characteristic length and velocity and D the diffusion coefficient:

$$\frac{\text{diffusion time}}{\text{convection time}} = \frac{\frac{L^2}{D}}{\frac{L}{V}} = \frac{LV}{D} \equiv \text{Pe} \tag{16}$$

Figure 9 shows particles of 1µm and 10nm respectively flowing at v=30 µm $^{-1}$ in a 10 µm wide lamina. The particles have very different diffusion constants and the difference in the effect diffusion has on the two streams of particles is

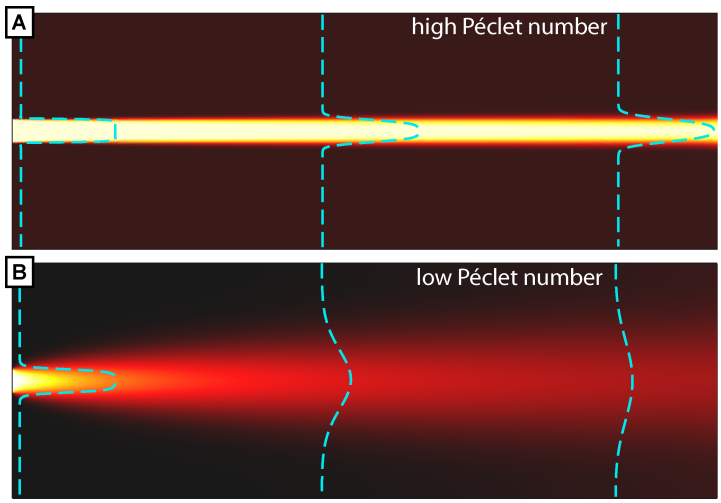

***F**igure 9 Simulation (COMSOL Multiphysics® 3.4 (COMSOL AB, Stockholm, Sweden)) of a 10 µm wide stream of particles entering from the left into a channel 100 µm by 300 µm with an average flow velocity of 30 µm s^{-1}. (A) Particles with a radius of 1 µm are characterized by Pe = 40 000. The particle stream is only very slightly broadened by diffusion. (B) Particles with a radius of 10 nm are instead characterized by Pe = 400. During the time taken for the particles to traverse the channel the stream is considerably broadened. The concentration profile in both cases is shown in blue.*

[11] At 25°C $k_B T \approx 4 \cdot 10^{-21}$ J.

pronounced. **F**igure 9A shows how at high flow rates and therefore high *Pe* the effects of diffusion are relatively small over the length of the channel and the stream remains well defined. The stream of 10nm particles however, characterised by a much smaller *Pe*, becomes greatly broadened as can be seen in **F**igure 9B. In DLD devices where streams of particles are created it is essential that Péclet numbers are high enough that the streams do not become significantly blurred due to diffusion.

'Deterministic' refers to the fact that the method, unlike many other separation techniques such as size exclusion chromatography for example or the microfluidic H-filter developed by Yager *et al* [79], does not rely on diffusion to achieve separation. As explained by Giddings [16] when diffusion is used there is always a trade-off between allowing enough time for diffusion to occur and minimizing the detrimental effects of zone broadening due to too much diffusion. DLD does not rely on diffusion and so separations can be run arbitrarily fast ($Pe \to \infty$), provided the criteria for low *Re* numbers are met. The importance of diffusion in DLD devices will be dealt with more specifically in chapter 3.5.3.

2.3.4 Dielectrophoresis

DEP is the movement of polarisable particles due to the forces they experience in a non-uniform electric field and was explored in the 1960s by Pohl [110-113]. The dielectrophoretic energy, W_{DEP}, and force, $\boldsymbol{F}_{\mathrm{DEP}}$, on a spherical particle are given by [114]:

$$W_{DEP}(x,y,z) = -2\pi\varepsilon_m r^3 \,\mathrm{Re}\left(f_{CM}\right)\left|E_{RMS}(x,y,z)^2\right| \tag{17}$$

$$\mathbf{F}_{DEP} = -\nabla W_{DEP}(x,y,z) = 2\pi\varepsilon_m r^3 \,\mathrm{Re}\left(f_{CM}\right)\nabla\left|E_{RMS}(x,y,z)^2\right| \tag{18}$$

where f_{CM} is the Clausius-Mossotti factor:

$$f_{CM} = \frac{\varepsilon_p^* - \varepsilon_m^*}{\varepsilon_p^* + 2\varepsilon_m^*}, \tag{19}$$

$$\varepsilon^* = \varepsilon - j\frac{\sigma}{\omega}. \tag{20}$$

In Eqs. 17 and 18 ε_{m} and ε_{p} are the permittivities of the medium and the particle respectively, r the particle radius and $\boldsymbol{E}_{RMS}$ the root-mean-square value of the electric field. ε_{m}* and ε_{p}* are the complex permittivities as defined by Eqs. 19 and 20 where ε is the permittivity and σ the conductivity of the particle/medium and ω is the angular frequency of the applied field.

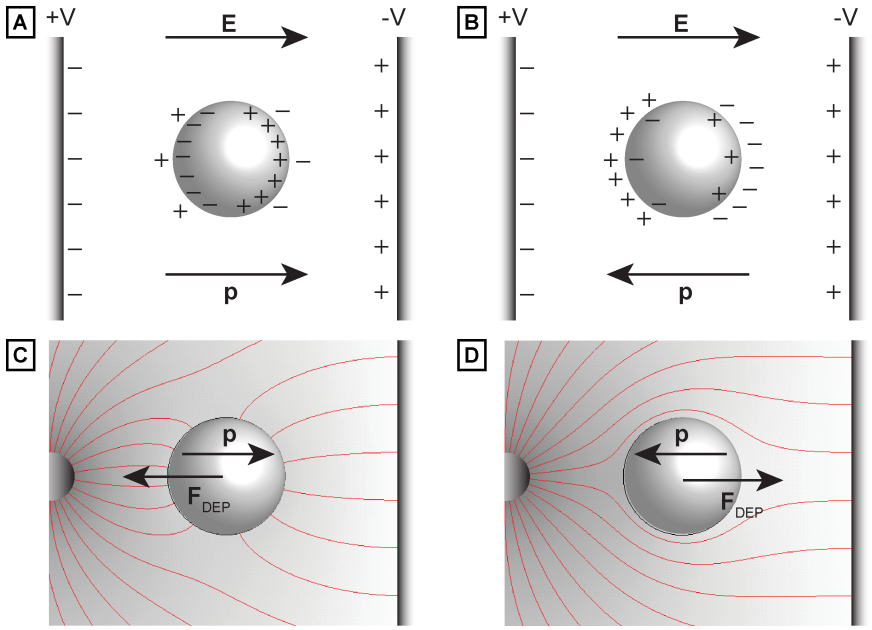

*Figure 10 Particles become polarised differently depending on the relationship between their polarisability and that of the suspending medium. (a) If a particle is more polarisable than the suspending fluid then more charges build up on the inside of the particle/fluid medium interface and a net dipole, **P**, is induced that is parallel with the electric field. (b) If the particle is less polarisable than the suspending medium less charge builds up on the inside of the boundary and **P** points in the opposite direction to the field. (c) If a particle more polarisable than the suspending medium is placed in an electric field gradient it will experience a force in the direction of the gradient. This is positive DEP. (d) In the opposite case the particle experiences negative DEP.*

We can consider what happens to f_{CM} in the limits where either ε_m or ε_p go to zero. If the particles are more polarisable than the surrounding medium (see Figure 10A), we let $\varepsilon_m \rightarrow 0$ and we get $f_{CM}=1$. If the opposite is true (see Figure 10B), then $\varepsilon_p \rightarrow 0$ and we get $f_{CM}=-0.5$ so the range of $f_{CM}=[-0.5,1]$ (see Figure 11*)*. It is the real part of f_{CM} that decides in which direction the DEP force will act. In general, if we have $\mathrm{Re}(f_{CM})>0$ then the potential energy of the particle will have a minimum where the electric field is highest. These particles will be pushed away from regions with a low electric field and towards regions with a high electric field. This effect is known as positive DEP (pDEP) (see Figure 10C). If on the other hand $\mathrm{Re}(f_{CM})<0$ then the potential energy will be largest where the electric field has a maximum resulting in a reversal of the force (see Figure 10D). Force towards areas of low electric field is known as negative DEP (nDEP). Choosing the frequency such that the sign of f_{CM} is different for the particles of interest makes separations using DEP possible. For example between 1.1 and $1.3 \cdot 10^6$ Hz the particles in Figure 11 with $\sigma_p=0.01$ (solid line) have a negative f_{CM} whereas

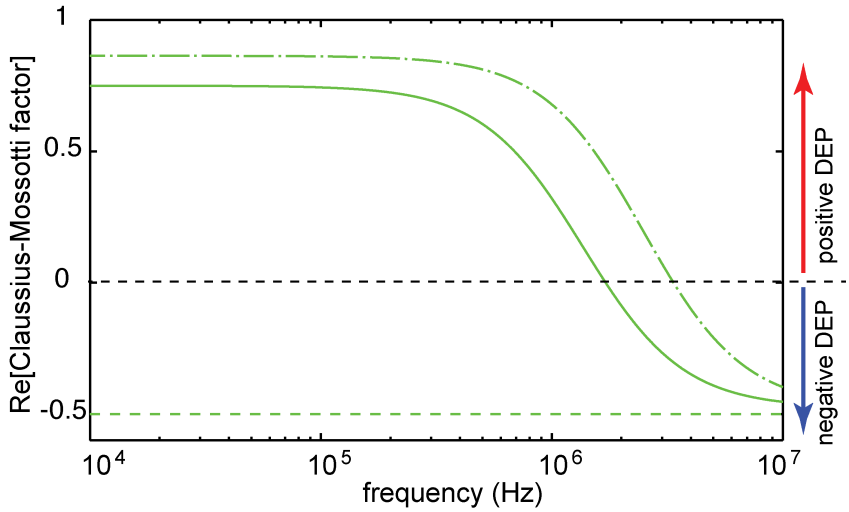

Figure 11 The electric dispersion (f_{CM} as a function of frequency) for a 100nm colloidal particle. The solid line shows ε_p =2.55·ε_0, ε_m =78·ε_0, σ_p = 0.01 S·m^{-1}, σ_m = 0.001 S·m^{-1}, (ε_0 = 8.85·10^{-12}). The dash-dot line is the same but with σ_p = 0.01 S·m^{-1}. The dashed line is for a medium with high conductivity, σ_m = 0.18 S·m^{-1} (like the TBE buffer used in Paper II).

those with σ_p=0.02 (dash-dot line) have a positive f_{CM} which would result in DEP forces in opposite directions.

Electric field gradients can be generated using the geometries of electrodes or by modifying the field using insulators (see Figure 13). It is the insulating properties of PDMS, in which we fabricate our separation devices, which we use to achieve DEP and modify the separation behaviour of particles.

2.3.5 Particle rotation and deformation

The shape and deformability of cells can be important for separation and analysis as discussed in chapter 1. In Papers III and IV we develop DLD devices that are sensitive to shape and deformability and use this sensitivity to separate cells. The behaviour of non-spherical and deformable particles in simple shear flows is reasonably well known. However, the shear flows in DLD devices cannot be considered simple and the situation is further complicated by the high degree of interaction between particles and the posts that make up the separation arrays as described in chapter 3. We will return to the specifics of particle shape and deformability in DLD devices in chapter 5, but first we will look briefly at what is known about the importance of shape and deformability on particle behaviour in simple shear flows with a focus on red blood cells which are important for the work in both Papers III and IV.

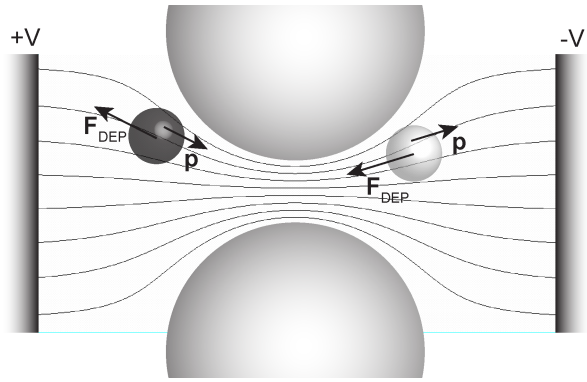

Figure 13 Electric field gradients can be created in microfluidic channels using insulating constrictions that squeeze field lines together. The dark particle is experiencing negative DEP and the light particle is experiencing positive DEP.

In the absence of interactions with channel surfaces, at low Reynolds numbers, the hydrodynamic centre of mass of a particle moving in a velocity gradient will move with the average velocity of the displaced fluid. The difference in drag forces exerted on the two sides of the particle (that in the slower flow and that in the faster flow) cause different particle motions depending on the deformability of the particle, see Figure 12. Jeffery described the motion of rigid ellipsoids in simple shear flow at zero Reynolds number as rotations about the vorticity axis[12]

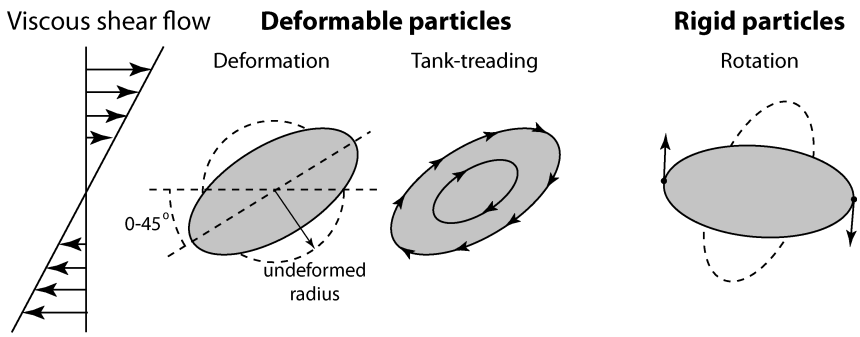

Figure 12 The behaviour of particles in simple shear flows. Rigid particles rotate in Jeffery orbits and deformable particles become aligned depending on the balance of interfacial tension and viscosity. When aligned rotational flow is set up inside the particle, an effect known as tank-treading.

[12] The vorticity axis is perpendicular to the flow gradient. For example for a 2D flow the vorticity axis would be perpendicular to the plane of the flow.

along closed orbits (Jeffery orbits) that depend on the initial conditions [115]. A deformable particle on the other hand, such as a spherical droplet, will deform into an equilibrium shape, an ellipsoid, and become aligned at an angle between 0° and 45° to the flow direction depending on the balance of interfacial tension and internal viscosity; 45° when surface tension dominates over the internal viscosity of the drop and 0° when the surface tension is negligible [116]. Inside the deformed droplet the fluid rotates about the centre of the drop in a motion known as tank-treading.

Goldsmith and Marlow [116] report that RBCs transition from rigid particle behaviour (rotation) at shear stresses <<0.1 Pa to deformable particle behaviour (tank-treading and alignment) as shear stresses increase to >0.1 Pa. They also saw an increase in the diameter of the RBC of 1.05 μm due to deformation of the cell as the shear stress was increased from 0 to 0.4 Pa.

Red blood cells flowing through capillaries are also known to transition from their normal discocyte shape to a parachute shape as flow rates increase, a transition that decreases the fluid resistance of blood in the microcirculation [117-119].

As mentioned above, while the deformation and orientation of cells has a large effect on their behaviour in DLD devices it is important to stress that both orientation and deformation are affected to a large degree by interactions with posts and other surfaces within a device. There has to our knowledge been little theoretical work done in this direction. However the work by for example by Noguchi and Gompper [119] would be an excellent starting point in any theoretical modelling of the red blood cells in DLD devices.

2.3.6 Note on time-reversible flows

At low Reynolds numbers fluid flow is time reversible. This means that if the direction of the pressure gradient is reversed, the velocities reverse but it should not be possible to distinguish between the two flow directions based on a snapshot of the flow pattern alone, as the pattern would be identical in both cases. However in order to visualize a flow we need to be able to see individual particles. As **F**igure 9 shows, with particles present in the flow it is often easy to see in which direction the flow is moving. This is because the behaviour of individual particles is not time reversible. In this case it is diffusion, a random process that is responsible for the non-reversibility and we can see that the flow is from left to right. Steric interactions or collisions between particles and channel walls are also non-reversible as discussed by Loutherback *et al* [120] and by Balvin *et al* [121]. In general, at low Reynolds numbers, viscous drag forces particles to follow streamlines in a reversible way whereas diffusion and steric interactions are non-reversible.

3 Deterministic Lateral Displacement

3.1 DLD in a nutshell

DLD devices use arrays of micrometre-sized posts to divide a flow of fluid into many narrow, parallel streams. As suspended particles flow through these arrays, interactions with the posts and the patterned fluid flow lead to two dominant outcomes. If particles are small enough they follow the average fluid flow direction, defined by the sidewalls, and if they are large enough they move at an angle to the flow decided by the geometry of the array. The transition between these two modes is sharp and for hard spherical particles occurs at a critical

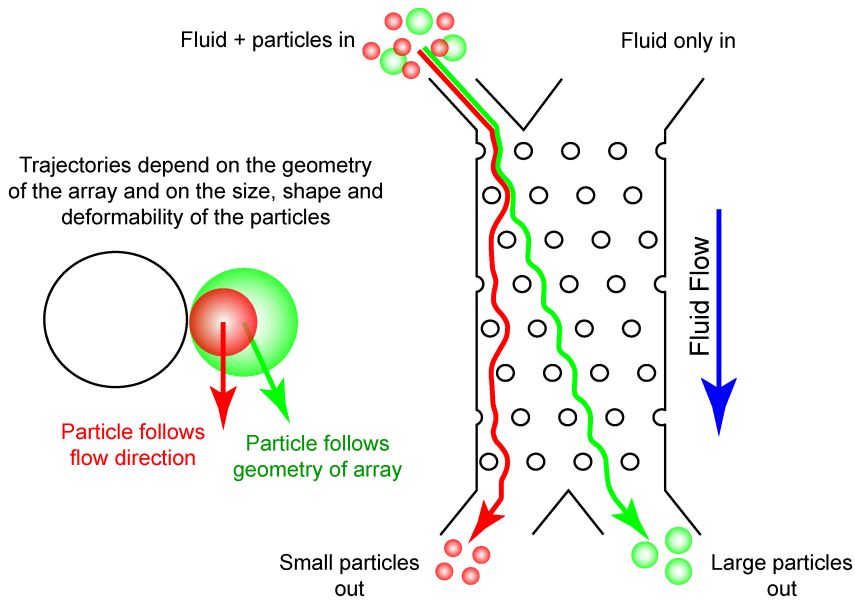

Figure 14 Separation in a DLD device depends on whether particles are able to follow the fluid flow or whether they are forced to follow a direction determined by the geometry of the array.

particle radius, R_c, which is always smaller than the gaps between the posts. Because particles follow different trajectories the separated fractions can be continuously collected at the end of the device. The trajectory a particle follows also gives information about its effective size. In this chapter we will look in detail at how the geometry of an array determines the critical size and how the properties of the particles determine whether they are smaller or larger than this critical size which in turn determines which trajectories they will take.

3.2 DLD - A more detailed description

The functional part of a DLD device consists of one or several row-shifted arrays of posts, which we begin be describing in chapter 3.2.1. It is the flow of fluid through these arrays and the interaction of particles with the resulting fluid flow patterns that give rise to DLD and so an understanding of these flow patterns is essential. We will first consider the nature of flow through arrays of posts in chapter 3.2.2 and then introduce particles to these flows in chapter 3.2.3. After looking closer at some of the factors that can influence the behaviour of particles in DLD devices in chapter 3.3 we finish the chapter with a review of the applications of DLD to date.

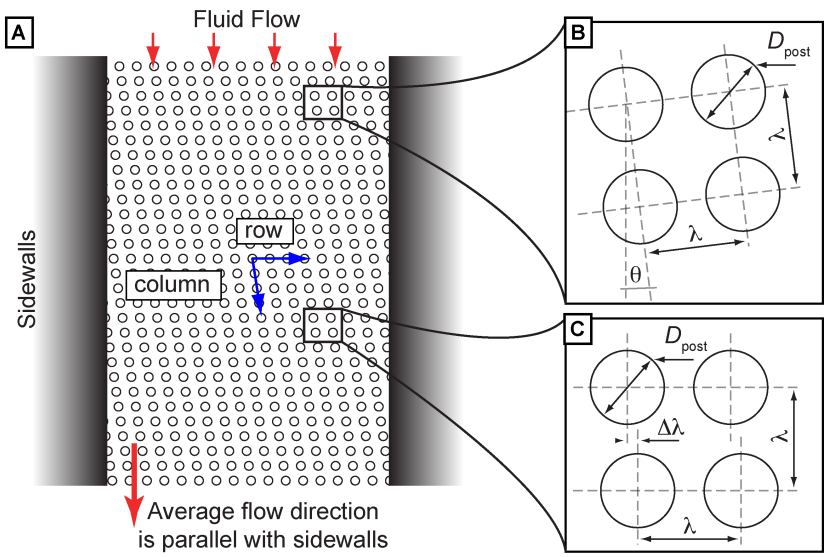

Figure 15 Post array geometries. (A) The sidewalls in a device define an average flow direction. Each row is shifted laterally with respect to the previous row. There are two ways to achieve this. (B) A rotated square array as used in Paper I (C) A rhombic array as used in Papers II, III and IV.

3.2.1 Row-shifted post arrays

The post arrays used in DLD devices are periodic. In each of our devices we keep the centre-to-centre, λ, spacing of the posts in the rows (perpendicular with the walls) and columns (almost parallel with the walls) equal. If the average flow direction is defined by sidewalls (see Figure 15) then "Row-shift" refers to the fact that each successive row along the flow direction is shifted by a distance $\Delta\lambda$ perpendicular to the flow direction. If in row number N+1 the posts have the same lateral positions as in row 1 then we say that the array has a period N[13]. There are two ways to achieve this shift. Tilted square arrays, shown in Figure 15B, have rows and column perpendicular to one another but rotated relative to the sidewalls and rhombic arrays as shown in Figure 15C in which rows are perpendicular to the side walls but columns are tilted at an angle relative to the sidewalls. In Paper I the arrays used were of the rotated square array type whereas those presented in Papers II, III and IV where of the rhombic type. While there may be small differences in these two types of row-shifted arrays, for example with regards to fluid resistance along different directions in the array as discussed by Inglis [14], rhombic arrays are simpler to draw in CAD software and are therefore the type we predominantly use. We therefore confine discussions here to the case of rhombic arrays. For rotated square arrays $\Delta\lambda$ can be calculated as $\lambda\tan(\theta)=\lambda/N$ and the arguments for rhombic arrays are assumed to hold true.

3.2.2 Flow through row-shifted post arrays

The total fluid volume flux between two posts in row 1 (see Figure 16 for an example of an array with N=5) can be defined as Φ_{gap}. Due to the periodicity of the array and the laminarity of the flow, Φ_{gap} can be divided into N laminae, which we will call Φ_i where i=1 to N, where the boundary between each laminae is defined by bifurcations around posts. Due to symmetry each of these laminae carries an equal volume flux of Φ_{gap}/N and follows a cyclic path through the array as depicted in Figure 16a. The positions at which the laminae pass between the posts are, again due to the laminarity of the flow, well defined and can be numbered P_i also for i=1 to N. As we will see in the next section it is the width of Φ_1 at position P_1 that determines the behaviour of particles and so we need to determine this width.

[13] Arrays with non-integer row-shifts are studied in Paper III of the related publications but are outside the scope of this thesis. As is discussed in this paper non-integer row-shifts give rise to multiple sorting modes. Using sedimentation as a driving force in order to achieve arbitrary row-shifts we have been able to experimentally demonstrate the existence of such modes. (J. P. Beech and J. O. Tegenfeldt, *Gravitationally driven deterministic lateral displacement devices*, The 13th International Conference on Miniaturized Systems for Chemistry and Life Sciences, Jeju, Korea, 2009, 779-781.)

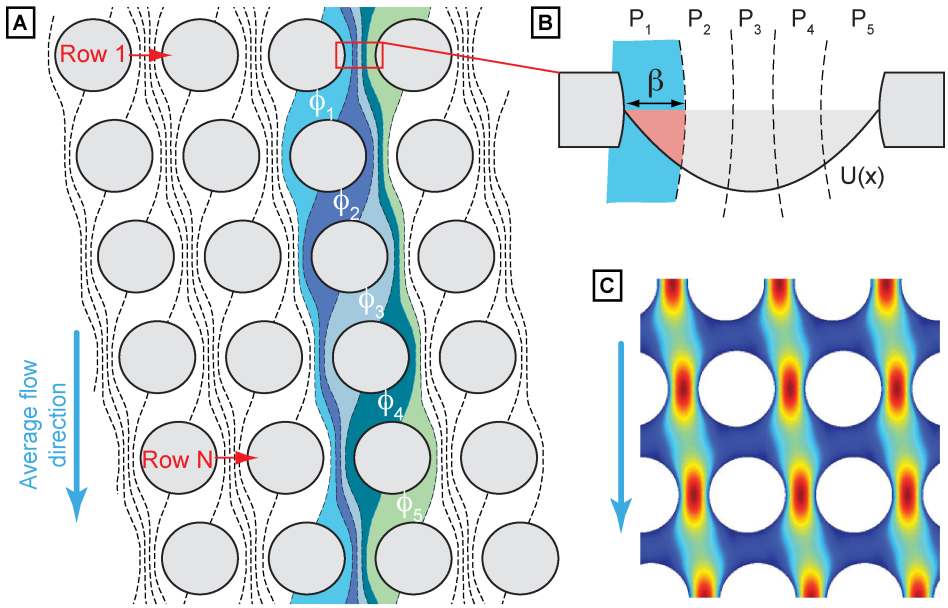

Figure 16 Fluid flow through a row-shifted array with a period, N=*5. (A) The flow becomes bifurcated by the posts and is divided into a series of laminae. Each of the laminae, labeled* $\phi_{1,2,\ldots,5}$*, moves through the array passing between the posts at 5 well-defined positions, which we number* P_1 *to* P_5*. A lamina that passes between two posts in a specific row at* P_N *will in the subsequent row occupy* P_{N-1}*. This is repeated until the lamina is back at* P_1 *after one period,* N*. (B) Positions* P_1 *to* P_5 *that the laminae occupy as they move through the array. Because of the flow profile the laminae have widths that depend on which of the positions they occupy. (C) Finite-element simulation of flow through a post array. The colour map shows the velocity profile with red fast and dark blue slow.*

Figure 16B and c show the flow profile between posts that we assume, for the time being, to be parabolic. Because the fluid flux in a lamina is conserved ($\Phi_i=\Phi_0 \,\forall\, i$), its width depends on its velocity and therefore its position, P_1, P_2, $P_3, \ldots, P_N$, in the flow profile. Due to the stick boundary conditions at the surface of the post the fluid velocity is lowest here and the width of the lamina is therefore widest at P_1 and P_N. This width, which we will refer to as β, can be calculated by solving the following integral:

$$\Phi_1 = \frac{1}{N}\,\Phi_{gap}$$

$$\int_0^{\beta} u(x)dx = \frac{1}{N}\int_0^{d} u(x)dx \qquad (18)$$

Assuming a parabolic flow profile:

$$u(x) = \left[\frac{d^2}{4} - \left(x - \frac{d}{2}\right)^2\right], \tag{19}$$

where d is the distance between posts and is equal to λ-D_{post}. The solution to the integral is:

$$\beta = \frac{d}{2}\left[1 + 2w + \frac{1}{2w}\right], \tag{20}$$

where

$$w^3 = \frac{1}{8} - \frac{N^{-1}}{4} \pm \sqrt{\frac{N^{-1}}{16}\left(N^{-1} - 1\right)}. \tag{21}$$

The correct root of w^3 is

$$w = \left[\frac{1}{8} - \frac{N^{-1}}{4} \pm \sqrt{\frac{N^{-1}}{16}\left(N^{-1} - 1\right)}\right]^{(1/3)} \left(-\frac{1}{2} - i\frac{\sqrt{3}}{2}\right). \tag{22}$$

By assuming that $1/N \approx \beta/d$ we arrive at the following approximation which is easier to handle and has a small error for commonly used periods, $N>10$:

$$\frac{1}{N} = \frac{\int_0^{\beta} \frac{d^2}{4} - \left(x - \frac{d}{2}\right)^2 dx}{\int_0^{d} \frac{d^2}{4} - \left(x - \frac{d}{2}\right)^2 dx} = \frac{\left[\frac{d\beta^2}{2} - \frac{\beta^3}{3}\right]}{\left[\frac{d^3}{2} - \frac{d^3}{3}\right]} = 3\left(\frac{\beta}{d}\right)^2 - 2\left(\frac{\beta}{d}\right)^3 =$$

$$= \left(\frac{\beta}{d}\right)^2\left[3 - 2\frac{\beta}{d}\right] \approx \left(\frac{\beta}{d}\right)^2\left[3 - 2\frac{1}{N}\right] \approx 3\left(\frac{\beta}{d}\right)^2 \Leftrightarrow$$

$$\Leftrightarrow \frac{N}{3} \approx \left(\frac{\beta N}{d}\right)^2 \Leftrightarrow \beta \approx \sqrt{\frac{N}{3}} \cdot \frac{d}{N} \tag{23}$$

This equation turns out to be quite a good approximation, despite the fact that particles strongly perturb the flow as it passes the posts. It was used in Papers I and II.

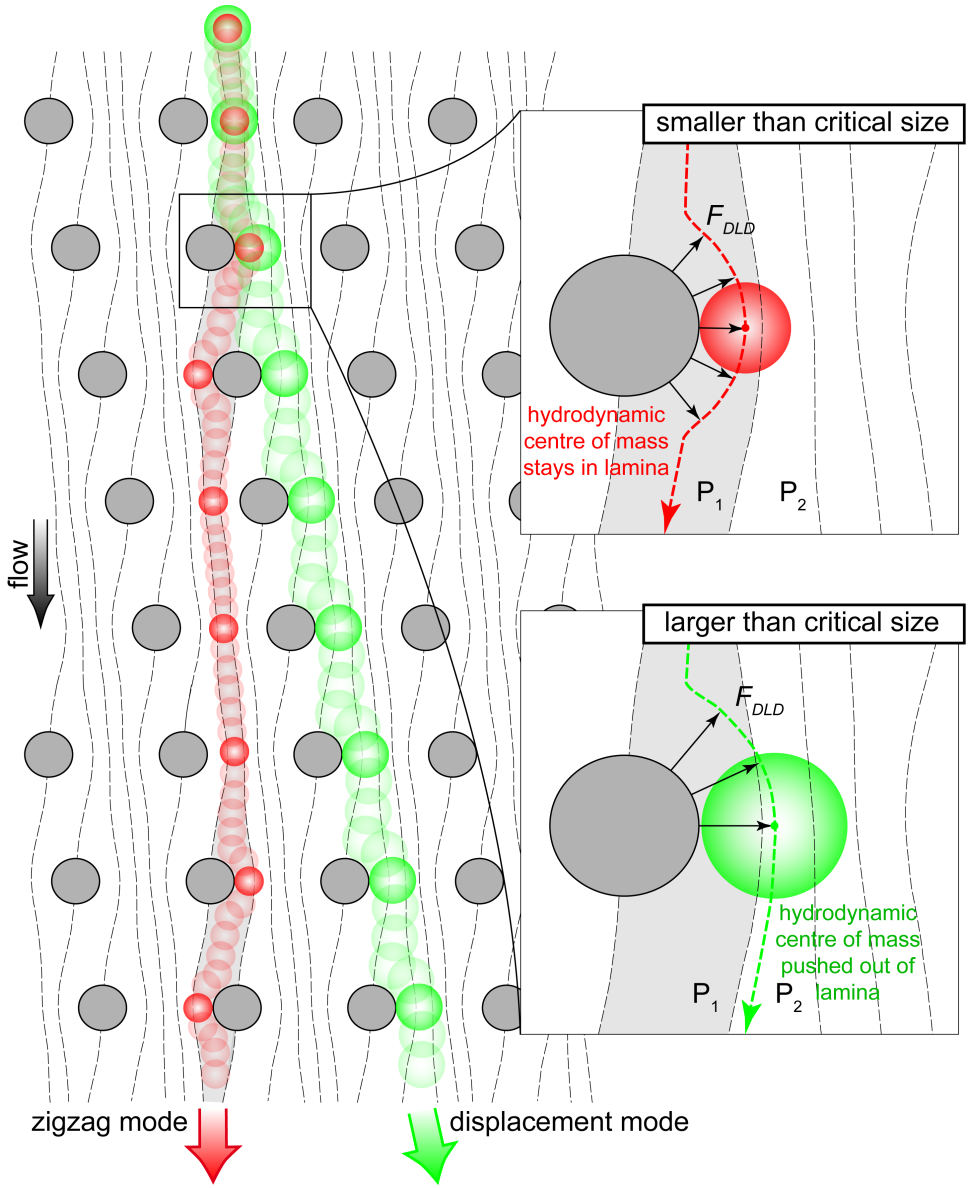

Figure 17 Particles moving through an array with N=5. The hydrodynamic centre of mass of the red particle fits into the lamina at the decision point and follows the flow direction (zigzag mode). The hydrodynamic centre of mass of the larger green particle is forced out of the lamina at the decision point due to interaction with the post and becomes more influenced by the trajectories of the neigbouring laminae, moving on the opposite side of the subsequent post. This is repeated at every row and the particle is forced to follow the direction of the columns in the array (displacement mode).

3.2.3 DLD – Particles and the critical radius

Now that we have described the flow of fluid through a row-shifted array of posts we can consider what will happen to particles suspended in that fluid. Due to the viscous drag force described in chapter 2.3.1, particles will follow streamlines wherever possible remaining within a lamina but they will also, as was explained in chapter 2.3.2, interact sterically with posts and will, depending primarily on their size, be forced to change lamina. When particles change lamina at each row they follow trajectories that are defined by the array rather than by the flow direction. The transition between following the flow direction and following a direction defined by the array geometry occurs at a well-defined particle size that we call the critical diameter.

Figure 17 shows fluid and suspended particles in an array with a period of 5, similar to that in Figure 16 but with smaller posts for clarity. An example lamina containing one N^{th} of the total flow between posts is shown in grey. Particles whose hydrodynamic centre of mass[14] fit into a lamina at P_1 will remain within the lamina and will therefore move through the array in the average flow direction whereas larger particles are displaced by the post into P_2[15]. This displacement occurs at every row causing these larger particles to follow the columns, which are tilted at an angle, $\theta = \arctan(\Delta\lambda/\lambda)$, relative to the fluid flow. The terminology we use for these two modes reflects the character of their trajectories and is the same as that used by Huang *et al.* [6]: particles that follow the flow move in the *zigzag mode*; deflected particles move in the *displacement mode* (see Figure 17).

In the previous section we derived the width of the lamina at P_1, β, as a function of the array parameters, d and N. We can now define the critical size in a DLD device as $D_{c0}=2\beta$[16]. *(The zero here is to denote that no other forces such as DEP forces, or changes in either the array geometry or the particles are being considered. These will be added later)*. An analytical expression for an approximation of the critical size is:

$$D_{c0} \approx 2 \cdot \beta \approx 2 \cdot \sqrt{\frac{N}{3}} \cdot \frac{d}{N} = \alpha \cdot \frac{d}{N} \tag{24}$$

Here $d = \lambda - D_{post}$ is the inter-post distance and $N = \lambda/\Delta\lambda$, is the period of the array as defined in Figure 15. The unit-less parameter α can be used to compensate for any effects that we have missed in the derivation of D_{c0}; it contains

[14] This is the point in the particle that never crosses lamina (without the infuence of applied forces) and is for a hard sphere at low *Re* the same as the centre of mass

[15] Displacement into P_i for $i > 2$ will have the same result.

[16] In Papers I-III we use D_c and in Paper IV we have used R_c. In this thesis I use both D_c and R_c. In all cases $D_c = 2 \cdot R_c$.

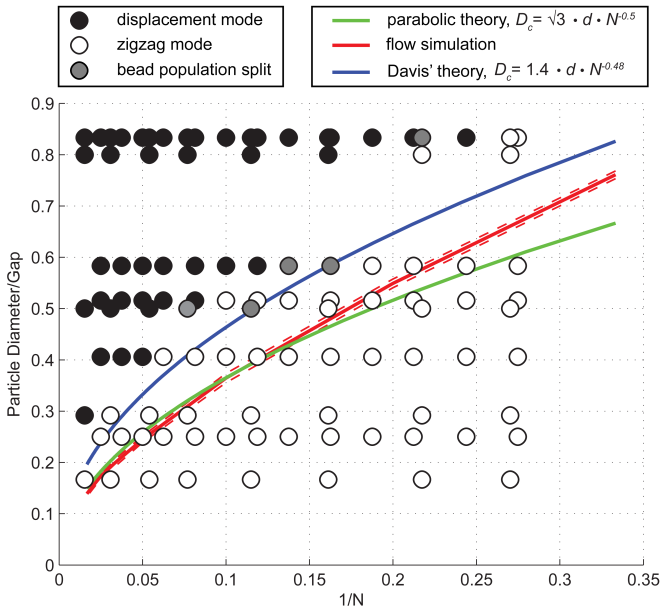

Figure 18 A collection of experimental results. The ratio of the particle diameter to the gap between posts is plotted as a function of N^{-1}. Black shows particles in displacemnt mode, white in zigzag mode and grey signifies that the bead population was split (beads in both modes). Two different theories, green =parabolic and blue = Davis and also simulations of theoretical diameter based on the width of 2/N of flow (2·β) with no particle present = red are shown.

for example the effects of the flow profile on D_{c0} and the various effects that array geometry has on the shape of the profile. For plug flow, which has a linear profile with slip at the walls, α would be equal to 1 and for parabolic flow $\sqrt{N}/3$.

The devices used in papers I and II were designed using equation 24. The value of α can be measured using the stretching method described in Paper I and used to refine the subsequent generation of devices.

Another way to determine how the critical size depends on array parameters is to do so empirically. Figure 18 shows a type of plot developed by Davis [122] that can be used to do this. In this case the plot shows experimental data collected by Stefan Holm and myself. The ratio of the particle diameter to the gap is plotted against N^{-1}[17] for many different gap sizes, particle sizes and array periods and the mode in which the particles move is indicated by the type of data point. In this case a black dot indicates that the particles are moving in the displacement mode and a white dot that they are moving in the zigzag mode. The polystyrene

[17] The inverse of N is used in this case for easy comparison with the results of Davis and Inglis who use the shift fraction $\varepsilon = 1/N$ rather than N in their equations.

microspheres used in these calibration experiments are not monodisperse. They have a distribution in their diameters that can be approximated by a Gaussian with a mean size, $\langle D_{part} \rangle$, and a standard deviation σ_{part}. The CV (coefficient of variation) is defined as $\sigma_{part} / \langle D_{part} \rangle$ and is commonly between 1% and 10%. This means that sometimes the critical size in a device lies within the size distribution of the beads and they therefore become separated into two fractions. Grey dots signify when this occurs. In this kind of plot a power law of the form:

$$\frac{D_{part}}{d} = a \cdot N^{b} \tag{25}$$

can be fitted to the data by choosing a and b such that the resulting function delineates the black and white dots (the grey dots should lie on the line). Figure 19 shows, in green, a fit based on the parabolic theory, which underestimates the critical size. The red line is based on calculating β from simulations and neglects the effects of the particles on the flow, it also underestimates the critical size although it does better for small N. Davis found empirically that the best fit to his data was given by equation 25, which is shown fitted to our data in blue.

$$\frac{D_{part}}{d} = 1.4 \cdot N^{-0.48} \tag{26}$$

Equation 26 was used to design the devices presented in Papers III and IV.

3.3 Factors that affect the critical size in an array

Equation 26 is, due to its simplicity very useful for developing devices, but this simplicity comes at a cost. The problem is that many factors that are not present in equation 26 can have an effect on the critical size. These effects are mostly small but can become important under some specific circumstances. Because these effects are difficult to quantify we will consider them here in a qualitative manner and look at when each effect may become important.

Firstly, array parameters other than the gap, d, and the period, N, have an effect on the flow profile and therefore on D_{c0}. We will consider device depth, which we vary in Papers III and IV, and the ratio of the post diameter to the gap size d. Unfortunately we do not have access to particle imaging velocimetry[18] with which to measure the actual flow profiles in our devices. Instead we can use the finite element method, implemented in

[18] Images are taken in rapid succession of fluorescent tracer particles moving in a flow. Image analysis is then used to calculate flow fields.

Comsol™ to solve the Navier-Stokes equation and simulate flow in arrays in which we vary these parameters.

3.3.1 Post diameter to gap size ratio

Figure 19 shows the effect that post diameter, D_{post}, has on the flow profile when the device depth (10 µm) and gap d (10 µm) are kept constant. Figure 19A shows the velocity field for D_{post}=10 µm and 1 µm respectively and it is evident that the profile is more plug-like for the smaller post. Figure 19B shows flow

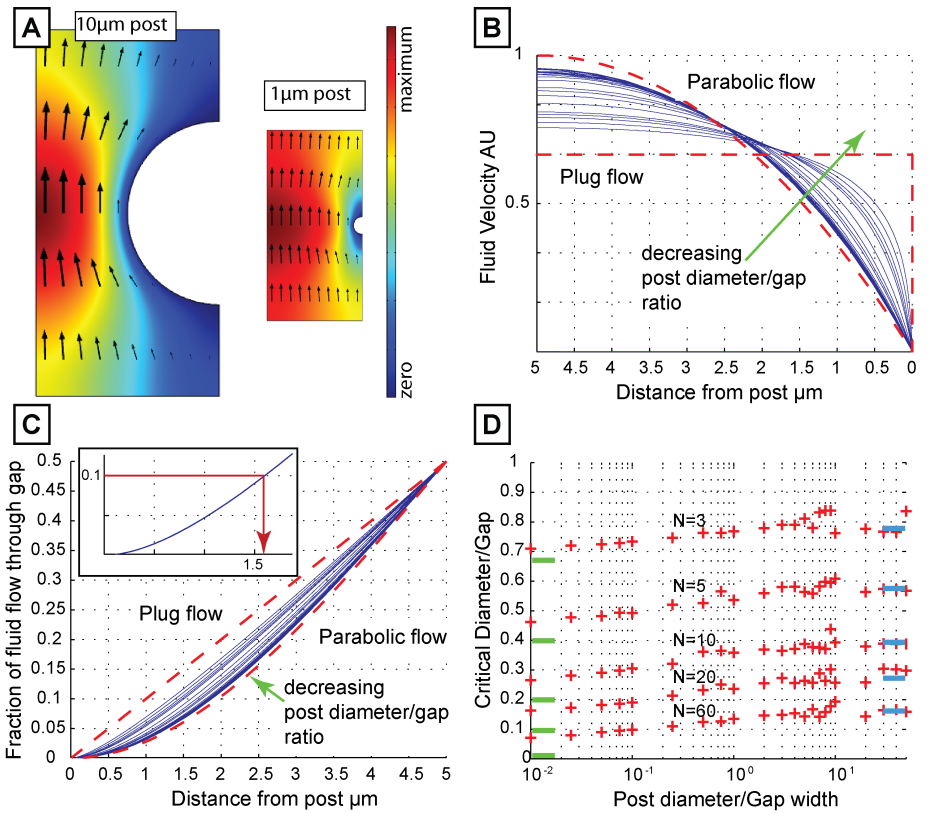

Figure 19 Flow velocity profiles as the post diameter/gap ratio is changed. (A) Simulations of flow between posts. In these examples the posts are 10µm and 1 µm respectively. The gap and depth are constant at 10µm. (B) Flow velocity profiles for many post diameters. All profiles are normalised so that the area under the curve (the flow rate) is the same. The red lines are profiles for plug flow and parabolic flow. (C) The fraction of the total flow as a function of distance from the post. The critical diameter can be read from this plot for any array period N. The inset shows how the critical radius can be estimated for N=10, and a post diameter/gap ration of 1. For 1/N=0.1 of the total flow the critical radius is roughly 1.6µm. (D) The critical diameter (approximated by 2/N) as a function of post/gap ratio for several periods N. The green lines to the left show 2/N for plug flow and the blue lines to the right show 2/N of the flow for a parabolic flow profile. (The noise is due to limitations of mesh sizes in the simulations).

velocity profiles for many post diameters. All profiles are normalised so that the area under the curve (the flow rate) is the same. The red lines are profiles for plug flow and parabolic flow. For large posts the flow is almost parabolic but as the posts become relatively smaller the profile becomes more plug-like. The fraction of the total flow as a function of distance from the post for each of the profiles in Figure 19B is plotted in Figure 19C. The critical diameter can be read from this plot for any D_{post} and N as is shown in the inset. In this example N=10, D_{post}=10 μm and 1/N=0.1 of the total flow occupies β=1.6 μm. $D_{c0} \approx 2\beta$ is therefore approximately 3.2 μm.

While 2β is only an approximation of the critical size the effect that the post size to gap ratio, D_{post}/d, has on it is still interesting and indicative of the effect on D_{c0} itself. Figure 19D shows how D_{c0}/d (calculated as $2\beta/N$) changes as a function of D_{post}/d for several N. The blue lines to the right show 1/N of the flow for a parabolic flow profile. The fact that the slopes are equal means that the absolute change in D_{c0} as D_{post}/d changes is the same for any N. However, because D_{c0} is smaller for larger N the relative effect is much greater. In this example, with N=60, in going from 500 μm posts to 0.1 μm posts the critical size is halved.

3.3.2 Device depth

The effects of device depth can be explored in the same manner as that presented in the previous section. In this case d and D_{post} are kept constant at 10 μm and the depth of the device is varied from 1 to 10 μm. Figure 20A shows the velocity field for the two extremes. Figure 20B and C show the flow profiles and the fraction of flow volume as a function of distance from the post in the same manner as those in Figure 19. Figure 20B shows how for the shallowest devices the flow profile becomes super plug-like and a large fraction of the volume flow is occurring near to the surface of the post. The effect of this is to reduce D_{c0} and as with the post diameter/gap ratio the relative effect is larger for larger N. While this effect is considerable it only becomes so as the device becomes very shallow. In fact, as the depth is decreased, before the effect becomes pronounced the device would become too shallow to allow particles above the critical size to enter. However, for very thin disc-like particles or long thin rod-like particle this effect could be utilized to reduce the critical size.

Note: Semiconductor nanowires of diameters ~100 nm and lengths of several micrometres can be fabricated in ordered arrays over areas of several cm^2 [123]. While it would not be trivial to integrate these into microfluidics devices, doing so might make it possible to use them as posts in DLD devices. Using small gaps, large N and with the effects discussed above it might be possible to achieve very small critical sizes. For example with d =1 μm and N =100 the critical diameter according to equation 25 would be ~150 nm. If the device were fabricated to 1 μm depth both the post/gap ratio and the device depth/gap ratio would be 0.1 and it might be possible to decrease the critical diameter to significantly below 100 nm.

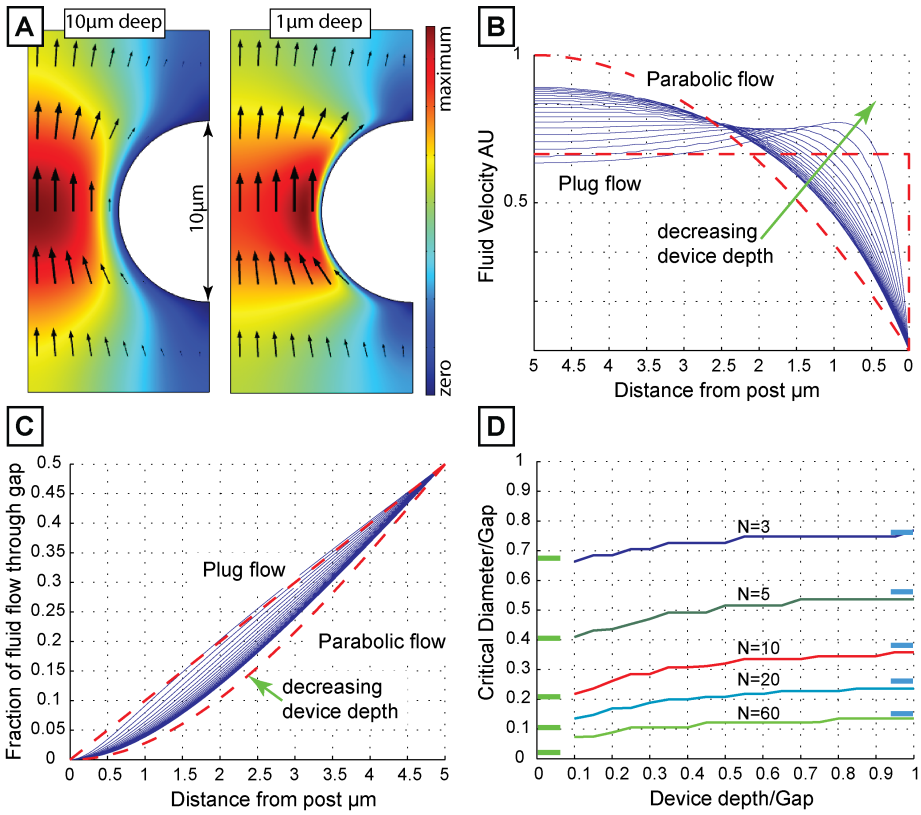

Figure 20 Flow velocity profiles as the depth of the device is changed. (A) Simulations of flow between posts. In these examples the posts and the gaps are both 10 and the depths are 10 µm and 1µm respectively. (B) Flow velocity profiles for many device depths. All profiles are normalised so that the area under the curve (the flow rate) is the same. The red lines are profiles for plug flow and parabolic flow. As the device becomes more shallow the profile becomes more plug-like. At 1-3 µm the profile is 'hyper-plug-like' with an area of high velocity close to the post (C) The fraction of the total flow as a function of distance from the post. The critical diameter can be read from this plot as described in Figure 19. (D) The critical diameter (approximated by 2/N) as a function of post/gap ratio for several periods N. The green lines to the left show 2/N for plug flow and the blue lines to the right show 2/N of the flow for a parabolic flow profile. As the device becomes shallower 1/N of the flow occupies less space. The fact that these lines are parallel means that the relative change is greater for large N.

3.3.3 Post shape effects

The shape of posts affects the shape of the fluid flow velocity profile and therefore the resultant critical size. Loutherback *et al* explored triangular posts in their DLD devices. Triangular posts lead to a skewing of the normally symmetric flow profile such that the 1/*N* of the flow that defines the critical size is narrower on one side of the gap and broader on the other. This is of interest because a

smaller critical size can be achieved for a given gap size[19] [124] but also because the non-symmetry means that the resultant device has different critical sizes in the forward and backward flow direction which the authors used as a microfluidic ratchet [120]. In our work we use circular posts throughout.

3.3.4 Edge effects

The description of flow through post arrays in 3.2.2 holds for infinitely wide arrays. At the interface between the array and the sidewall flow can become perturbed in a way that changes the critical size locally causing particles to follow the sidewalls instead of their intended trajectories and leading to an undesired decrease in resolution. In Papers I and II the particles being separated are focused in a stream that is far from the sidewall and so these effects can, and have been neglected. In the types of devices shown later in Figure 25 particles fill the entire device and so move close to sidewalls. This is also the case for those devices used in Papers III and IV in which we wanted to make maximum use of the available space. This is achieved by focusing the sample close to one sidewall, effectively halving the required width of the device compared to those used in Papers 1 and II. Inglis reports a method to modify the array-sidewall interface in such a way that the perturbations to the critical size are minimized [125] and we used this method when designing this device. The idea is to modify the size of the gaps between the sidewalls and the posts along the edges. If particles are being displaced from left to right then the gap between the left sidewall and the nearest post, d_{left}, is given by equation 25, and the gap between the right side wall and the nearest post, d_{right}, is given by equation 26 where d is the gap in the bulk of the array N the period and n the row number.

$$d_{left} = d\sqrt{\frac{n}{N}} \tag{25}$$

$$d_{right} = d\sqrt{2 - \frac{n}{N}} \tag{26}$$

[19] The decrease in the effective radius when using equilateral triangular posts instead of circular posts was show nto increase with N. For N=10, R_c decreased to ~75% and for N=100 it decreased to ~55% of the value for circular posts with the same gap.

3.3.5 Anomalous modes

The theory presented in this chapter is based on array periods, N, that are integers. These are achieved by row shifts of $1/N$. In arrays with row shifts of M/N, where M is an integer that is not a divisor of N, particles can move in more than the two normal modes and these arrays consequently have more than one critical size. We have shown experimentally that these modes exist[20] and a theoretical description can be found in Paper III of the related publications. The devices presented in Papers I to IV however are all of the $1/N$ type.

An alternative description of the mechanism of DLD has been given by Balvin *et al [121]*. Balvin explored the trajectories of millimetre-sized spherical particles driven by sedimentation through large arrays constructed in Lego™ (this is effectively a scaled up version of the work we presented at Microtas 2009, see the footnote below for details). In their description particles can only follow the direction of the driving force if the interactions with posts are fully reversible. Irreversible interactions between particles and posts lead to the locking of particles into different trajectories that correspond to lattice directions in the array, behaviour that was also seen in simulations by Frechette and Drazer [126].

Quek *et al* performed 2D numerical simulations of particles with varying deformability in DLD arrays [127]. They found that rigid particles that are larger than half the gap size could move in a mixture of the zigzag and displacement modes. They considered this motion to be a third mode that they named the dispersive mode due to the fact that it leads to a broadening of the particle distribution at the outlet compared to the inlet. The authors state that the limitations of a 2D simulation might give rise to this behaviour and while they cite the experimental literature they do not point to any examples of this behaviour. We have seen that large rigid particles, with diameters larger than half the gap size, are displaced less than expected; see Figure 2 of Paper III. This might be related to the effects discussed by Quek *et al* although no broadening was observed for these particles suggesting that the behaviour is not yet fully understood.

[20] J. P. Beech and J. O. Tegenfeldt, *Gravitationally driven deterministic lateral displacement devices*, The 13th International Conference on Miniaturized Systems for Chemistry and Life Sciences, Jeju, Korea, 2009, 779-781.

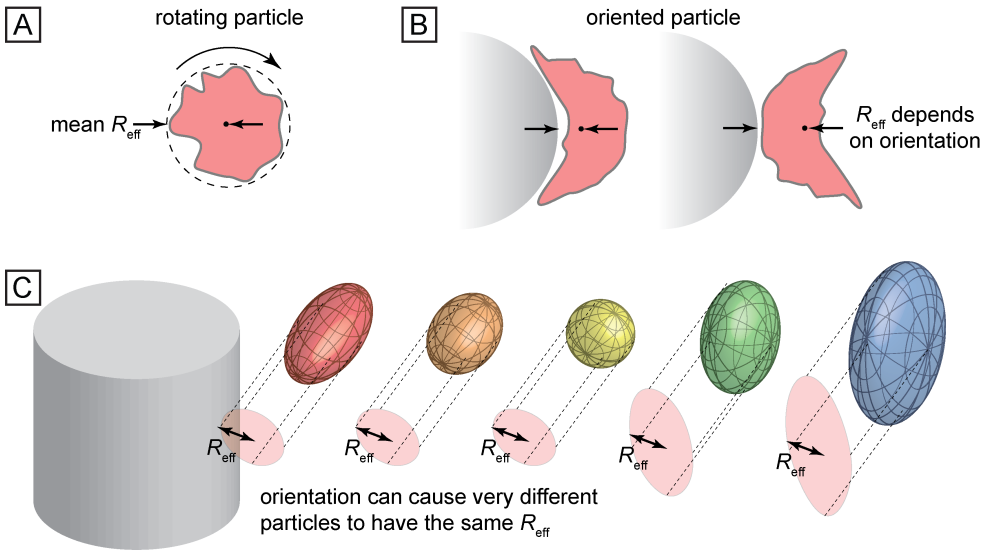

Figure 21 The orientation of non-spherical particles determines their effective size. (A) A randomly rotating particle will have a mean R_{eff} as it moves through a device. (B) If the particle adopts a specific orientation at the decision point in the array (as it moves past a post) then R_{eff} will, for some shapes, depend strongly on the orientation. (C) This effect means that particles with very different shapes can have the same R_{eff} making it impossible to separate them.

3.4 The effective size of particles

In our simplified model we consider the critical particle size as the projected distance of the hydrodynamic centre of gravity of the particle from the surface of a post along a line joining the centres of two posts. Since this is where the trajectory of the particle is decided, we refer to this location as the decision point. For rigid spherical particles the projected distance is equal to the radius of the particle and is invariable under rotation or the application of shear forces since the particle cannot change shape. For particles that are either permanently non-spherical or that are deformable and can temporarily become non-spherical the projected width will depend on both particle orientation and on the degree of deformation. We can define an effective size, R_{eff}, for a particle of arbitrary shape and deformability as the radius of a hard spherical particle that would follow an identical trajectory through a device. It is the relation between R_{eff} and R_{c} that determines the trajectory of a particle.

3.4.1 Particle shape

As discussed in chapter 1, biological particles come in many shapes. For non-spherical particles R_{eff} depends strongly on the orientation that the particle adopts as it moves through the decision point, as summarized in Figure 21. In chapter 2.3.5 we considered the rotation of non-spherical particles in shear flows and alluded to the fact that interactions with posts dominate. What we see in our devices is that, provided they have room to rotate, particles always align themselves such that it is their smallest dimension that dominates R_{eff}. This can greatly limit the kind of particles that can be resolved in DLD devices, as shown in Figure 21C, but it also presents an opportunity. Controlling the orientation of particles makes it possible to choose which particle dimensions contribute to R_{eff}. This in turn makes possible both the measurement of, and separation by, particle shape parameters. In Papers III and IV we control the orientation of particles using device depth, which limits the ability of particles to align and minimize their effective sizes. In Paper III we use this effect to improve the separation of non-spherical particles of different shapes and in Paper IV we use the same approach to measure size and deformability in different particle orientations.

3.4.2 Particle deformation

As described in chapter 2.3.5 velocity gradients give rise to shear stresses that can deform soft particles. Figure 22 shows how the shear rate is distributed in the

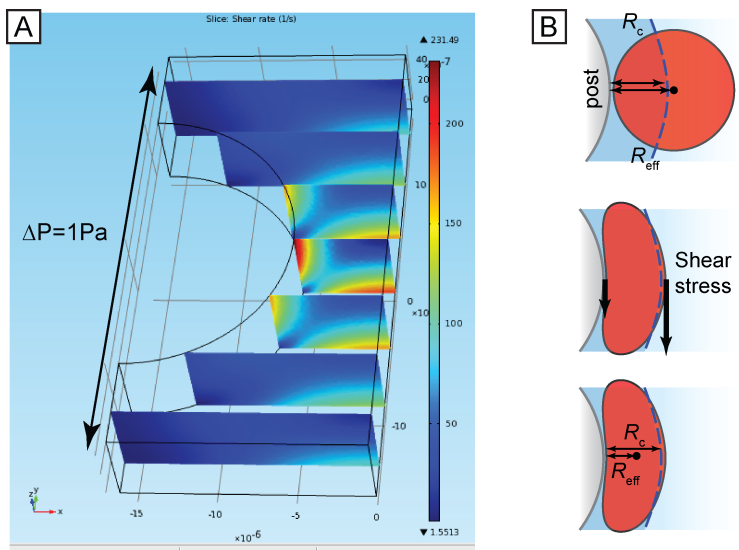

Figure 22 Deformation due to shear stress.(A) The colour map shows the shear rate in a fluid flowing between two posts. The shear rate and therefore the resulting shear stress on the particle is greatest between the posts at the decision point. (B) Shear stress deforms particles decreasing their effective size.

fluid in a typical device. The exact nature of the shear stress a particle will experience in this shear field is difficult to determine since the particle perturbs the flow. Depending on its mechanical properties, the particle will deform, which in turn changes the perturbation. What is more, interactions with posts can also give rise to particle deformation. Despite the complexity of the deformation we can still capture the general behaviour in a simple way by considering R_{eff}. Particles of the same size and shape but with different mechanical properties will have different effective sizes in DLD devices.

Paper IV shows how DLD can be used to approach both shape and deformability measurements and separations.

3.5 Other device-particle interactions

3.5.1 Post-particle interactions

Any forces, other than purely steric interactions, between particles and posts will change the effective size of the particles. Repulsion between particles and posts will increase the effective size of the posts (or particles) and attractive forces could have the opposite effect (Paper II is based on using DEP forces to do this). Large attractive forces can lead to the adhesion of particles to posts and clogging as described in the following section. During the inflammatory response leucocytes are known to interact with selectins expressed by epithelial cells in blood vessel walls. The interaction is strong enough for the cells to adhere to the surface despite shear forces from the flowing blood but weak enough for them to be able roll along the wall in order to find sites through which they can leave the blood vessel. This, or similar, rolling effects could influence the point at which particles lose contact with the posts and therefore which flow stream the particle will follow. Choi *et al* recently used rolling to separate cells in a microfluidics device with a principle different to DLD [128] but based also on selection of flow streams and we believe that the excellent resolution of DLD could be used to perform adhesion based separations with higher resolution than Choi reported. Frachette and Drazer simulated particle trajectories through post arrays and found that particles with equal radius but different surface roughness followed different trajectories [126]. At present we minimize the effects of surface interactions by chemically modifying the inner surfaces of our devices, see chapter 4.3, however post-particle interactions would be an interesting direction to follow in the future.

3.5.2 Flow perturbations by particles and particle-particle interactions

As particles move through our devices they perturb the surrounding flow field. It is this perturbation partly that leads to the discrepancy between the width of the unperturbed first lamina and the critical radius (compare equations 24 and 26 and Figure 18); as the particle moves between two posts the width of the first lamina changes. The perturbation is dependant on the relationship between the particle size and the gap size. Particles much smaller than the gaps in a device have little effect on the flow and Equation 25 works well enough but those that almost fill the gaps cause large perturbations, not only within the gap they are traversing but also in the surrounding gaps. This underlies the effects seen in the numerical simulations by Quek *et al* [127]. As particle concentrations increase, these perturbations that can extend several posts in distance, will overlap further changing the critical size in the device.

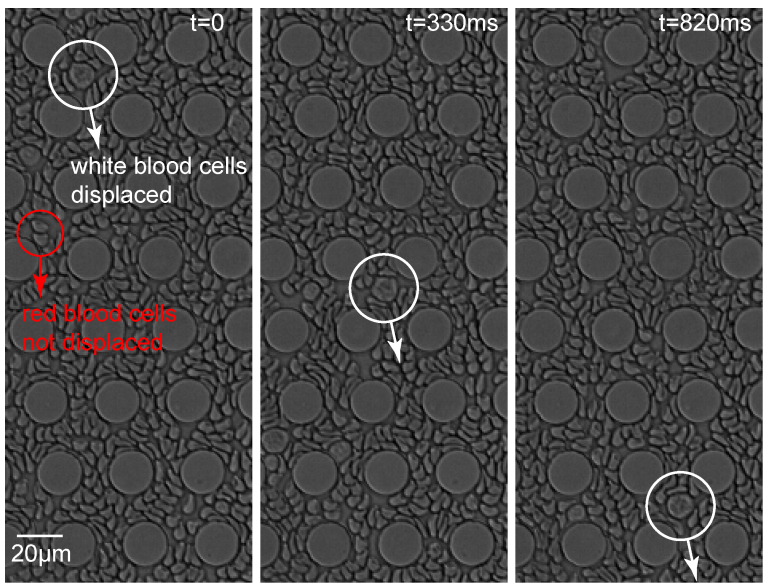

Figure 23 DLD devices are able to separate white and red blood cells even at particle concentrations above those of whole blood (50%). This is due to the deformability of the cells, which have evolved to move through capillaries that can be smaller in cross section than the cells themselves.

Devices can become clogged by particles, either because they adhere to the inner surface of the device, because they are too large to fit between posts or because they enter a gap at the same time and become stuck by the keystone effect [129]. Clogging can cause major problems in microfluidics in general specifically

when working with biological samples and DLD devices are no exception. Clogs cause the following problems: they change the critical size locally decreasing resolution, they increase the resistance in a device, decreasing throughput and they cause loss of sample. It is almost always clogging that limits the lifetime of a device.

Estimating the probability of particles becoming trapped due to steric interactions is a complex problem. Very small particles can move very close to the surface where the flow is slowest affording them time to interact with the surface. The larger particles are in relation to the gaps and the higher the concentrations, the higher the probability of keystoning. This can limit the maximum concentrations of hard particles to below several ‰ by volume. Soft particles such as red blood cells on the other hand are able to flow through our devices at concentrations approaching 100% as can be seen in Figure 23.

The above effects are all difficult to quantify. We have as yet not measured the effects of very high particle concentrations on the critical size but we see that the devices are able to displace white blood cells even at the extremely high concentrations shown in Figure 23. The problem of adhesion can be minimized by the use of surface coatings, see chapter 4.3. In general we minimize the negative effects of particle-particle interactions by keeping particle concentrations low when working with hard particles and by designing devices with as large gaps as possible in relation to the particles we want to analyse in order to minimize both flow perturbations and clogging.

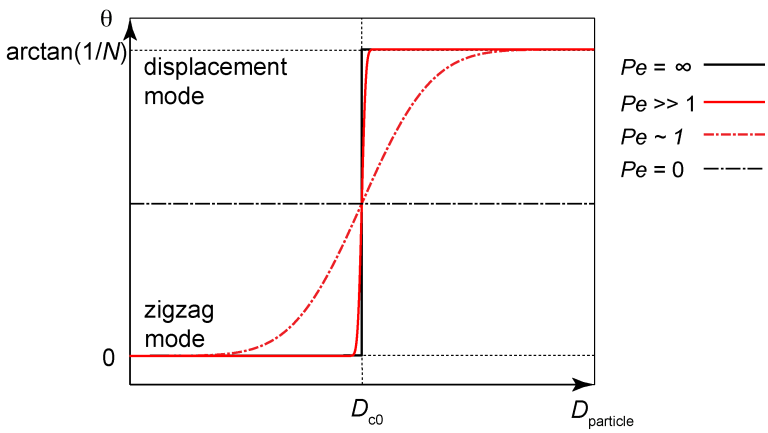

Figure 24 The effects of diffusion on the transition between zigzag and displacement modes. With no diffusion (Pe =∞) the transition is a step function. As the relative effects of diffusion increase (Pe decreases) the transition broadens. As Pe → 0 diffusion begins to dominate and at Pe = 0 no separtion occurs.

3.5.3 Diffusion

Diffusion broadens streams of particles as discussed in chapter 2.3.3 and also leads to the migration of particles between lamina. If particles diffuse a distance of $|D_{particle}-D_{c0}|$ they will be able to make the transition from the zigzag to the displacement mode or visa versa. For the micrometre-sized particles that we have investigated, at average flow velocities of 100μm s^{-1} to several cm s^{-1}, Péclet numbers are large and diffusion can mostly be neglected. If one wants to separate sub-micrometre particles however diffusion can become important. Particles that have diameters very close to D_{c0} will be very sensitive to the effects of diffusion and will diffuse back and forth between the two modes often. Figure 24 shows how diffusion acts to broaden the transition between the zigzag and displacement modes. In the deterministic limit (high Péclet number) the transition from zigzag to displacement is a step function. As the Péclet number is decreased the transition is broadened. This effect, shown as symmetric about D_{c0} in the figure, actually tends to shift D_{c0} to the left. The shift originates in the fact that diffusion acts differently on particles in the zigzag mode than it does on particles in the displacement mode, and it is expected to be more pronounced for larger posts. For more details of this effect the reader is referred to the discussion in Paper III of the related publications and that by Heller and Bruus [108].

3.6 Applications of DLD

To date, DLD devices have been put to use in the separation of diverse particles. The technique has been used to separate chromosomal bacterial DNA of differing lengths [6]. Davis *et al* used DLD to isolate cell-free plasma from whole blood and also to separate blood cells into size-based fractions [7]. Inglis *et al* used hydrodynamic cell size in DLD devices to distinguish healthy from malignant lymphocytes [130] and also detected changes in the hydrodynamic size distribution of blood platelets due to the effects of thrombin and refrigeration [14]. Morton *et al* likened the behaviour of particles in DLD arrays to the behaviour of light in refractive media and used DLD to stear, focus and disperse streams of particles [11]. Because particles are caused to move across streamlines in a DLD device they can be moved through laminar flow streams containing different chemistries. Morton *et al.* used this fact to lyse cells, stain the nucleus upon release and subsequently separate the stained nucleus from the unwanted debris [131]. Nucleated RBCs, a source of information on maternal, fetal and neonatal health were separated from whole blood using DLD followed by a magnetic separation technique by Flejter *et al* [8]. Large cells for tissue engineering were enriched by Green *et al* [9]. Inglis reported highly accurate DLD devices for the separation of

fungal spores [12]. As recently as this year, Inglis showed a two-layer device that makes better use of a smaller device area by having fluidic in and outlets on a separate layer to the separation array itself. This device was able to concentrate white blood cells from whole blood by a factor of 20 with a high throughput ~100 µl/min. [13]. Also this year, Jönsson *et al* separated water droplets in oil based on their size. Some droplets contained yeast cells, which caused the droplets to shrink, and these shrunken droplets where separated from empty drops that were present at 40 times higher concentrations [15].

3.7 Conclusions about DLD theory

From this discussion we conclude that there are many factors that influence both D_{c0} and D_{eff} in DLD devices and that the theory is still in its infancy. Despite this it is still possible to design devices using the principles we have discussed that will have D_{c0} close enough to the desired value for devices to be useful. However, if one wants to take full advantage of the exceptional resolution in a DLD device, close is not always good enough. Empirical studies can help us to develop devices for specific tasks but in general devices that either have multiple D_{c0} or that are tuneable are more versatile.

As well as the design of the arrays themselves it is also important to consider the properties of the particles one wishes to analyse. Particle shape and deformability affect R_{eff}. Particle concentrations will also influence the outcome of separations, more so for rigid particles, and although high particle concentration means high throughput, concentrations should be low enough that changes in the relation between R_{eff} and R_c do not become limiting. Also steps should be taken to ensure that particles to do not adhere to the surfaces of devices as clogging negatively affects device performance.

For sub-micrometre particles diffusion can limit separations and high flow speeds should be used to ensure high Péclet numbers.

A thorough understanding of all of these effects can be gained through simulations, but only by simulating in 3 dimensions with particles influencing the flow, which is no easy task and outside the scope of this thesis.

The simple theory presented here provides useful heuristics when designing devices. The art of designing DLD devices is the art of arranging things such that it is the particle characteristics of interest that decide particle trajectories but also to ensure that devices are able to cope with actual samples for long enough to give the desired results, whether it be the analysis of one µl of blood that may only take seconds or the continuous filtering of large volumes of drinking water that may take days or even weeks.

4 Device design and fabrication

In this chapter we will consider the practicalities of designing, fabricating and running devices according to the principles laid out in the previous chapter. We will first consider how the mechanism of DLD can be implemented in devices. The exact way in which this is done depends on the nature of the sample and on the desired outcome: particle concentration, separation or analysis and on the required throughput. Arrays can be used individually to achieve bimodal separation or in series to separate samples into multiple fractions.

As well as the post arrays where separation takes place, devices require a means of introducing and collecting samples and in some cases particles need to be imaged before, during and/or after their journey through the device. In future, true Lab-on-a-chip devices will be self-contained [59] but at this, the development stage, devices need to be connected to external pressure sources in order to induce flow, electrical connections to implement DEP (see Paper II) and to microscopes with which the results of experiments can be observed, recorded and analysed.

4.1 DLD device concepts

4.1.1 Separation or concentration – Device modes

Without the need to focus a sample, a device with only one inlet can be used to increase the concentration of particles with $R_{eff} > R_c$ by displacing them into the side-wall of a device, see Figure 25A. This can be a useful approach to increase the concentration of larger particles relative to a background of smaller particles or to remove a fraction of unwanted larger particles from a sample.

In order for complete separation to occur the displaced particles need to be able to move into a fluid that is initially free of sample components. The flow of sample next to an ‘empty’ buffer can be created in two ways. Flow focusing, see Figure 25B, is achieved using separate inlets for sample and buffer streams and, as explained in 0, requires the control of pressure or flow rates at several inlets and/or outlets.

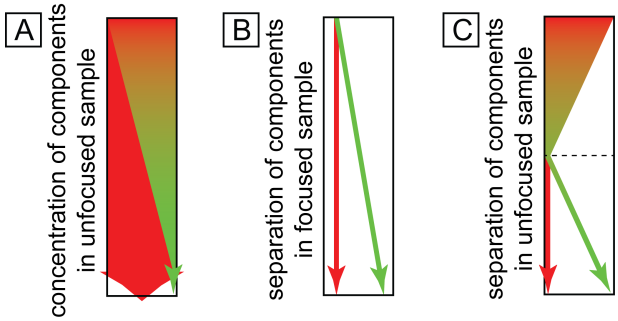

Figure 25 The ability of DLD devices to displace only those particles with specific properties can be used in different modes. (A) Without focusing, a subpopulation of particles can be concentrated. (B) A focused stream of particles can be separated into fractions. (C) DLD can be used to first focus a sample and to then separate it into fractions.

Alternatively, DLD itself can be used to focus the sample prior to separation as shown in Figure 25C. An array with R_c smaller than the effective size of all of the particles of interest can be used to focus the particles against the wall. Once focused, subsequent arrays can be used to separate the particles.

The advantage of flow focusing lies in the greater control over the relative amounts of sample and buffer that can be introduced into the device and the degree of focusing that can be achieved. Controlling pressure or flow rates using the methods explained in chapter 4.1.3, is easily done in the laboratory environment but might require more instrumentation than is practical or affordable for cheap and portable devices [59]. Devices based on DLD focusing require only one inlet and, while they are not as versatile as devices that use flow focusing, they are considerably easier to use.

4.1.2 Single and multiple array devices

The devices used in Papers I and II each contain one array with one critical size only based on the parameters shown in Table 2. Such devices can be used to separate particles into two fractions: those smaller than the critical size, and those larger as shown in Figure 26A. Figure 26A also shows the specific layout used for the device in Paper I.

In order to separate particles into more than two fractions, multiple arrays with parameters that result in multiple critical sizes can be used in series. A device with n arrays in series can separate a sample into n+1 fractions. Figure 26B shows an example with n=3.

The devices used in Papers III and IV consist of 13 sections and are therefore able to separate particles into 14 fractions. Each section has a specific critical diameter, $D_{c,n}$ (n=1,2,…,13), which are increased in steps of 0.5 µm by decreasing N and where each section gives rise to a lateral displacement of ~160 µm for

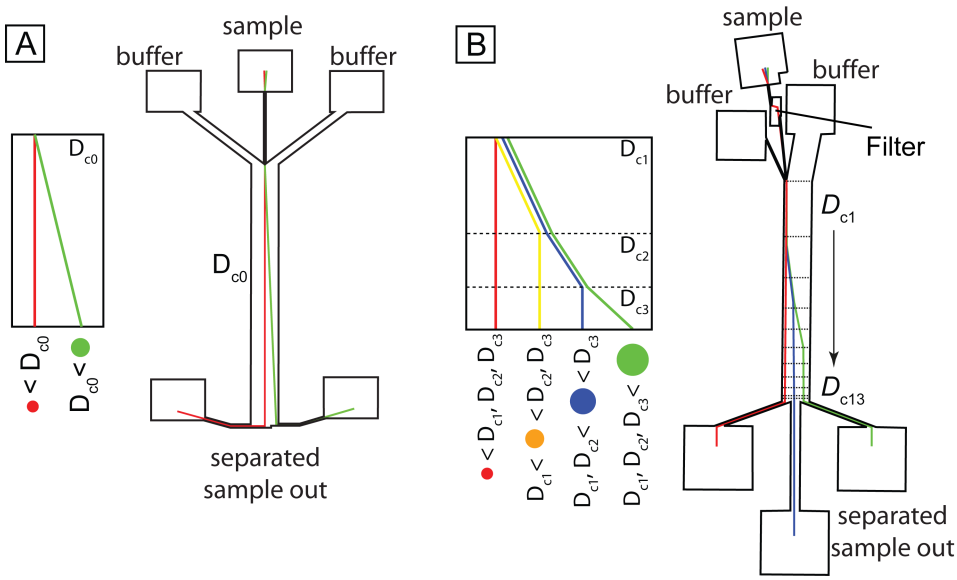

Figure 26 Devices can be designed to separate particles into two or multiple fractions. (A) A device with one array gives bimodal separation (two fractions). (B) Multiple arrays in series give multimodal separation (many fractions).

Table 2 Parameters for the devices used in Papers I to IV. The devices in Papers I and II were designed using the parabolic theory. For reference the values for the critical diameter calculated using Davis' theory are added. The devices used in Papers III and IV where designed using Davis' equation and have 13 critical diameters achieved by changing N. The range of values of N *used and the resulting D_c are shown here. The exact values can be found in the supplementary information to Paper III.*

Device	Row Shift $\Delta\lambda_n$ [µm]	Period N_n	Post diameter D_{post}[µm]	Gap d [µm]	Critical Diameter $D_{c,0}$ [µm]
Paper I	2.7[§]	20	30	54 *	13.94[†] 17.95[‡]
Paper II	1.2[§§]	10	30	12	4.38[†] 5.56[‡]
Papers III and IV	0.8 – 8.8[§§]	40 – 3.6	20	12	2.9 – 9.0[‡]

*Unstretched. [§]Rotated square array. [§§] Rhombic array. †Calculated using $D_c=2\cdot\sqrt{1/3}\cdot d\cdot N^{-0.5}$. [‡]Calculated using $D_c=1.4\cdot d\ N^{-0.48}$

particles with diameters larger than $D_{c,n}$. The range of values of N is given in Table 2 and the exact values can be found in the supplementary information to Paper III. The total displacement for a particle with diameter D_{eff} is given by $x_{particle} \sim 160\ \mu m \cdot \sum_{n=1}^{13}(D_{particle} > D_{c,n})$. The Boolean term within the brackets equals 1 if true, else 0. Particles are separated into 14 fractions with diameter thresholds ranging from 3 to 9 μm in 0.5 μm steps.

4.1.3 Injecting, focusing, imaging and collecting particles

Both before and after separation, particles need to be temporarily stored in reservoirs. These reservoirs can be on the device itself, as shown in Figure 28 and Figure 27 or they can be external to the device and connected via tubes. We use 1.5 ml centrifuge tubes as off-chip reservoirs but more commonly we glue reservoirs directly onto devices. In both cases a pressure difference needs to be generated between the inlet and outlet reservoirs in order to generate a flow through the device. In Papers I and II this was achieved by keeping inlet reservoirs at ambient pressure and applying vacuum at the outlet reservoirs, and in Papers III and IV by keeping the outlets at ambient pressure and controlling the pressure independently in each of the inlets.

These methods have their relative advantages and disadvantages. Applying vacuum to the outlets to drive flow is generally easier to do without expensive pressure controllers. Open inlet reservoirs make it very easy to introduce sample at any point during an experiment without the need to turn off the flow whereas connections need to be removed before anything can be introduced when controlling inlet pressure. The situation is reversed for the outlets. Changing the pressure at the outlets changes the overall flow rates but sample focusing is fixed and depends on the careful design of the inlet channel geometries, see chapter 2.2.2 for a description of hydraulic resistance. Working with samples and buffers of varying viscosities can be problematic in this case as the amount of focusing depends on the viscosities of the fluids for a given set of applied pressures. Greater control over sample focusing can be achieved by independently controlling the pressure, and therefore the flow rates, in each of the inlets. While this is easily done in a well-equipped microfluidics lab it is more dependent on expensive periphery equipment. In this case also, outlets must be carefully designed with the correct resistances in order for the sample to be collected in the desired manner.

Simple vacuum pumps are very suitable for the types of devices shown in Figure 25A and B[21], whereas sample focusing is more easily done with pressure

[21] In fact overpressure at the inlet generated with a simple pump or syringe would work equally well for these types of devices.

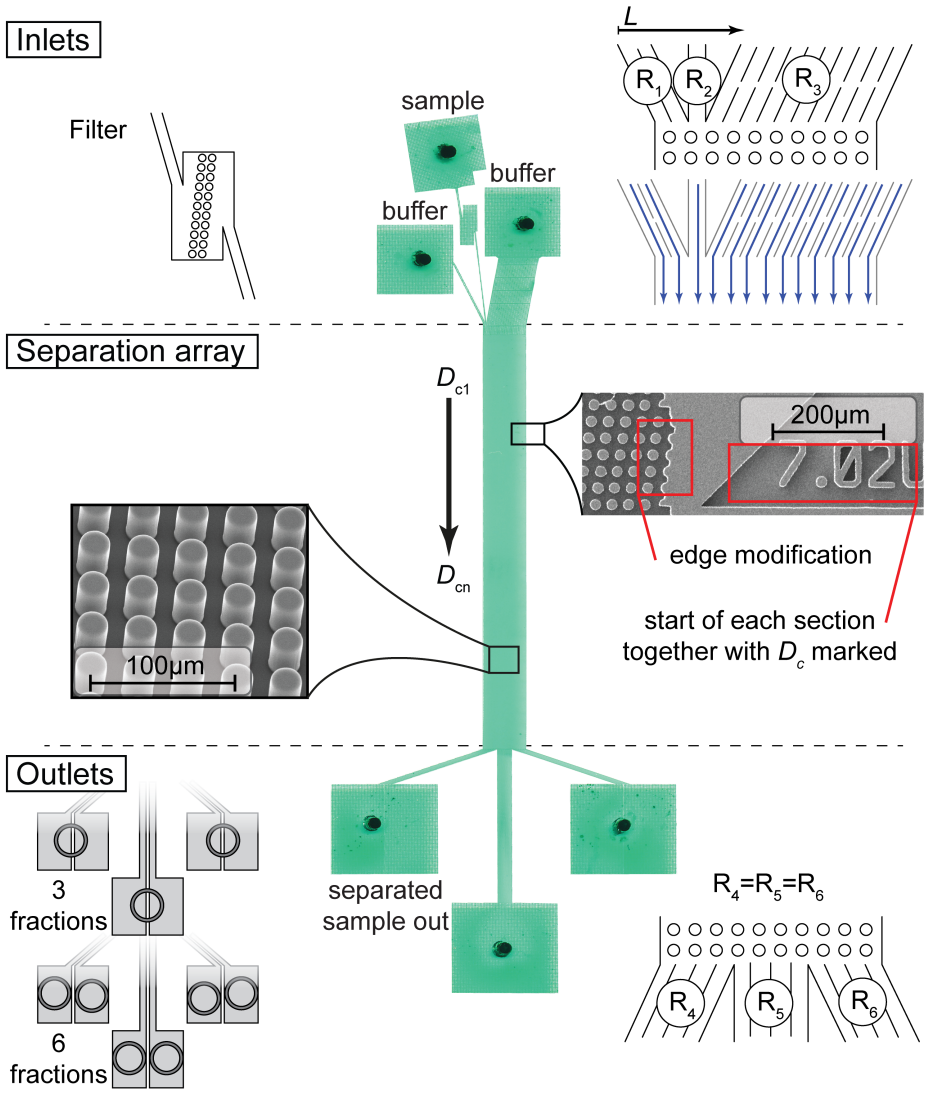

Figure 27 An overview of the components that make up a functioning DLD device. Three inlets allow the sample to be focused in a narrow stream. Inlets and outlets are designed with resistances that allow the device to function equaly well with either controlled over –pressure at the inlets or vacuum at the outlets. An inline filter catches particles that would otherwise clog the device. The device has a range of critical sizes so that samples can be separated into 14 discrete streams. Outlet channels are arranged such that either 3 or 6 fractions can be collected. (It is of course possible to have 14 outlets and collect all 14 fractions although unnecessarily complicated at the development stage). Each of the separate arrays are dilineated with markers and all edges are modified as describes in chapter 3.3.4.

controllers. Of course the maximum possible control is achieved by controlling pressure on all inlets and outlets but this is seldom necessary.

In order to minimize clogging, inline filters can be added to the sample inlet. In the devices used in Papers III and IV, see Figure 27, the filter had the same gap size as the separation array. Any particles that would get trapped in the array are removed before hand by the filter. As the filter becomes clogged the resistance increases, which in turn can affect the introduction of sample to the device. It is important to design these filters with a large enough volume so that excessive clogging does not occur over the time scales required for the experiment taking into account the nature of the sample in each specific case.

Provided devices are transparent, imaging particles during experiments is easy; the type of microscope used places the only constraints. If transmission microscopy is be used then it is important that inlet and outlet reservoirs and tubing do not obscure the regions of interest in the device. Placing the reservoirs 2–3 cm apart is sufficient for most microscopes. High-magnification objectives often have short working distances and so it can be important that the device has at

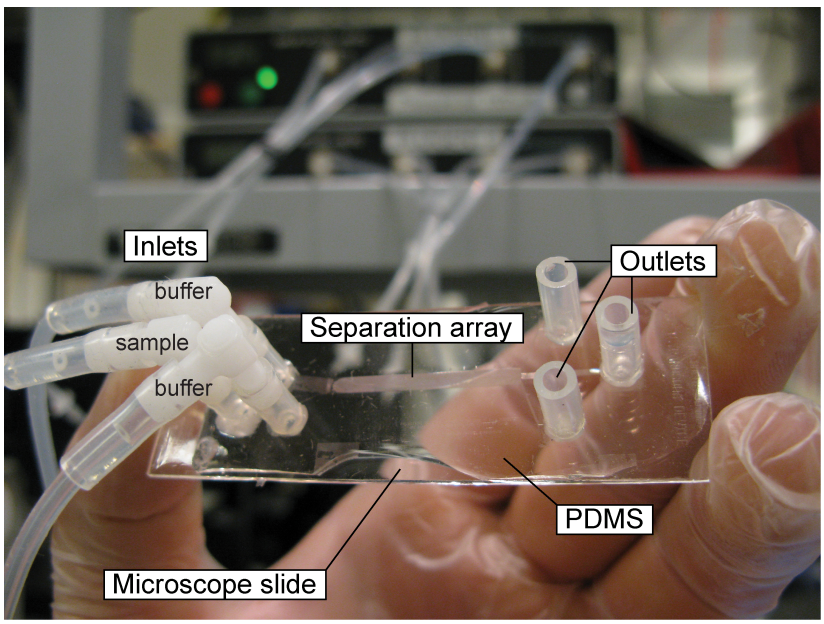

Figure 28 A photograph of a typical device (this is the device used in Papers III and IV).

---

[22] In fact overpressure at the inlet generated with a simple pump or syringe would work equally well for these types of devices.

least one side that is very thin. The images of red blood cells in Paper IV (Figure 1e, f and g) were acquired with a 100x objective with a working distance of 130-200 μm, designed for use with thin coverslips. In order to do this the PDMS device was sealed with a number 1 glass cover slip (~150 μm). These thin devices are fragile and can be difficult to work with and in most cases normal microscope slides (~1mm) can be used.

In Paper II alternating electric fields are applied between the inlets and the outlets of a device, which was done simply by dipping platinum electrodes into the reservoirs.

Descriptions of the pressure devices, microscopes, cameras and other peripheral equipment used in Papers I to IV can be found in Appendix 4.

4.1.4 Throughput

Throughput is normally measured in the volume of sample that devices can deal with per unit time and 'high throughput' most commonly means high volume throughput. However, it is often more relevant to consider the number of particles separated per unit time, so that in this case the concentration of particles that the device can successfully deal with is very important. The detection of rare cells in blood provides a very good example of this. If the cells are present at very low concentrations, 10 per ml for example, then in order to find 100 cells using a device that can deal with whole blood it would be necessary to analyse 10ml of blood, a reasonable task for a microfluidics device. Many methods however require the dilution of blood, in some cases by as much as 1000 times. In this extreme case 10 Litres of diluted sample would need to be analysed. As well as the problems of dealing with such large volumes of sample in microfluidics devices, both access to large volumes of dilution media and the disposal of large volumes of contaminated waste can be problematic.

In Paper III, and in Figure 22, we show that our device can deal with whole blood. However, focusing the sample with a sheath flow of buffer is equivalent to temporarily diluting it, even if the sample is once again concentrated at the exit. The amount of buffer required to run the device depends on the amount by which the sample is focused and varies, in the device in Paper III, between ~10-50 times the sample volume. In many cases, such as the precise analysis of small volumes of sample, this focusing is necessary and dilution is acceptable. In other cases the width of the sample stream can be increased in relation to the sheath flow, increasing throughput. The types of devices shown in Figure 25A and C require no sheath flow and are therefore the optimum designs for high throughput. However it should be noted that it is the maximum concentration of particles after concentration at the wall that will determine the useful concentration of sample that can be introduced into the device. Consider whole blood for example, which has a particle concentration of approximately 50%. It will be possible to concentrate the blood to more or less 100% as shown in the previous chapter but

this will only entail a focusing of the sample to half the inlet width. If blood is to be focused to 1/10th the inlet width then it would first need to be diluted 5 times.

High pressures generate high flow rates increasing throughput but as discussed in chapter 3.4.2 high shear rates can result in particle deformations that can negatively affect separations. Sufficiently high shear rates can alter the physiological state of cells and can even cause cells to lyse and these factors should be considered at the design stage. Also the materials used to fabricate devices have inherent limitations with regard to the pressures they can withstand. As described in Paper IV we have used pressure differences of 1 bar across our PDMS devices without negatively affecting the devices themselves, however red blood cells, while not lysing suffered considerable deformations greatly changing their effective sizes. We have not as yet tested the limits of our devices with respect to shear stresses and cell viability but this would be an interesting topic for future studies.

Finally, the deeper a device is, all else being equal, the larger the volume throughput. When using shallow devices, see Papers III and IV, throughput can instead be improved by running many devices in parallel, which can be achieved by stacking many thin devices on top of one another[23].

4.1.5 Dynamic range

The range of particle sizes that a DLD device can deal with is limited by the size of the smallest constriction in the device. This is normally the size of the gaps in the arrays but can also be the depth of the device (see Papers III and IV); particles larger than this minimum dimension will become stuck and clog the device causing the problems described in chapter 3.5.2. Generally, the larger the gaps the better, as the device can accept a broader range of particle sizes and be less susceptible to clogging avoiding the problems described in the previous chapter. The larger the ratio of the gap to the critical size, d/D_{co}, the greater the margin and because d/D_{co} is proportional to $N^{0.48}$, arrays with larger N are less susceptible to clogging. Larger gaps also result in arrays with lower resistance and potentially higher throughput. However, large N also means small angle trajectories and devices need to be longer in order to achieve the same relative lateral separation as arrays with smaller N. Even if device size is not a limiting factor, diffusion can be, see chapter 3.5.3. Separation is only possible if the rate at which lateral displacement occurs is greater than the diffusion rate and very small angular separations may require very high flow rates in order to overcome

[23] J. P. Beech, T. Mäkelä, P. Majander and J. O. Tegenfeldt, *Throughput Through Thin-Film Fluidics,* The 12th International Conference on Miniaturized Systems for Chemistry and Life Sciences, San Diego, USA, 2008, 1492–1494.

diffusion. $3>N>60$ is the range of periods that we find practical for micron sized particles.

It is not only the range of particle sizes that can pass through a device that is important. It is only at the critical size in the device that any useful separation occurs and so the dynamic range, DR, is also useful to consider. DR can be defined as the ratio of the largest to the smallest useful separation that the device can perform. For DLD devices this is equal to the ratio of the largest critical size to the smallest critical size. A device with only one array has only one critical size and DR=1. In tuneable devices DR is greatly improved. As described in Paper I, deforming an array can change the critical size by a factor of 2, which doubles DR for a single array provided that the device is deep enough so that the decrease in depth upon stretching is negligable. DEP forces can be used to decrease the critical size by a factor of at least 3, as described in Paper II, which not only increases the dynamic range from 1 to 3 but it also increases the margin between the critical size and the gap decreasing the probability of clogging.

The devices used in Papers III and IV have critical sizes from 3 μm to 9 μm and have therefore DR=3. In these devices the gap is kept constant throughout so that provided a particle is smaller than the gap it will be able to traverse the entire device. Cascaded arrays with successively smaller gaps can be used to achieve a DR of more than 20 [7] provided the largest particles are removed via side-channels after each step in the cascade so that they do not clog subsequent arrays.

4.2 Fabrication techniques

There are many materials from which microfluidics devices can be fabricated and many methods have been used to pattern them as mentioned in chapter 1.3. While we have experimented with devices fabricated using injection moulding [132, 133][24] and roll-to-roll imprinting [134] [25] the work presented in Papers I-IV has all been performed in devices fabricated using silicone rubber (PDMS) and glass.

[24] J. P. Beech and J. O. Tegenfeldt, *Capillary driven separation on patterned* surfaces, The 13th International Conference on Miniaturized Systems for Chemistry and Life Sciences, Jeju, Korea, 2009, 785-787.

[25] J. P. Beech, T. Mäkelä, P. Majander and J. O. Tegenfeldt, *Throughput Through Thin-Film Fluidics,* The 12th International Conference on Miniaturized Systems for Chemistry and Life Sciences, San Diego, USA, 2008, 1492–1494.

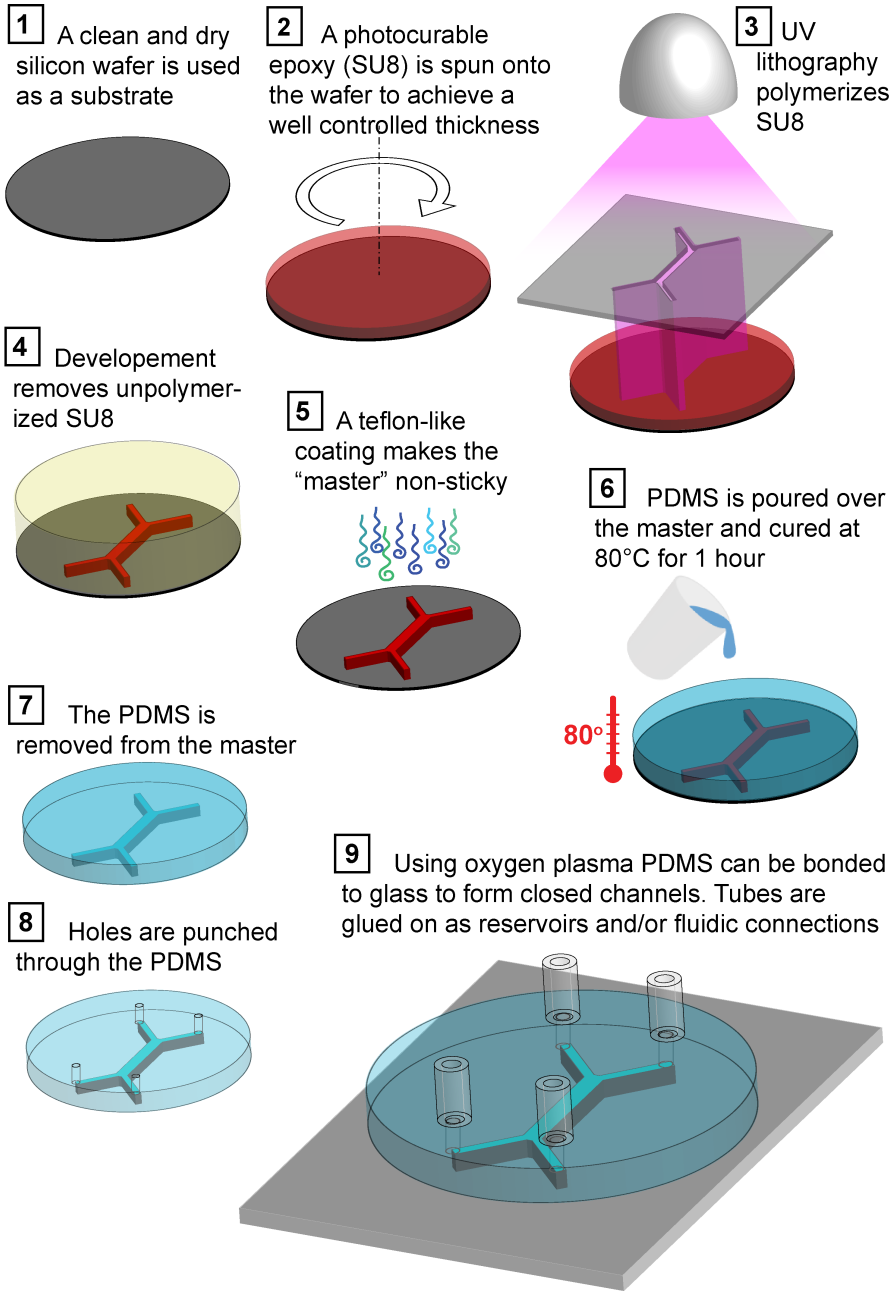

Figure 29 The basic processing steps of replica moulding. (A detailed description can be found in Appendix 4)

4.2.1 Silicone rubber and glass devices

Silicone rubber or polydimethylsiloxane, PDMS, is widely used to fabricate microfluidics devices using the method of replica moulding as developed by George Whiteside's group [135-139] and Stephen Quake [140]. PDMS is cheap, biocompatible and transparent in the wavelength range relevant for most fluorescent molecules (250nm – 1100nm). Importantly in the context of Paper I, it is an elastomer and in the context of Paper II, an electrical insulator.

The elastomeric properties of PDMS have been widely exploited in the microfluidics field, both for fabrication purposes and to achieve functionality in actual devices. Soft lithography is regularly done using PDMS stamps [135, 137, 141]. Yu *et al.* fabricated masters for replica moulding that could be inflated using gas pressure and were able to change the size and curvature of the resultant channels [142]. Various microfluidic components such as valves and pumps are made possible in multilayer devices [143] and Huh *et al* used the deformability of PDMS to create tuneable nano-channels [144]. Accelerometers [145], optical devices that use the deformability of PDMS to achieve tuneability [146-148] and stretchable electronics [149, 150] have also been reported. Deformable pillars and cantilevers in PDMS have been used to measure the forces that cells generate [151, 152] and a variety of other devices have been developed in which mechanical studies can be performed on cells [153-156]. In some cases the deformability of PDMS can be a limiting factor, high/low aspect ratios [135] or high pressures [157] can limit performance and should be considered at the design stage. In Paper IV relatively high pressures were used (1000mbar) but deformation of the device proved not to be a problem. Inglis reported a method based on thin layers of PDMS sandwiched between rigid glass slides that reduce the deformation of structures in fluidics channels [158] that could be useful in the event that deformation becomes a limiting factor.

As well as fulfilling the criteria necessary for our devices to function, the primary reason we chose to work with PDMS is the ease with which prototype devices can be fabricated. Designs, such as simple, straight microfluidics channels, can be taken from idea to functioning device in one working day, given access to all necessary equipment. More complicated devices such as those presented in Papers I-IV take longer to design, and requirements on the fidelity of device dimensions means that careful optimization of the process is often required, but the basic fabrication steps are identical.

A detailed description of the fabrication process and equipment needed is given in Appendix 3 and a summary in Figure 29. The basic idea of replica moulding is that a relief pattern is created on a surface, this can be in any resilient material with a non-sticky surface but we use SU8, a photo-sensitive epoxy resin. The pattern is created in the form of the desired fluidics channels. Liquid PDMS is poured over

this patterned surface and then cured. The cured PDMS, containing the channels, is removed from the mould, the channels sealed with glass or a flat sheet of PDMS and contacts made through which fluids can be injected and collected.

4.2.2 Constraints imposed by optical lithography and replica moulding

The following factors limit the range of feature sizes that we can use for our devices. The first limits are those imposed by optical lithography with SU8, which we use to fabricate masters. The resolution of the photo mask determines how well the posts can be positioned with respect to each other and this is usually on the order of a few 100 nm. SU8 structures can be fabricated at depths from 100nm to 100 µm with ease. Lateral dimensions however are limited to a minimum of 5-10 µm; the difficulty being to achieve vertical sidewalls, which are very important in DLD devices in order to ensure constant gap size over device depth. Most of the optimization done during fabrication is done while trying to achieve parallel walls. It is no problem to replicate features of this size in PDMS. What is important is that aspect ratios are kept within ~10:1, width to height (1:10 might also be a problem although we have not fabricated devices with these aspect ratios due the difficulty of fabricating the master in SU8). In the separation array this is never a problem due to the relatively small gap size. However, in order to make the connection of reservoirs to devices as easy as possible we add large inlet and outlet channels see Figure 27, and in these channels it is important to add supporting structures that keep aspect ratios below 10:1.

4.3 Surface coatings

In order to minimize the adhesion of particles to the inner surfaces of devices additions can be made to the buffers. Detergents such as sodium dodecyl sulphate (SDS) reduce the adhesion of polystyrene microspheres to PDMS. We used a 0.1% concentration in Paper II. Triblock copolymers bind to hydrophobic surfaces and reduce the adhesion of proteins and cells to PDMS [159]; they also reduce the adhesion of polystyrene microspheres in devices and Pluronics 127 at 0.1% was used in Paper I. Polyethyleneglycol (PEG) is also known to supress the adhesion of cells and proteins to PDMS. PEG is commonly grafted to poly-L-lysine that is positively charged. The resulting PLL-g-PEG thus easily binds to glass and other negatively charged surfaces (see Paper I of the related publications). All work with blood was performed in devices that were first treated with 0.2% PLL(20)-g[3.5]-PEG(2).

4.4 Running a typical experiment

The starting point for most experiments is a patterned piece of PDMS at the stage shown in step 7 of Figure 29. PDMS casts can be stored for as much as a couple of years in this state without any noticeable degradation. The final fabrication steps are normally performed within a day or two of the planned experiments. After plasma bonding of the device it is important to fill the channels with water as soon as possible as the hydrophilicity of the plasma treated PDMS significantly decreases over the course of a few tens of minutes. The glue we use to attach reservoirs takes ~1 hour to dry and so gluing is performed after first wetting the channels. When wetting channels the most important thing is to avoid trapping air bubbles, as these can be difficult to remove. Devices with several in/outlets are best filled from one inlet only until all channels are wetted. Once the glue is dry the reservoirs can be filled with buffer. The device is mounted in the microscope, connected to a pressure source and then flushed. When working with blood, at this point 0.2% PLL(20)-g[3.5]-PEG(2) is pumped through the device for several minutes. After flushing, the sample can be pipetted into the reservoir and the experiment performed. Wherever possible, buffers and other solutions used in the devices should be filtered to remove any particles that might clog the device. Avoiding the pumping of excessive amounts of fluid through the device prior to measurements can further minimize clogging. Also performing any surface modification or rinse steps by flowing from the outlets to the inlets ensures that any unwanted particles are trapped at the outlets where they cause much less of a problem than they would if they clogged the inlets. More specific information can be found in conjunction with each paper.

5 Papers I – IV Developing DLD devices

When this project started, DLD had been shown capable of size-based separations with high resolution. Our goal was to add functionality to DLD devices and by so doing broaden the field of application for the method. This chapter summarizes the work that is presented in Papers I-IV to those ends (the Papers themselves are appended).

5.1 Paper I - Using the elastomeric properties of PDMS to tune DLD devices

Paper I presents a proof-of-concept for a tuneable DLD device. The basic idea is that a DLD device, fabricated in PDMS, an elastomeric polymer, can be deformed and that this deformation will change *d,* the gap size between the posts, thereby making it possible to tune the critical size in a dynamic manner.

5.1.1 The advantages of tuneability

The advantages of tuneability are several. DLD is fully capable of separating 1.00 µm from 1.01 µm radius particles but it remains a challenge to design and fabricate a device with a critical size exactly in the right place, between 1.00 and 1.01 µm. What is normally done is that one hedges ones bets by designing and fabricating devices with many separation parameters that cover the range of interest, in this case from 0.8 µm to 1.2 µm for example. But in order to ensure that one critical size hits the target (between 1.00 and 1.01 µm) the steps in critical size should be on the order of 10 nm or smaller, which can mean many steps and very long devices. If we instead fabricate a tuneable device with a critical size near to 1 µm (within the dynamic range of the device) then we can tune the critical size to the desired value based on observations of the actual separation performance. *Tuneability*, together with continuity, would make it possible to perform separations with live feedback, where for example image analysis is used to evaluate the results of a separation and the running parameters are adjusted accordingly in order to reach the desired outcome at each given point in time. This

can be a powerful tool in the analysis of biological systems that are in their nature dynamic.

Tuneability can also be useful when the effective size of the particles in the system of interest is not fully known or when they change with time and experimental conditions. It is also useful when the separation properties of the devices change in time due to sticking of particles or proteins to the inner surfaces of the device, the effect known as fouling. The situation is summed up in the review by Toner *et al.* [53] for the case of blood-cell separation in microfluidic devices, '…they are not very accommodating to changes in properties of the samples being separated. Separating target cells of new size usually requires a new design or at least a new device with modified dimensions'. Toners statement is certainly true for DLD, where the size and shape of the cells change depending on experimental conditions and as they grow.

The ability to change the critical size in a device also makes it possible to switch the lateral displacement of specific particles on and off. This could be used for label-free, particle specific switching for example to control the local chemical environment of the particles.

5.1.2 Stretching PDMS

Stretching, squeezing, bending or shearing the block of PDMS containing the DLD array are ways by which stress can be applied and will result in a strain, or in other words a change in the geometry of the array. We choose to create strain in a device by stretching it and designed and built a chuck to do this, see Figure 2 in Paper 1 and Appendix 4. This chuck was designed to hold a device in a microscope, allow for connections to pumps for pressure control and to apply controlled stress during on going separations. If a force, F_n, is applied normally to one face of a block of PDMS, with cross sectional area A, then (if the opposite face is fixed) the stress, σ, is given by:

$$\sigma = \frac{F_n}{A}. \tag{23}$$

This stress will give rise to an elongation *dl* of the PDMS block. If the initial length of the block was l_0 then we can define a strain ε as:

$$\varepsilon \equiv \frac{dl}{l_0} = \frac{\sigma}{E}. \tag{24}$$

Where E is Young's modulus. The strain generated globally by stretching the entire block of PDMS is mirrored on all scales as depicted in Figure 30. Using the setup shown in Appendix 4, for example, it is relatively easy to change the length of a ~1cm long device by ~10 μm. This gives a strain of $\varepsilon = dl/l = 10 \cdot 10^{-6}/10^{-2} = 0.1\%$,

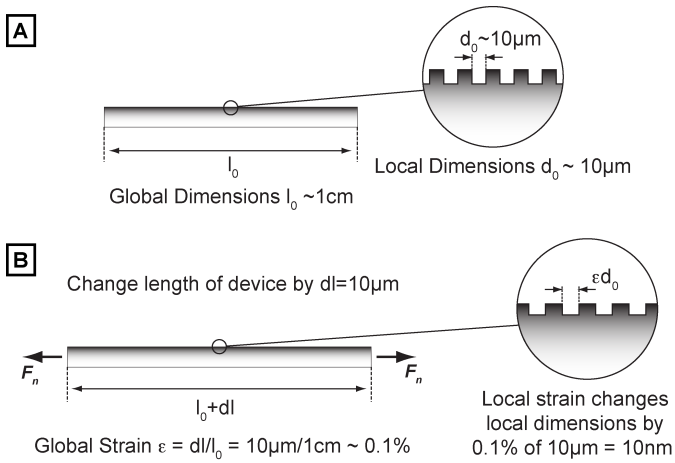

Figure 30 Deformation of an elastomer occurs at all scales. (A) The global dimensions of the device can be several centimetres and the local feature size is most often ~10μm. (B) If a global strain is applied then it gives rise to an equal local strain. Global strains of 0.1% are easy to achieve by stretching a device. This relates to a change in local dimensions of ~10nm.

which relates to a change in the inter-post distance *d* of ~0.1%·10 μm~10 nm in an array where the posts are ~10 μm apart.

Note about Poisson's ratio: Poisson's ratio, γ, is the ratio of the transverse strain, or the contraction of the material perpendicular to the applied stress, to the axial strain, or the extension of the material in the direction of the applied stress,

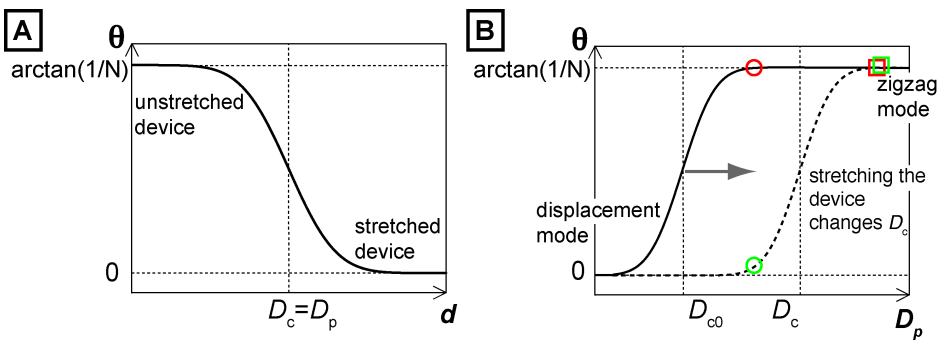

Figure 31 The effect stretching has on the behaviour of particles in a DLD device. (A) The trajectory of a monodisperse population of beads with diameter D_p in a device with $D_{c0} < D_p$. As d and therefore D_c is increased the beads make the transition from the displacement mode to the zigzag mode. At the inflection point the critical size is equal to the size of the beads. (B) The trajectory of beads in a device as a function of particle size. Stretching moves the curve, making it possible to choose D_c to suit the system one wishes to separate. Before stretching, particle larger than D_{c0} (red circle and square) are not separated. After tuning they can be separated (green circle and square).

$\gamma=\varepsilon_{trans}/\varepsilon_{axial}$. *PDMS is an ideal elastic material and has a Poisson's ratio of 0.5. This means that the volume does not change under deformation and that for stretching in the x direction* $dl_y/l_{y0}=dl_z/l_{z0}=-0.5\cdot dl_x/l_{x0}$. *This means that as the device is stretched such that d increases the distance between the rows and the depth of the device will decrease. As far as the distance between rows is concerned it has no effect on* D_c. *The stretching will change the angle* $\theta = \arctan(\Delta\lambda/\lambda)$ *and should be considered when observing trajectories. However because the positions of the outlets also change, there is no change in the relative positions of the particles as they exit the device. This transverse contraction will also affect the depth of the channels. The importance of device depth is described in Papers III and IV. Care should be taken that particles do not become trapped due to decreases in device dimensions due to transverse contractions.*

5.1.3 Changing the critical size

Figure 31 shows the effect that stretching has on the trajectories of particles. Figure 31A shows how a monodisperse population of spherical microspheres that are larger than the critical size in the unstretched device are displaced. As the device is stretched and *d*, the gap between the posts, increases the critical size increases according to Equation 26. As the critical size in the device is scanned across the size of the particles they make the transition into the zigzag mode. For monodisperse particles the width of this transition is due solely to a distribution in the critical size in the device stemming from irregularities in the array geometry and on diffusion. A distribution in particle sizes will also contribute to this broadening. Figure 31B shows how the trajectory of a particle depends on its size (solid line) and how stretching the device moves this curve (dashed line). Tuning is performed in the following way. The red circle and square represent particles that are both larger than the critical size. They are consequently both in the displacement mode and cannot be separated. By stretching the device, the critical size can be increased until the smaller of the two particles falls into the zigzag mode at which point separation occurs as shown in green. In Paper I we demonstrate this using polystyrene microspheres of 10 μm and 16 μm diameters.

5.2 Dielectrophoresis in DLD devices

Paper II provides the first demonstration that DLD can be used for separations based on parameters other than size. The idea is that particles very close to the critical size are very sensitive to small perturbations that might cause them to switch between zigzag and displacement modes. This means that very small, short-range interactions can be greatly amplified by the mechanism of DLD. In this particular example we amplify short-range dielectrophoretic forces.

Dielectrophoresis is the movement of polarisable particles due to the forces they experience in a non-uniform electric field as described in chapter 2.3.4. Since Pohl's first particle manipulations using DEP in the 1960s [110-113], the technique has developed in two main directions. Non-uniform electric fields have been generated in two ways, either using the geometries of electrodes [160] or by modifying the field using insulators [161]. The introduction to Paper II reviews the fields of Electrode-based and Electrodeless or Insulator-based DEP.

Briefly, Electrode-based methods can be catagorized as batch methods that only deal with samples one batch at a time; DEP migration [113, 162], DEP affinity [163] and DEP field flow fractionation (DEP FFF) [164, 165], or as continuous methods; Travelling Wave DEP (TWDEP) [163, 166, 167] and Isomotive Nonuniform Field DEP [168, 169]. DEP forces have also been used for the barriers needed to focus and switch particles in microchip-based flow cytometers [168, 170-172].

5.2.1 Insulator-based DEP in PDMS devices

Electrodeless or insulator-based DEP (I-DEP) is based on the ability of insulating obstacles, placed between electrodes, to deform the electric field. The insulator-based approach has several advantages when compared to electrode-based methods. Complex channels with insulating constrictions can easily be fabricated in PDMS using soft lithography or alternatively in thermoplastics using imprint-lithography or injection moulding as described in chapter 4.2. While these same steps are used to fabricate the channels for electrode-based methods the integration of electrode arrays requires additional fabrication steps. Electrodes are prone to fouling and running electrodes at low frequencies can cause electrolysis, which can affect buffer composition and pH, degrade electrodes and lead to bubble formation, which for microfluidic systems can be detrimental. Insulator-based methods make it possible to position electrodes in reservoirs at the ends of the device or to position integrated electrodes [173] well away from microchannels and structures where bubbles can cause problems and these devices can therefore be run at low frequencies and even at DC, see Appendix 4 for details of the experimental setup. While the correct choice of electrode configuration can create extremely high field gradients these gradients are localized near to the surface of the electrodes and DEP forces fall off quickly in the channel above the electrodes. However, the electric field in an insulating constriction is modulated through the entire depth of the channel, perpendicular to the direction of constriction.

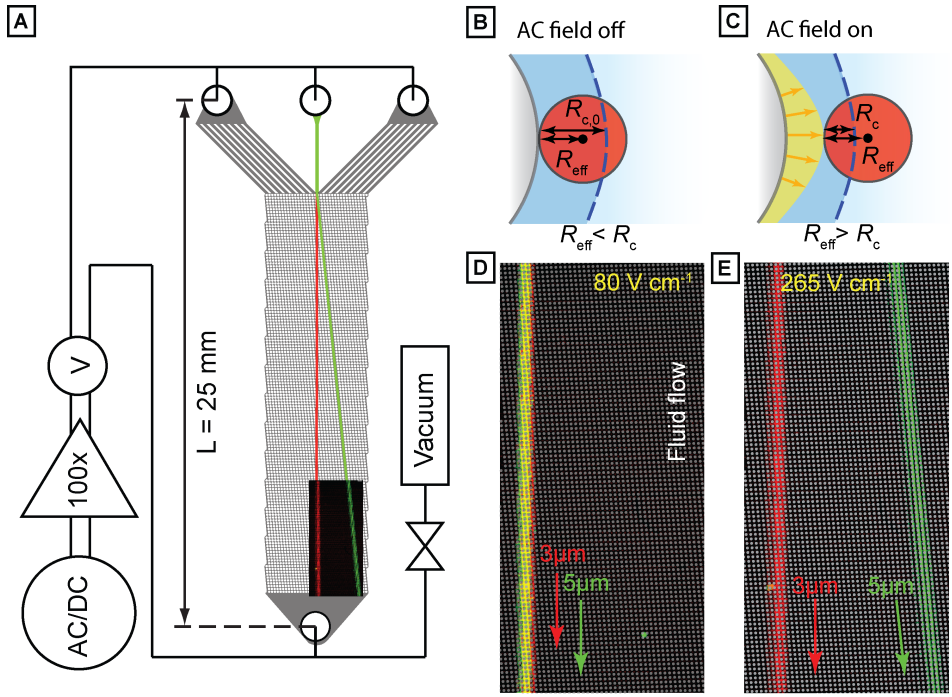

Figure 32 Applied AC electric fields change the critical size in DLD devices. (A) The red and green particles are smaller than the critical size in the device and follow the flow. (B) The DEP force is volume dependent and therefore greater for the larger particle which is forced into the displacement mode. (C) A micrograph taken at two wavelengths and averaged over 500 frames of 3 μm (red) and 5 μm (green) diameter polystyrene beads moving with the pressure-driven flow from left to right through a device with Dc0 = 6 μm shown relative to the device and fluidic and electric connections. (D) In this case the beads are hydrodynamically focused into a stream of approximately 200 μm in width. An AC field at 100 Hz with a magnitude as high as 80 VRMS cm-1 has no effect on the trajectories of the particles. The grey overlay highlights the location of the posts. (E) Same as previous image but at 265 VRMS cm-1 3 μm < Dc < 5 μm and the 5 μm beads have therefore made the transition from the zigzag mode to the displacement mode.

5.2.2 DEP forces tune the critical size in DLD devices

When an electric field is applied along a post array the field lines become squeezed together in the constrictions between the posts as described in chapter 2.3.4. This generates areas of high field gradient exactly at the decision point for particle sorting, and highest at the surface of the post. A particle with a negative Clausius Mossotti factor will experience a force away from the surface of the post as it flows past. Consider a particle that is below the critical size in the device, like the red and green particles in Figure 32A. The velocity of the particle past the post determines the time that the DEP force acts on the particle. Given

sufficient time the DEP force will push the hydrodynamic centre of mass of the particle out of the first lamina and into the second, as shown in Figure 32B for the green particle. The result is that DEP can be used to force a particle to move in displacement mode that would otherwise move in zigzag mode.

Because the DEP force is proportional to the volume of the particle it requires a smaller field to push larger particles into the displacement mode than smaller particles. Figure 32D shows 3 µm and 5 µm particles (red and green respectively) moving through a device with a critical diameter of 6 µm with an applied field of 80V cm^{-1}. Being smaller than the critical size both bead types are in the zigzag mode. When the field is increased to 265V cm^{-1} the 5 µm beads make the transition into the displacement mode and they become completely separated from the 3 µm beads. In Paper II we show how even the 3 µm beads transition into the displacement mode as the field is further increased.

While we show that it is possible to tune size-based separations of otherwise identical particles in DLD devices using DEP we also argue in the outlook that we would like to use the devices to separate particles that are the same size but that differ in polarizability, such as live and dead cells.

5.2.3 Surface charge-based separation

We have since performed experiments with beads of very similar sizes but with different charged groups on their surfaces (unpublished results). Figure 33 shows two types of beads being separated in a device very similar to that used in Papers III and IV but with critical diameters ranging from 1 µm to 4.5 µm in steps of 0.5 µm. 2.0 µm beads with carboxylate surface groups are shown in red and

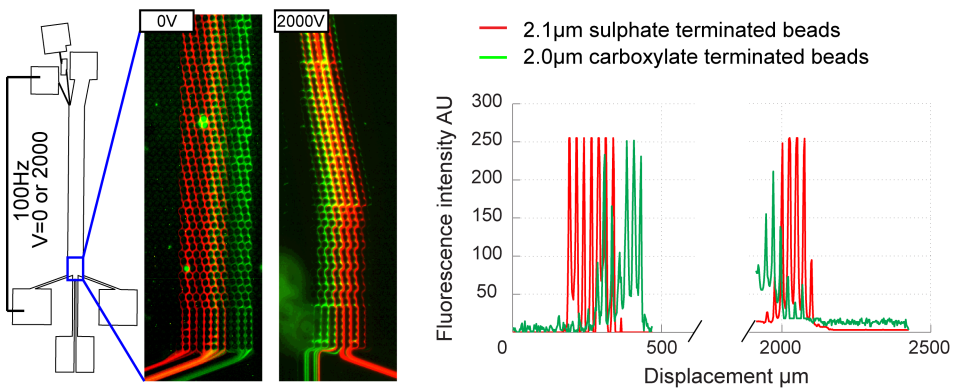

Figure 33 Separation based on surface charge. At zero applied voltage 2.1 µm beads (green) are displaced to a greater extent than the 2.0 µm beads (red). When a voltage of 2000 V is applied across the length of the device instead the 2.0 µm beads, which are more negatively charged due to carboxylate surface groups, are displaced to a greater extent than the 2.1 µm beads which have sulphate surface groups and are less negatively charged.

2.1 μm beads with sulphate surface groups are shown in green. The carboxylate beads are much more negatively charged than the sulphate beads.

With no applied electric field the marginally larger 2.1 μm sulphate beads are displaced more than the 2.0 μm carboxylate beads. The striped appearance of the particle distributions is due to the fact that the device consists of sections containing different critical sizes and that the beads have a dispersion in diameter. The device creates one fraction containing 2.0 μm beads only, one fraction containing both types of beads and one fraction of 2.1 μm beads. When a voltage of 2000 V at 100 Hz is applied across the ~2 cm long device both bead types are displaced by considerably more. The 2.0 μm, carboxylate beads are however, despite being smaller than the sulphate beads, displaced even further. While we have as yet not measured (or calculated) the f_{CM} for the two types of beads these results show that particles can be separated based on a difference in the surface groups using our method. We believe that the frequency dispersion in f_{CM} can be used to perform separations of cells based on differences in dielectric properties.

5.3 Separating parasites from human blood

Papers I and II dealt with spherical particles but as we discussed in chapter 1 many different types of biological particles are non-spherical. The red blood cells and *Trypanosoma cyclops*, shown in Figure 34, are good examples. Paper III presents the first example of the use of particle shape to greatly improve particle separation in DLD devices.

The diagnosis of Human African trypanosomiasis, caused by *Trypanosoma* parasites [174][26] relies on finding parasites in the blood, a difficult task as explained in Paper III. Standard parasitological techniques currently used are estimated to give false negatives in 20-30% of cases [175].

In order to avoid the use of dangerous drug treatments [176] it is essential to diagnose the disease in its early stages when parasites are present in the blood at very low concentrations in a huge background of blood cells. Most of the current methods are focused on increasing the trypanosome concentration by removing the background cells, predominantly RBCs. Given that 1 ml of blood might contain

[26] Sleeping Sickness in humans is caused by *T. brucei* which is morphological very similar to *T. cyclops*. Because of the dangers and strict regulations when working with *T. bruccei* we used *T.cCyclops* as a model organism.

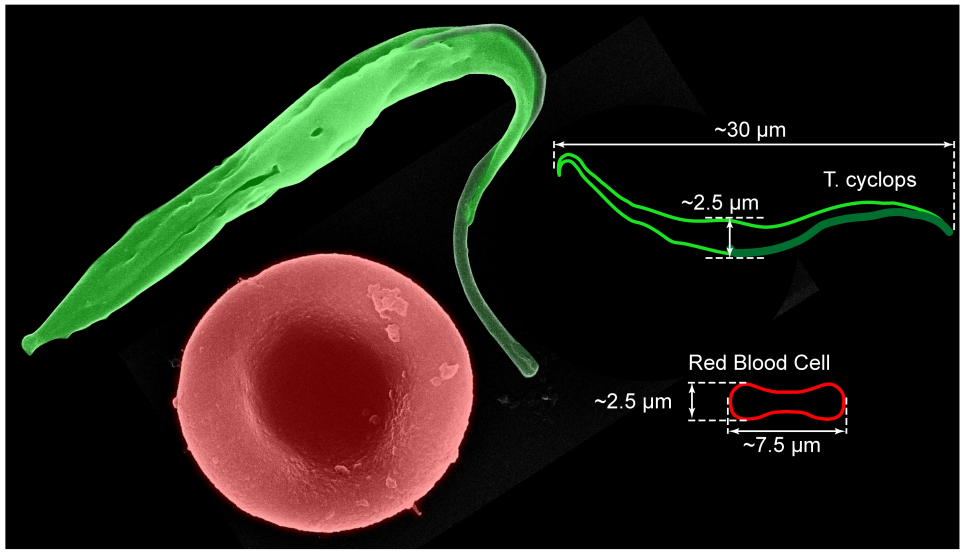

Figure 34 Scanning electron micrograph of a T. Cyclops *and an RBC. The similarity in the thickness of the cells make it difficult to separate them in standard, deep DLD devices.*

fewer than 100 parasites [30], but on the order of $5 \cdot 10^9$ RBCs, $0.35 \cdot 10^9$ platelets and $7 \cdot 10^6$ WBCs the task is not trivial.

Currently the best trypanosome separation technique is the mini-Anion-Exchange Centrifugation Technique (mAECT), which has been reported of having a detection limit of 100 trypanosomes per mL of blood. This method exploits the negative surface charge of RBCs to remove them from a blood sample while neutrally charged trypanosomes pass through the column and can then be concentrated by centrifugation. A large field-study in 2004 concluded the sensitivity of mAECT to be 75.3%, cost per test almost €3 and time per test half an hour [177]. Beside the cost, the test is not ideal for use in the resource-poor regions where the disease is endemic due to the need of bulky equipment and trained personnel.

A cheap, portable microfluidics device, able to rapidly and reliably find parasites in blood, would have a large impact on the treatment of this much-neglected disease. The fact that trypanosomes differ in multiple biophysical ways from blood cells (including surface charge as previously exploited in anion exchange chromatography), size, shape and motility offer the potential for new routes to separation of trypanosomes from blood cells using new advances in microfluidics. Our approach is to develop DLD devices capable of performing this task based on the size and shape of the blood cells and parasites. The width of the parasites is almost identical to the width of the RBCs, see Figure 34, making

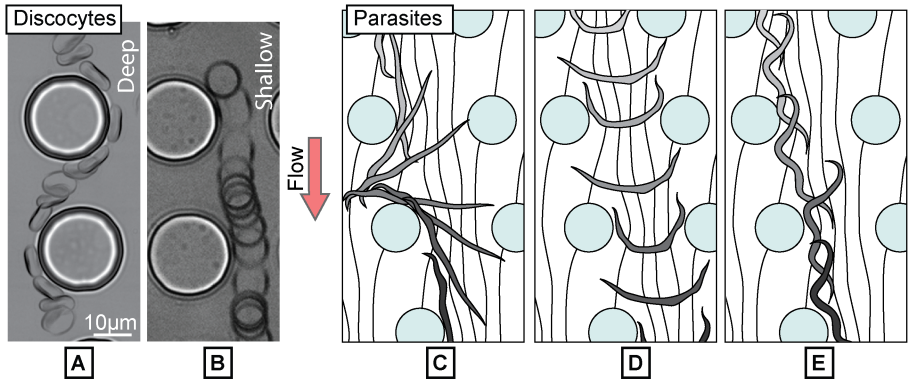

Figure 35 Modes of transport through DLD arrays for disc-shaped particles (RBCs) and long soft particles (parasites). (A) Given enough space, RBCs rotate and their thickness determines their effective size. (B) In a shallow device RBCs are unable to rotate and their effective size is determined instead by the diameter across the disc. (C) The long thin parasites rotate also but are influenced by many flow streams, which increases their effective size. (D) After rotating the parasites often become trapped in a u-shape between posts, this gives them the maximum possible effective size. (E) Parasites are often bent which also increases their effective size. The bent shape can be static or dynamic (due to constant motion of the flagella). Flagella motion gives the parasite a larger average size.

separation in conventional DLD devices very difficult and necessitating a new approach.

5.3.1 Optimizing DLD devices for parasite detection

In starting this project we were aware of the similarity in the thickness of both RBCs and parasites and of the difficulties this would entail due to alignment giving the cells identical critical sizes as described in chapter 3.4.1. Based on the results of previous work[27] with RBCs in which we controlled their effective size by controlling their orientation we believed that DLD devices could be developed in which the effective sizes of RBCs and parasites would differ enough for separation to occur.

Our approach was to use the depth of the devices to limit the amount by which cells become aligned. The effect of device depth on the orientation and effective size of RBCs can be seen in Figure 35A and B. In deep devices (deeper than the largest dimension of the particles), RBCs assume an orientation perpendicular to the device as they pass through the decision point, so that the *thickness* of the cells determines their effective size. In a shallow device (shallower than at least one

[27] J. P. Beech and J. O. Tegenfeldt, *Shape-based particle sorting – a new paradigm in microfluidics*, The 13th International Conference on Miniaturized Systems for Chemistry and Life Sciences, Jeju, Korea, 2009, 800–802.

dimension of the particles) however, the RBCs are forced to move with the disk in parallel with the device, so that the *overall diameter* of the RBCs determines their effective size. We predicted that parasites, being long and narrow would not experience the same increase in effective size in shallow devices and that we could use the approach to achieve separation; as it turned out, depth also effected the behaviour of the parasites but fortunately in a way that we were able to exploit to improve separation.

While testing devices of various depths we found that the long, thin parasites moved in a manner very different from spherical or disc-shaped particles. Figure 35C-E give an overview of how the parasites move through the device used in Paper III. Parasites rotate in the array just like RBCs. Their length however, 33.5 µm, is large compared to the gaps between the posts, which is 12 µm throughout the device. In devices that are as deep or deeper than the length of the parasites they are able to rotate such that their effective size is minimized and they take very similar trajectories through the device as the RBCs do, meaning that they are not separated. As the device depth is decreased interactions between the walls of the device and the parasites increase as with the RBCs. However, because of the long, thin shape of the parasites, rather than becoming simply aligned as the RBCs do, the parasites begin to interact with the posts and the pattern of flow streams in a few specific new modes, shown in Figure 35C-E, that dominate their behaviour.

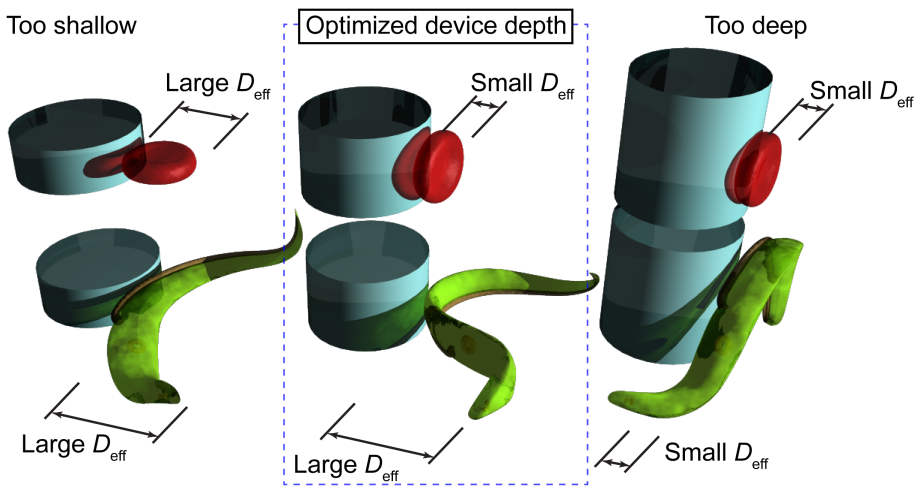

Figure 36 In very shallow devices (4.5µm) both RBCs and parasites have a large effective size and separation is poor. In deep devices (30µm) separation is also poor due to the similarity in the thickness of the cells. The optimum device depth for separation of these particles is a depth that allows RBCs to orient themselves such that they adopt their smallest possible effective size, but shallow enough that the effective size of the parasites is maximized by the effects shown in Figure 35.

Each of these modes confers an increase in the effective size of the parasites and the shallower the device is, the larger the increase becomes improving the separation between parasites and RBCs. This improvement continues until the device reaches a depth of ~8 μm, at which depth the RBCs also experience confinement and their subsequent increase in effective size again reduces the effectiveness of the separation. Figure 36 illustrates the overall behaviour of the cells at different device depths. In Paper III we compared three devices with depths of 4 μm, 11 μm and 33 μm. We define F_p as the fraction of trypanosomes at the exit of the device from which 99% of RBCs have been removed and use this as a figure of merit for the performance of the devices. Table 3 summarizes the results of the separations at the three device depths. The table shows the total distance the cells are displaced, the effective sizes (diameter) that this relates to and the performance in each case, given by F_p. In our particular device, the separation was most effective, by a considerable margin, at a device depth of ~11 μm[28].

Table 3 A summary of the results from Paper III.

Device depth [μm]	Total displacement [μm]		Effective size [μm]		F_p [%]
	RBCs	*T. cyclops*	RBCs	*T. cyclops*	
4	944±123	1386±424	~5-6	~5-9	53
11	36±44 24±75*	980±330 841±259*	≤3 ≤3*	~4-7 ~4-6*	99.5 99.6*
33	9±23	66±105	≤3.5	≤5	14

*values obtained for concentrations equivalent to whole blood, lymphocytes have an effective size of ~6.5-7.5 μm and were also separated from the parasites.

5.3.2 Easy to use high-throughput devices

The device presented in Paper III was developed in order to find device parameters that can be used to achieve the separation of parasites from RBCs. In order for a diagnostic device to be of use in the field it must be able to detect parasites at extremely low numbers. For example at some periods during HAT infection the levels of parasites in the blood can be as low as ~100 per ml. This means that somewhere in the range of 100 μl to 1 ml might need to be processed and this should preferably be done in a few tens of minutes. The exact volume depends on the fraction of parasites that evade detection in the device, which

[28] We expect the difference in the effective sizes of RBCs and parasites to increase further as the device approaches 8 μm in depth although we have yet to varify this.

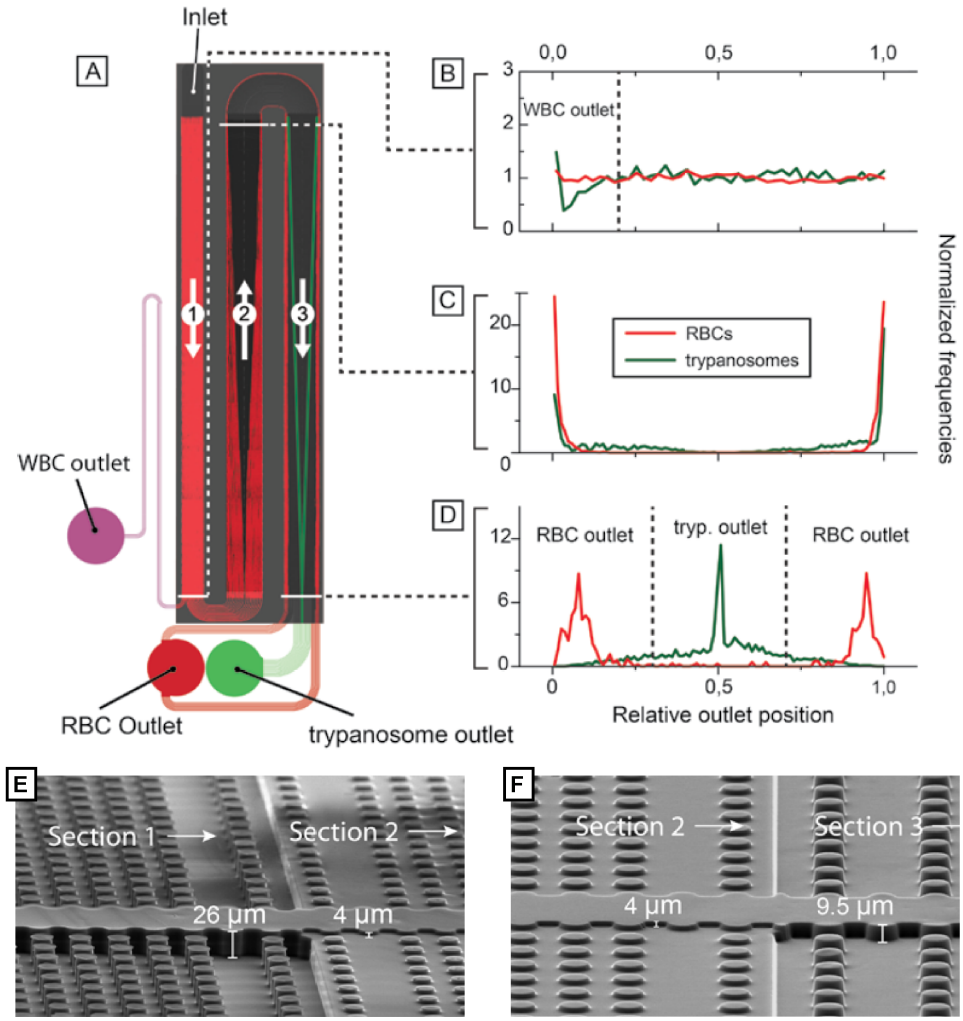

Figure 37 (A) An overview of the device with an overlay of a mosaic-image (coloured red) created by multiple time-integrated micrographs of RBCs travelling through the device. The path of the trypanosomes overlap the RBCs until section 3 were they diverge, as illustrated by the green lines. (B-D) Measurements of the RBC and trypanosome frequency after each of the three sections. No displacement occurs for RBCs and trypanosome in the first, deep, section were WBC are removed. In the second, shallow, section both cell types are laterally displaced to the side of the channels creating a cell-free stream in the centre. The third section is identical to the second, except for the depth. This increased depth together with the shear field of the fluid act to align the RBCs against the posts decreasing their effective size from ~7.5 µm (the diameter) to ~2.5 µm (the width). The increased depth is however not enough to affect the behaviour of the longer trypanosomes which continue to be laterally displaced, this time towards the centre. (E and F) Show SEM images of the transitions between section 1-2 and 2-3 respectively. (Figure adapted from S. H. Holm, J. P. Beech, M. P. Barrett and J. O. Tegenfeldt, Multiple depths in a deterministic lateral displacement device for field-diagnosis of sleeping-sickness, The 15th International Conference on Miniaturized Systems for Chemistry and Life Sciences, Seattle, Washington, USA, 2011, 527–529 by kind permission from Stefan Holm.)

needs to be known and taken into account in order to avoid false negatives. For example finding just one parasite is proof positive of infection but care must be taken when calculating how much blood is analysed before concluding that the patient is parasite free with a high level of confidence. This device however was not optimized for high throughput since the sample is focused into a very narrow stream; see the discussion in chapter 4.1.4.

We are currently developing multi-layer, high throughput devices that do not require flow focusing and are therefore very easy to use[29]. The aim is to increase the throughput, sensitivity, robustness and ease of use of these devices such that they might find use as diagnostics tools in the field where they are most needed.

5.4 Size, shape and deformability based separations

Morphology has been used successfully for centuries for classification of species across all kingdoms of life ranging from bacteria to mammals and identification of disease through histological samples. During the past decades there has been an increasing fundamental interest in the connection between the shape of cells, their overall function and the underlying molecular networks. Characterization of cell shape is typically carried out using microscopy by direct observation. Automated imaging cytometry systems have been developed for increased throughput (for example Amnis, Cellavision and CompuCyt). Optofluidics devices have been used to simplify the imaging and to improve resolution. However for cell sorting immunostaining followed by FACS remains the main workhorse. Although a highly powerful technique it does not give any accurate morphological information. Deformability of cells is also an important clinical indicator of a wide range of medical conditions as discussed in chapter 1.

Despite the importance of shape and deformability, and the possible benefits of microfluidics-based methods sensitive to these parameters, few approaches have been successful. In fact, no microfluidics based methods have been developed that are able to both measure the size, shape and deformability of particles and to separate the particles based on these parameters. In Paper IV we demonstrate how DLD devices can be used to approach this problem and present the first

[29] S. H. Holm, J. P. Beech, M. P. Barrett and J. O. Tegenfeldt, *Multiple depths in a deterministic lateral displacement device for field-diagnosis of sleeping-sickness*, The 15th International Conference on Miniaturized Systems for Chemistry and Life Sciences, Seattle, Washington, USA, 2011, 527–529

continuous, passive method that is sensitive to size, shape and deformability and potentially able to deal with the large numbers of cells necessary for diagnostics on a single cell basis.

5.4.1 Measuring the shape and deformability of cells

The mechanical properties of individual cells have been measured using a variety of methods such as micropipette aspiration [178, 179], atomic force microscopy [180], electrodeformation [181], magnetic twisting cytometry [182], optical tweezers [183] and optical stretchers [184] and while these methods allow the detailed study of small numbers of cells their throughput and therefore application to diagnostics is limited. A method with higher throughput that found some clinical use in the 1980s is membrane aspiration [185, 186] where blood is forced through a membrane in which pores are smaller than the size of the cells and the fluidic resistance is measured. Although this method is inherently simple, both size and deformability contribute to results and only average values are measured. Due to the small size of the pores, clogging can also be a problem. Similarly, methods such as flow cytometry and ektacytometry give bulk values of size and spherical eccentricity [187], and deformability [188] respectively for large populations of cells but neither method is capable of picking out subpopulations that differ in either shape or mechanical properties.

Techniques that use shear forces such as those caused by laser cavitation bubbles [189], flow through microcapillaries [190] and in a rheoscope between counter-rotating discs [191] give information on the mechanical properties of cells and, at least in the case of the rheoscope, are able to measure distributions in mechanical properties. These methods rely heavily on image analysis, which ultimately limits the number of cells that can be analysed per unit time. Furthermore they are purely analytical methods and cannot be used to perform separations.

Microfluidics based methods were covered in chapter 1.

5.4.2 Sorting cells by size, shape and deformability using DLD

In reference [7] Davis *et al* note that flow velocity affected the critical size of RBCs in their DLD devices. In the supporting information they show how the amount of displacement decreases for increasing flow velocities and speculated that this could be due to preferential orientation of the cells or to deformation of the cells into a “sausage shape”, but no efforts to exploit this behaviour were reported. Building on this work we have since shown (Paper III) that orientation is indeed important. In Paper IV we look closer at particle orientation and also explore particle deformation and the effect it has on particle trajectories in our device as driving pressure and the resulting shear forces are changed.

Due to shear forces from the carrier fluid and normal forces from the stationary posts, a deformable particle will change shape as it moves through a device as shown in Figure 38A and B. A change in driving pressure from 5 mbar to 800 mbar corresponds to average flow velocities in the range 110 $\mu m \cdot s^{-1}$ to 18 $cm \cdot s^{-1}$ and wall shear rates (the maximum rate at the surface of the posts) in the range 100 to 16400 s^{-1} for the ~11 μm deep device used in Paper IV. Although by no means simple, the deformation caused by shear stresses at these rates of shear can to first approximation be simplified to an elongation along the flow direction together with a compression of the particle perpendicular to the flow direction at the decision point, which decreases the effective size of the cell. This decrease in the effective size changes the trajectory of the cell and can be detected as a change in the position of the cell as it exits the array.

Gradually changing the rate of shear by changing the driving pressure and looking at the resulting change in the position of the cells at the end of the device, is equivalent to measuring the strain as a function of the applied stresses and we can thus gauge the deformability of cells and also find optimum parameters for the separation of subpopulations based on mechanical properties. What is more, controlling the orientation of the cell as presented in Paper III we could probe any anisotropy of the deformability.

The central concepts that we put forward in Paper IV are the following. Cell size, shape and deformability all affect the trajectories of cells through DLD devices. If we perform particle separations in DLD devices at low rates of shear, particles retain their shapes and can be separated into size-based fractions where it is the smallest dimension of the particle that most often defines this size. Changing the depth of the separation device allows us to control the orientation of particles as they move through our devices allowing us to perform measurements on different particle dimensions giving us the ability to infer information about particle shape and to leverage shape for separation. Lastly, by changing the rate of shear and looking at the resulting change in the effective size of particles we can gauge their deformability and also find optimum parameters for the separation of subpopulations of more or less deformable particles. All in all this gives us the ability to choose the relative contributions of size, shape and deformability to the behaviour of particles in our devices making possible applications such as the analysis, concentration or separation of particles based on any combination of these parameters.

5.4.3 RBCs as a model system

We evaluated our method using RBCs. The morphologies of RBCs are in many cases indicative of clinical conditions such as various types of anaemia. The mechanical properties of RBCs are also of great interest and a Mokken *et al* review the many factors affecting RBC deformability [192]. We also discussed in

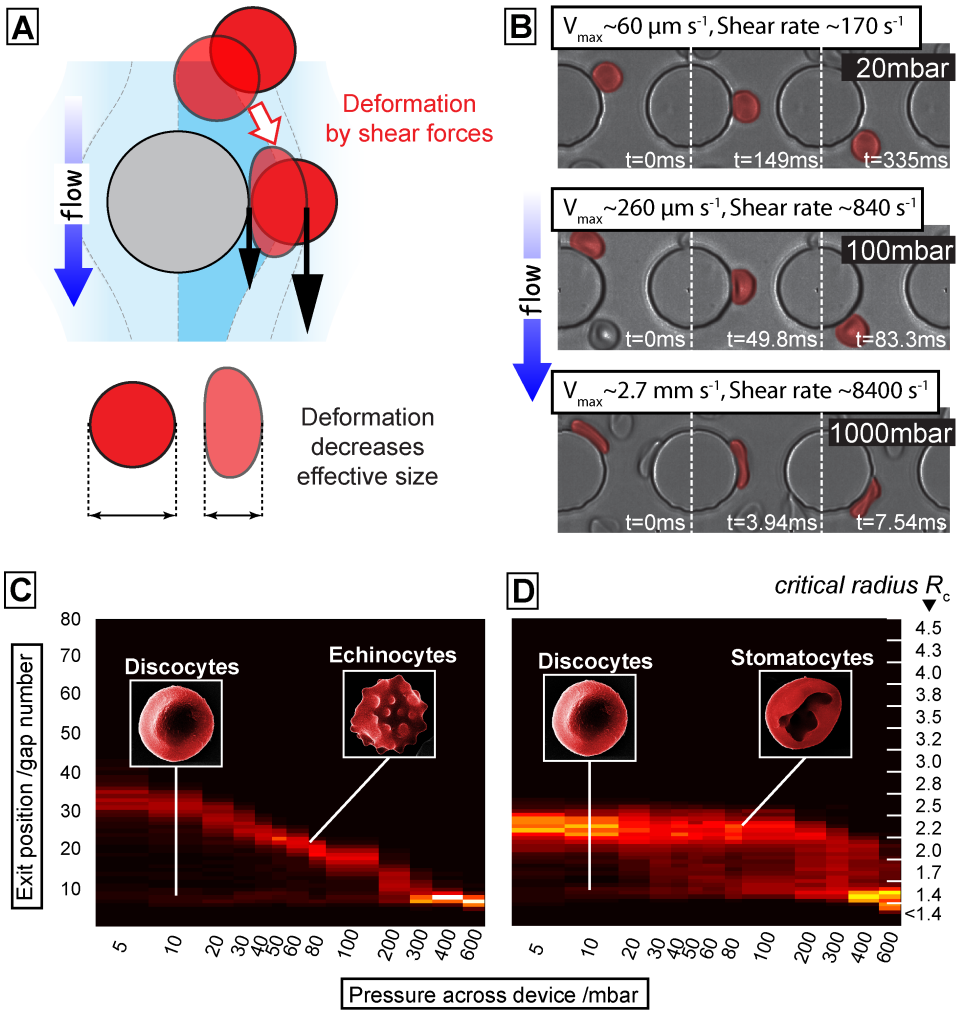

Figure 38 Deformation of cells and cell fingerprints. (A) As a cell moves through the decision point it is deformed by shear forces and the effective size decreases. (B) The shear stress on a cell can be varied by varying the driving pressure. Using a high-speed camera we can verify the deformation of the cells at the decision point. (C and D) By plotting the exit position (effective size) of many cells as the shear rate is varied we acquire characteristic fingerprints for different cell types. These fingerprints hold much information about the size, shape and mechanical properties of the cells. We see for example subpopulations of cells with different shapes and also the slope of the curve tells us that echinocytes are more deformable than stomatocytes.

earlier chapters how malaria affects the stiffness of RBCs. As well as being clinically relevant in their own right, because RBCs are both readily available and their shapes and mechanical properties are easily changed they constitute an

excellent model system for cells in general although it is important to keep in mind that they lack a nucleus and are therefore very much simpler than most other cells.

RBCs are, under normal physiological conditions, biconcave discs. In order to move through the cardiovascular system, which is in many places smaller than the disc-shaped cells, they must be able to readily deform. What is more, many agents are known to cause RBCs to change shape and deformability. Cationic amphipaths, low salt and low pH [193, 194] for example cause the formation of more spherical RBCs, with mouth-like invaginations, known as a stomatocytes. Anionic amphipaths, high salt, high pH [193, 194], ATP depletion and interaction with glass surfaces result in crenated, or spiky, RBCs known as echinocytes. This series of shape changes is known as the stomatocyte-discocyte-echinocyte main sequence. The shapes and the order in which they occur is independent of the agent used and the main sequence is therefore considered to be universal [195]. Examples from this main sequence are shown in the SEM images in Figure 39. Lim *et al* [195] used the bilayer couple theory originally proposed by Sheetz and Singer [23] to explain why these shape changes occur.

The membrane of the living cell is commonly described by the fluid mosaic model [196]. The cell membrane consists of a two-dimensional fluid of phospholipids, a bilayer, into which proteins and protein complexes are incorporated. The most prominent model used to explain RBC shape, the bilayer couple theory [23, 195] relies on an asymmetry in composition between the two leaflets of the bilayer so that they will react differently to perturbations while remaining coupled to one another. If for example the area of one leaflet is altered relative to the other the resulting strain in the other leaflet will be relieved by bending the bilayer in analogy to the bending of a bimetallic strip upon heating. This bending can have a dramatic effect on both the shape of the cell, as can be seen in Figure 39, and on its mechanical properties. In the current work we use sodium salicylate and Triton X-100 to modify the relative areas of the leaflets and thereby the shapes of RBCs.

5.4.4 Sodium salicylate and Triton X-100 change the morphologies of RBCs

Sodium salicylate (SS) is an aspirin derivative. It is known to incorporate into the outer leaflet of the RBC and is therefore an echinocytic agent. Concentrations of SS significantly less than 2 mM lead to the formation of a population of echinocytes with a broad distribution in shapes including stomatocytes, discocytes and echinocytes [5]. It is believed that this spread in morphologies stems from the distribution in cell age, cytoskeletal differences and/or metabolic rate. As the concentration of SS is increased the mean shape of the populations is driven towards the echinocytic. At 2mM 98% of RBCs will adopt echinocytic forms, with the remaining 2% keeping there discocytic shape [5].

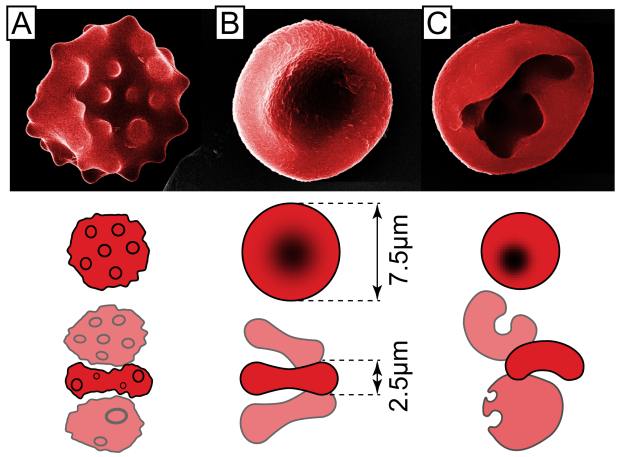

Figure 39 False coloured SEM images showing how the morphologies of red blood cells can be altered by the addition of substances that incorporate into either the inner or outer leaflet of the cell membrane. (A) Sodium salicylate causes the formation of echinocytes. (B) The normal shape of a red blood cell is a biconcave disc. Cells with this morphology are named discocytes. (C) The addition of small amounts of Triton X-100 causes the formation of stomatocytes. In all cases there is a distribution in morphologies as described in [5].

The non-ionic surfactant Triton X-100 is known to be a potent stomatocytic agent. However, care must be taken when using Triton X-100 to induce stomatocytes as the surfactant is also a haemolytic agent. The ability of RBCs to change shape without being lysed depends on the buffer. We found that when using autoMACS^{TM} (BSA and EDTA) as a buffer, a concentration of 0.06% Triton X-100 gave sufficiently well-formed stomatocytes that where stable over the time scales, ~1 hour, of our experiments. As with echinocytes, the population of stomatocytes formed is not completely homogeneous, and a small number of the cells retain a discoid shape.

5.4.5 Fingerprints for cells types

Plots of the type shown in Figure 38D and E (more are shown in Figure 2 of Paper IV) constitute fingerprints for cell types that contain a wealth of information about the size, shape and deformability of the cells. Examples of the information contained in these plots are:

1. Because this particular device is deep it is the thickness of the cells that we measure and we see that echinocytes are thicker than stomatocytes in their undeformed states.

2. The slope of the curve tells us that the echinocytes are more deformable than the stomatocytes.
3. The stomatocytes seem to have a more complex mechanical structure than the echinocytes. The data shows a bistable situation with a quite resilient conformation up to a relatively high shear rate at an applied pressure of about 200mBar that quickly snaps into a different conformation indicating a possible underlying buckling transition.
4. In both cases we can resolve the subpopulations of cells that retain their disc shapes.
5. At the highest shear rates the effective size differences disappear and it is no longer possible to resolve differences in shape.

In conclusion, deformation changes the morphology of cells and separations based on the unperturbed morphology are best done at low rates of shear. Controlling shear rate allows us to measure effective size changes and therefore deformability and controlling particle orientation confers to some degree the ability to measure size and deformability in different directions across the cell. The size of posts and distance between rows of posts in our devices could be used to change the time scale of deformation and recovery independently of flow rate, which we believe could be used to measure elastic properties, viscous properties and overall deformation independently from each other.

6 Conclusions and outlook

In my thesis I have presented a series of improvements to the method of deterministic lateral displacement that I have developed together with my coworkers. In this final chapter I will begin by summarizing our results. I will then take the opportunity to speculate about which future directions I believe might be fruitful to pursue. As the papers themselves contain discussions along these lines, I will limit myself to the most exciting examples.

6.1 Summary of results

We have used controlled deformation of an entire device fabricated in PDMS to continuously tune the spacing between features, and shown how this principle can be used to tune a sorting device allowing not only fine adjustment, relaxing the strict fabrication requirements, but also making new modes of operation possible for these types of devices.

We have also shown how tuneable size separation can be achieved by combining DLD with DEP and how by modulating the voltage drop over the channel thus altering the dielectrophoretic force acting on the particles traversing the device, we can decrease the critical size in a simple and controlled manner by over 50%. It should be possible to resolve biologically relevant differences in $\mathrm{Re}(f_{CM})$ for particles of equal size and we have demonstrated this for microspheres with different surface groups. The method has other benefits such as reducing the probability of clogging and simplifying fabrication by allowing increased gap size between the posts for a given critical size. The introduction of DEP to DLD opens up for sorting based not only on size but also on dielectric properties of the particles of interest without any labelling. Moreover, the exact dielectric features of interest can be selected by choosing a corresponding frequency or combination of frequencies.

We have successfully shown how particle orientation, controlled via device depth, can be used to accentuate morphological differences making possible the sorting of otherwise indistinguishable particles in DLD devices. We have separated *T. cyclops*, a non-pathogenic relative of *T. brucei* from RBCs opening up for a cheap, simple to use, point-of-care, diagnostics tool. Work has begun on the

next generation of devices that we have designed to be simpler, to have both a higher throughput and a lower detection limit and also with features for the capture and concentration of the parasites.

Finally, we have shown how DLD can be used to achieve simple, continuous, measurements of size, shape and deformability. By running devices at different velocities we can expose the particles to different shear rates. Due to their deformation their effective size changes, which we can detect in the device. By plotting the output distribution we can thus create deformability fingerprints of different particles. Because deformation changes the morphology of cells, separations based on the native morphologies are best done at low rates of shear. Controlling shear rate allows us to measure effective size changes and therefore deformability and controlling particle orientation confers to some degree the ability to measure size and deformability in different directions across the cell. We can also choose the relative contributions of size, shape and deformability when performing separations.

6.2 Future directions

By far the most interesting direction for future work would be the application of our methods to medical diagnostics. Our methods hold great potential as tools for the detection of blood-borne parasites such as trypanosomes, malaria and bacteria and also to the detection of other rare cells such as circulating tumour cells. Here, two related but different approaches could be taken. 1) The excellent resolution of DLD, and the sensitivity to size, shape, deformability and dielectrophoretic properties that we have shown DLD capable of could be maximized for laboratory-based, label-free, high-throughput manipulations. Applications could encompass the screening of large volumes of blood for rare cells or the isolation of cells from large cultures. 2) The inherent simplicity and robustness of DLD devices could be brought to bear on the problems of field diagnostics. The focus here would be on increasing throughput and sensitivity while making devices that can work rapidly in a sample-in answer-out fashion with minimal reliance on peripheral equipment.

The combination of the different sorting mechanisms and driving forces that we have explored is also a direction I believe has great potential. Although we chose to combine DLD with DEP due to its simplicity, it is conceivable that DLD could be used via the same approach to amplify any type of minute force interaction, such as for example magnetic, gravitational, optical, or adhesion forces. Using an elastic device in which the critical size is tuneable it should be possible to adjust the critical size so that it is very close to the effective size of the

particles of interest, thereby increasing the sensitivity of the separation to variations in any small applied forces or interactions.

Also, DEP forces might be used to control the orientation of particles as they move through the decision point in a device. This could conceivably be used to gain greater control over orientation than that offered by device depth. This might make it possible to separate particles that have the same cross-sectional dimensions but different lengths. An interesting example is the sorting of bacteria as a function of length, thereby dividing a heterogeneous population into synchronized subfractions in a simple, minimally invasive way without any chemical means.

The size, shape and distance between posts in our devices could be used to change the time scale of deformation and recovery independently of flow rate, which we believe could be used to independently measure elastic and viscous properties and overall deformation. A more detailed picture of the shear stresses experienced by cells and of those mechanical properties that affect R_{eff} will be elucidated in the future with the aid of 3D simulations and also using artificial cell analogues more simple still than red blood cells.

7 Populärvetenskaplig Sammanfattning

Hoppet väcks för sömnsjuka

Det sticker till i benet. Du viftar med handen, men alltför långsamt. Du ser en glimt av den ljusbruna flugan, stor som ett bi, och hör hur den surrar vidare genom den varma afrikanska eftermiddagen mot sitt nästa blodmål.

Tsetseflugans bett kliar. Inom ett par dagar har det förvandlats till en arg röd svullnad. Därinne förökar sig parasiterna. Inom ett år har parasiterna erövrat din kropp och din hjärna. Efter månader av sömnrubbningar och svåra neurologiska problem som till slut övergått i koma ger ditt utmattade försvarssystem vika. Du somnar en sista gång, den stora sömnen.

Sömnsjukan drabbar en halv miljon människor i Afrika (söder om Sahara) om året. Av dessa människor dör varje år omkring 60 000. Medicin finns, men den är farlig. Den mest använda, Melarsoprol, är baserad på arsenik och orsaker dödlig hjärninflammation i uppemot 5 procent av patienterna. Att medicinera i tveksamma fall där diagnosen inte är fastställd är inte bara dyrt utan även onödigt riskfyllt.

Nya diagnostiska verktyg behövs

En tidig och korrekt diagnos är mycket viktig för patientens prognos. För att ställa en diagnos måste parasiterna påvisas i blodet. Detta görs fortfarande, som det alltid har gjorts, genom att lägga ut några droppar av det misstänkta blodet på en glasbit. Med hjälp av mikroskop letar man efter parasiterna. Som en nål i en höstack finns de fåtal parasiter man letar efter bland hundra miljontals blodkroppar. Metoder finns att ta bort en del av blodcellerna, vilket underlättar letandet, men dessa metoder, som till exempel centrifugering, kräver relativt stora apparater. De kräver utbildade användare och tillgång till mängder med kemikalier. Räknar man in alla delsteg är processen både arbetsintensiv och tidskrävande. Hoppet är att metoderna i den här avhandlingen ska göra det möjligt för vem som helst att kunna hitta parasiterna i en droppe blod inom bara ett par minuter.

Lab-on-a-chip - Bra för mycket mer än sömnsjukadiagnostik

Ute på den Afrikanska landsbygden, där sömnsjukan förekommer, finns det sällan upprustade laboratorier. Det finns ett kraftigt behov av portabla diagnostiska verktyg som kan fungera lika väl i ett dammigt, provisoriskt tält som i en blänkande ren vårdcentral. För att vara användbara i dessa svåra förhållandena på den afrikanska landsbygden måste verktygen vara effektiva, billiga och bärbara. De ska helst också vara oberoende av annan kringrustning. "Lab-on-a-chip" är ett koncept där man kommer bort från dyr, tung, resurskrävande utrustning genom att krympa ner allt till några kvadratcentimeter - ett laboratorium i mobiltelefonformat.

Sömnsjukadiagnostik är bara ett exempel på hur Lab-on-a-chip verktyg skulle kunna göra skillnad. I naturkatastrof och krigsdrabbade områden där infrastukturen är utslagen eller i rymden och djuphavsmiljöer där det aldrig funnits infrastruktur skulle de här verktygen kunna användas för att samla in information

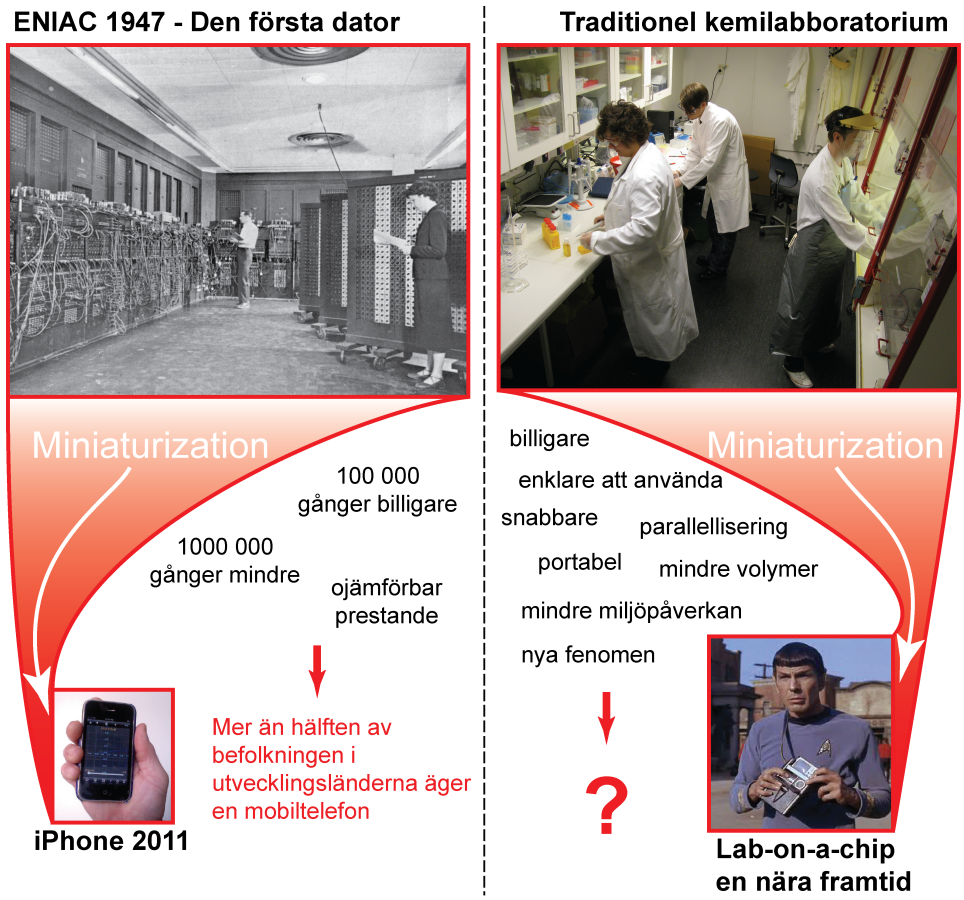

om både miljöns och människornas hälsa.

När "lab-on-a-chip"-tekniken används för diagnostik brukar det kallas för "Point-of-Care Diagnostics", (engelska för "diagnos vid sängkanten") och den har redan fått ett par stora genombrott. Några exempel är graviditetstestet och glukosmätaren för diabetiker. När medicinsk diagnostik bara kostar en droppe blod, några kronor och några minuter blir det inte bara lättare att tidigt upptäcka sjukdomar utan gör det också möjligt att följa sjukdomsförlopp i minsta detalj och avgöra till exempel om behandlingen fungerar som förväntat. Små kraftfulla diagnostiska verktyg kommer att leda till en revolution i personlig medicin likt den vi redan upplevt inom kommunikation och informationsteknologi och som lett till att fler än 50% av jordens befolkning, utveklingsländerna inkluderade, äger en mobiltelefon.

Partikelseparation

Ordet "partikel" kommer från latinets, particula, och betyder "liten del". Det används för såväl elektroner som sandkorn trots en skillnad på 20 storleksordningar i massa. Mycket av det arbetet som görs i forskningslaboratorier och i industriella processer handlar om att separera och sortera partiklar. Vissa processer kräver att man separerar partiklar från vätskor, och andra att man separerar partiklar från andra partiklar. Inom medicinsk diagnostik letar man ofta i kroppsvätskorna efter vissa typer av partiklar som ger information om patientens tillstånd. Som med sömnsjukeparasiterna och blodcellerna i exemplen ovan; när man separerar nålen från höstacken blir den betydligt lättare att hitta. I lab-on-a-chip är partikelseparation också viktig och kan utgöra hela eller bara ett steg i en diagnostisk process.

Separationens huvudidé är att man använder sig av krafter som påverkar partiklarna olika beroende på deras egenskaper. I fallet med höstacken och nålen är magnetiska krafter ett strålande exempel. Nålen skulle lätt kunna fiskas upp av en kraftfull magnet. Alternativt om höet och nålen slängdes i en behållare med vatten skulle höet flyta men nålen, på grund av sin högre densitet, sjunka. Den sistnämnda är samma mekanism som ligger bakom separation med centrifugering.

Mikrofluidik – Rörmokeri i miniatyr

Ett miniatyriserat laboratoriumbygge görs lättast med väldigt små byggstenar. De rör igenom vilka vätskorna ska flöda är oftast betydlig mindre än ett mänskligt hårstrå. I dessa mikrometerstora rörsystem beter vätskorna sig på ett sätt som är mycket annorlunda än det som vi brukar ser när vi stötar på vätskor till vardags. Om de kaotiska, virvlande och bubblande rörelser, som vi brukar förknippar med vätskor kan liknas med hur folkmassan rör sig på en flyplats, blir mikrofluidiska flöden mer som soldater som marscherar på ett torg. I dessa ordnade flöden uppstår det många nya fenomen som kan användas bland annat för att styra och kontrollerar partiklar. Den här avhandlingen dokumenterar våra försök att förstå

och använda några av dessa fenomen för att separera och analysera partiklar, främst i medicinska och diagnostiska syften.

Pelarskogar

Metoden vi använder är baserad på ett vätskaflöde genom en skog av mikrometerstora pelare. När en vätskeburen blandning av partiklar, som blod till exempel, flödar genom pelarskogen följer partiklarna olika banor. De enskilda banorna beror på partikelegenskaper som storlek, form och mjukhet men också på avståndet mellan pelarna och mönstret som pelarna är ordnade i. Väljer man rätt mönster och avstånd mellan pelarna efter de partiklar man vill analysera kommer de olika partiklarna att lämna 'skogen' på olika ställen. I slutet av pelarskogen kan partiklarna samlas upp och/eller analyseras. Att dela upp blod i sina beståndsdelar är ett typiskt exempel på vad som kan göras med den här metoden.

Att mäta på celler

Eftersom en partikels bana genom dessa pelarskogar beror på storlek, form och mjukhet så ger banan information om just de här egenskaperna. Det betyder att metoden inte bara behöver användas för att separerar partiklar utan även för att mäta på dem också. När man står i mataffären och ska välja en frukt så brukar man titta på fruktens storlek, dess form och man kanske även klämmer på den för att avgöra vilken tillstånd frukten är i. Samma sak gäller för våra celler. Storlek, form och mekaniska egenskaper innehåller mycket information om cellens tillstånd. Sickel-cell anemi är ett exempel på ett sjukligt tillstånd som ändrar cellers form. Malaria, cancer och HIV är exempel på faktorer som påverkar cellers mekaniska egenskaper. I våra pelarskogar kan vi klämma på tusentals celler varje sekund och avgöra hur stora de är, vilken form de har och om de är lika mjuka som de borde vara.

Framtiden

Det finns en del arbete kvar innan vår metod kommer att kunna användas för diagnostik av sömnsjuka, malaria eller cancer. Typiska problem som måste lösas har att göra med att de biologiska proven man letar i är väldigt komplexa och oftast kladdiga och att de saker man letar efter är så väldigt få. Jag vill visa med den här avhandling att, trots dessa svårigheter, de metoder vi har utvecklat skulle kunna utgör grunderna i enkla men kraftfulla diagnostiska verktyg. Det är min förhoppning att dessa verktyg komma att bidra till det stora målet att göra diagnostiska verktyg lika tillgängliga världen runt som mobiltelefoner är idag.

Appendix 1 The sizes and shapes of some cells of importance for medical diagnostics

Table A4 The components of human blood and some examples of rare cells and foreign bodies.

Cell	Number per µl	Shape	Dimensions [µm]	Ref
Blood cells				
Red blood cells (erythrocytes)	$4 \cdot 10^{-6}$ - $6 \cdot 10^{6}$	Biconcave discoid	7.81±0.63	-
Reticulocytes (young nucleated RBCs)	-	-	>5	[8]
White blood cells (Leucocytes):	~$6.6 \cdot 10^{3}$(total)			
Neutrophils	~$5.0 \cdot 10^{3}$	~Spherical	8.4±0.4	[197]
Eosinophils	~$2.0 \cdot 10^{2}$	~Spherical	-	-
Basophils	~40	~Spherical	-	-
Monocytes	-	~Spherical	8.5±0.4	[197]
Lymphocytes	-	~Spherical	6.5±0.5	[197]
Megakaryocytes (produce platelets)	-	-	19.4±3.0 (Adult) 15.3±1.7 (Neonate)	[198]
Platelets (Granulocytes)	$2 \cdot 10^{5}$	Oblate ellipsoid of revolution	3.62±0.74 diameter 0.93±0.32 thickness	[199]
Foreign bodies and other cells that might be of diagnostic interest				
2 human breast cancer cell lines MCF-7 and MDA-MB-231	-	~Spherical	18.1±1.8 18.2±2.8	[200]
Bacteria	-	Many shapes	0.5 - 5	-
Trypanosomes				
T. brucei	$<10^{2}$ to $>10^{4}$	Worm-like	33.5 x 2.5	[30]
T. cylops	-	Worm-like	30.0 x 1.5-3.5	[201]

Appendix 2 A review of particle separation and analysis methods

Group	Method	Separation/analysis mechanism	Separation/analysis criteria	Sample	Resolution	Throughput	Purity or efficiency	Enrichment ratio	Yield	Notes	References
Benchtop methods	FACS	Electric field switching	Detection of fluorescence label, or scattering	Any for which labels exist	-	70000 sorts/s*	-	-	99%	Labelling required, non portable	*BeckmanCoulter MoFlo™ XDP
			Forward scatter - size Side scatter - granularity	RBCs	Measurement of spherical index	1000 cells/s	-	-	-	Internal structure (granularity) effects measurements	[1]
	MACS	Capture in high gradient magnetic field	Presence of magnetic label	Rare cells in blood	-	10^{11} cells captured in 30 min	-	~20 000	-	Labelling required	[2]
	Imaging cytometry	Microscopic imaging and image analysis	Morphology, colocalisation of fluorescence	any	Limited by optical microscopy	2000 cells/s (Amnis ImageStream^X at 20x magnification)	-	-	-	-	Amnis, Cellavision, CompuCyte
	Coulter counter	Drop in electric current over a pore	Size	0.4µm to 1600µm particles	-	-	-	-	-	-	[3], BeckmanCoulter
	Mini Anion Exchange Centrifugation Technique (mAECT)	Anion exchange	Surface charge	Whole blood with T. brucei (parasites that cause sleeping sickness)	-	-	<50 parasites /ml	-	-	Cost per test 3Euro	[4]
	Centrifugation	Sedimentation at high g	Density and size	Cell lysate, organelles, nuclei, mitochondria, large macromolecules	Same macromolecules containing different isotopes of carbon and nitrogen	-	-	-	-	Requires large machines and can take hours per separation	-
Microfluidics-based cytometers	Photomultiplier 1D scanning in 384 parallel channels	No sorting	Localisation of fluorescently marked proteins	Yeast cells and mouse ovary cells	-	~2000 events/s, 384 separate samples of 1µl and 1000 cells in 6 min	-	-	Detection of cells above 0.01% of total number	-	[5, 6]
Adhesion based separation	Adhesion based separation	Adhesion of cells to immobilized ligands	Specific binding	Any cells for which specific ligands are known	Very specific	<20µl/min	-	<28 fold enrichment	As high as 100%	Ligands necessary, not continuous	[7]
Chip-based separation methods with applied fields	Acoustophoresis	Acoustic radiation pressure	Size, density and compressibility	Lipid vesicles (1%) from bovine blood (5%), diluted 20 times	Bovine RBCs from lipid vesicles (>1 µm)	0.3 ml/min	80% of lipids removed from 70% of blood cells	-	-	-	[8]
				Micro emboli (lipid vesicles) from human blood	Lipid vesicles from human RBCs (>1 µm)	-	No quantitative analysis performed	-	-	-	[8]
	Dielectrophoresis	Translational motion of charge-neutral matter in an electric field gradient	Increased dielectrophoretic response due to binding of beads	1:5000 target:non-target bacteria	Taged from non-taged	10^4 cells/s	-	250 fold (one round of sorting) 325 fold (after two rounds of sorting)	-	-	[9]
	Electrophoresis	Migration of charged particle in an electric field	Electrophoretic mobility	E.g. Different cell types based on surface charge	-	-	-	-	-	-	[10]
	Optical	Optical stretching	Deformability	Malaria infected – non-infected RBCs	Factor 2 in stiffness -	1 cell/s	-	-	-	No contact with surfaces is a benefit. No separation only analysis.	[11]
		Optical lattice	Size and index of refraction	-	-	-	-	-	-	-	[12]

Group	Method	Separation/analysis mechanism	Separation/analysis criteria	Sample	Resolution	Throughput	Purity or efficiency	Enrichment ratio	Yield	Notes	References
Passive chip-based methods	Pillars, weirs and membrane structures	Filtration through weir constrictions	Size (adhesion and deformability)	Microbes 0.2-5µm in water 10^6 /mL	-	0.2µL/min	-	-	97% of microbes trapped	clogging	[13]
		Filtration through microfabricated membranes	Size (adhesion and deformability)	Cultured CTCs spiked in human blood	17±1.5µm CTCs separated from most other blood cells	-	-	-	90% of CTCs captured (plus some other large blood cells)	-	[14]
		Louver array structures	Size + deformability	Endothelial cells and amniotic stem cells in amniotic fluid	Endothelial cells ~40µm from stem cells ~5µm	~60µl/hour	-	-	82.8% (97.1% after 2 runs in same device)	-	[15]
		Transit through constrictions	Size and deformability (debatably friction also)	Malaria (ring stage P. falciparum) infected RBCs spiked in 50x diluted blood	-	100 cells/min	-	-	-	No separation, device clogs after transit of 10^4 cells	[16]
	Pinched flow fractionation	size exclusion from patterned flows	Size and to some degree shape	RBCs and polystyrene spheres	1µm from 2µm particles	20µl/hour	-	-	-	-	[17-19]
	Hydrodynamic filtration	size exclusion from patterned flows	Size	Diluted blood 1%	RBCs from WBCs	1 L/min, or 10^3 cells/min @ 100 times dilution	-	-	97% of leukocytes in a pure fraction	Low concentration needed	[20]
			Size + shape	Budding yeast cells	-	-	-	-	-	-	[21]
			Size	Diluted blood 50%	Nucleated from non-nucleated RBCs (20nm for micron-sized polystyrene spheres)	0.35 ml/h, ~10^7 cells/min	Elimination of ~99.99% of RBCs	-	~99.99 WBCs retained	-	[22], [23]
	Deterministic lateral displacement	Altered trajectories through obstacle arrays based on size exclusion	Shape	Diluted blood spiked with parasites	-	-	-	-	99.6% of parasites at end of device with 99% of RBCs removed	-	Paper III [24]
			Size, shape and deformability	Diluted blood 20%, RBCs with altered morhologies	Discocytes, echinocytes and stomatocytes from one another.	-	-	-	-	-	Paper IV
			Dielectrophoretic properties	Polystyrene microspheres with different surface charge	-	-	-	-	-	-	Paper II [25]
			Microvascular behaviour of blood cells	Whole blood	Leukocytes from RBCs	>nl/s	-	34 fold enrichment of leukocytes-to-RBC ratio	67% of leukocytes recovered	Better than a single spin "buffy coat"	[26]
	Biomimetic - Mimicking microvasculature phenomena	Leukocyte margination	Microvascular behaviour of blood cells	-	-	5µl/min, 2·10^7 cells/min	-	-	75% (early stage infection) >90% (late stage)	Only works with high haematocrit (~40%)	[27]
		Margination of Malaria (P. falciparum) infected RBCs	Microvascular behaviour of blood cells	Defibrinated whole blood (sheep)	Plasma from blood cells	3-4µl/min	-	-	15-25% of cell-free plasma recovered	No clogging or haemolysis for 30 min of continuous functioning	[28]
		Zweifach–Fung effect	Size	Bacteria in 20x diluted blood	Bacteria from blood cells, several µm difference	57000 cells/s (all cells)	-	300 fold enrichment of bacteria	60% recovery of bacteria at 99.87% purity	-	[29]
	Inertial	Soft inertial microfluidics with sheath flow	Size and deformability	Cancer cells and WBCs	-	22000 cells/min	-	5.4x for Metastatic breast cancer cell 3.2x for osteocarcoma cells	96-97%	Difficult to separate effects of size and deformability	[30]
		Shear and wall induced lift	Size (volume)	Asynchronous cells	G0/G1 from G2/M phase cells	15·10^6 cells/hour	-	-	80-90% of cells in G0/G1 phase	90% of cells viable	[31]
	Pinched flow + Inertial	Cells focused by inertial effects and separated by pinched flow	Size	MCF-7 cells spiked into whole blood	CTCs from RBCs and WBCs	10^8 cells/min	-	3.25·10^5 relative to RBCs	>80% cell recovery	20x dilution of blood required. Overlapping cell sizes not resolved.	[32]

Appendix 3 Replica Moulding

The process of replica moulding with PDMS can be divided into three steps. The first step entails the fabrication of a structure, commonly called a master, which will function as a mould. For this we have used SU8, an epoxy-based photoresist, which can be patterned on a silicon substrate using photolithography. The second step is to cast a slab of PDMS on the master. The features defined in the surface of this slab become microfluidic channels when, in the third step, a glass slide or blank PDMS slab is attached forming closed structures. As part of this third step we can consider also the attachment of fluidic and electronic connections through which we can interface the device to external equipment such as pumps and electrical power sources. There follows a detailed description of the fabrication process together with a list of the equipment used. The numbers in the text refer to Tables A5-A8.

Photolithography of SU8 - making a master

Device designs were drawn using cad software (1) and transferred to chrome masks using a laser pattern generator (2).

Table A5 Material and equipment used in the fabrication of photomasks.

		Description of equipment/material	Model/product name	Manufacturer
Photomask fabrication	1	CAD drawing programme	L-Edit 11.02	Tanner Research, Monrovia, CA, USA
	2	Mask writer[1]	DWL66	Heidelberg Instruments GmbH, Heidelberg, Germany

[1]*All photomasks were fabricated by the author at the department of electrical measurements, LTH, Lund University, with the exception of those used in Paper III which were made to our design by Delta Mask, Enschede, The Netherlands.*

A silicon wafer large enough to accommodate the design (3) is prepared by baking at 200˚C for ~30 minutes in a convection oven (4). This removes any water from the surface of the wafer and promotes adhesion of the photoresist. The photoresist (5) is applied to the wafer by pouring directly from the bottle. Care should be taken not to introduce bubbles while pouring. Enough resist should be added to cover the middle 2/3 of the wafer. Tilting the wafer will then allow the resist to spread and cover as much of the wafer as possible. The final thickness is achieved using a spinner (6). The thickness of the resist layer depends both on the viscosity of the resist and on the spin rate. SU8 is available in a range of viscosities, which can be used to achieve various thicknesses. Figure A41 shows

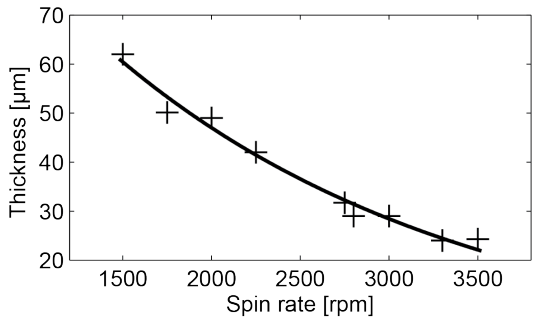

Figure A41 Spin curve for SU8 2050 on a 2" wafer.

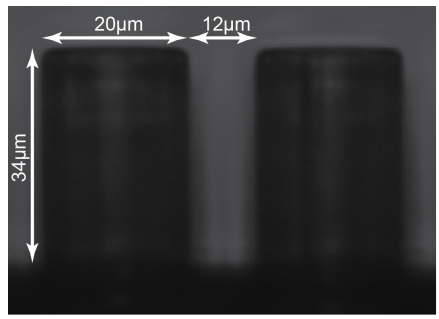

Figure A40 Optical microscopy image of a cross-section through a PDMS cast from Paper III. The master was made using the example recipe for 34 µm thick SU8 2050.

the thickness of SU8 2050 as a function of spin rate when following the recipe shown below. After spin coating the resist is soft baked in order to remove the solvent (7, 8), exposed with UV light using a contact mask aligner (9, 10). After exposure resist is baked again (post exposure bake, PEB) and then developed (11) under mild sonication (12). After development the SU8 is fully cross-linked in a convection oven (13) at 200˚C for 30 minutes.

Spin recipe for SU8 2050

1. 10 seconds @ 500 rpm
2. 60 seconds @ final spin rate, for example 3000 rpm gives 30 µm

note: On the spinner that I have used in this work (6) the SU8 that is thrown from the wafer has a tendency to form long airborne fibres (reminiscent of candy floss) that can land on the spun surface and form defects. Holding a piece of paper close to the edge of the spinning wafer collects the excess SU8 stopping these fibres from forming and ensuring defect free surfaces.

The exact baking times and exposure dose are very dependent on one another, on the wavelength of the light used and on the thickness of the resist layer and base-line parameters are given by the manufacturer, which are a good starting point for optimization. The following recipe was found to produce good resolution and parallel side-walls for SU8 of 34 µm thickness. (In order to achieve parallel side-walls that are only 12 µm apart and 34 µm high it was necessary to remove edge beads by dipping the edge of the wafer in developer.)

Example recipe for 34 µm thick SU8 2050

1. Soft bake 3 minutes @ 65˚C hotplate 1
2. Move to hotplate 2 @ 95˚C for 10 minutes
3. Remove edge beads if high resolution is required

4. Expose at 21 mW/cm^2 for 7 seconds. The mask aligner (10) is fitted with a filter that removes most UV radiation under 365 nm.
5. PEB 1 minute @ 65˚C hotplate 1
6. PEB 4 minutes @ 95˚C hotplate 2
7. Development can be done under very mild sonication for 2 min. Developer should be rinsed with IPA and the sample dried with flowing nitrogen. The sample should then be inspected under a microscope and further developed if necessary. Typically 4 min is sufficient.

PDMS has a tendency to stick to clean silicon surfaces, which can make demoulding without damaging either the master or the moulded PDMS slab very difficult. In order to facilitate demoulding a monolayer of fluorinated molecules (14) is formed using the same setup and recipe presented in [220].

Table A6 *Material and equipment for the fabrication of SU8 masters.*

		Description of equipment/material	Model/product name	Manufacturer
Fabrication of master	3	Silicon wafers 2” and 3”	-	Siltronix
	4	Convection oven	-	-
	5	Photoresist	SU8 2005, 2015, 2050	MicroChem, Newton, MA, USA
	6	Spinner	-	-
	7	Hotplate 1 (65˚)	-	-
	8	Hotplate 2 (95˚)	-	-
	9	Mask aligner 1	MJB3	Karl Suss, Munich, Germany
	10	Mask aligner 2	MJB4	Karl Suss, Munich, Germany
	11	Developer	SU8 Developer	MicroChem, Newton, MA, USA
	12	Sonicater		
	13	Convection oven (200˚C)		
	14	Anti-sticking treatment	1*H*, 1*H*, 2*H*, 2*H* – Perfluorooctyl-trichlorosilane	ABCR GmbH & Co, KG, Karlsruhe, Germany
	15	Glove box	-	-

Replica moulding – transferring the pattern to PDMS

PDMS and initiator (16) were mixed thoroughly at a ratio of 10:1 (by weight). The mixture was placed in a vacuum desiccator (17) until all air bubbles were removed (~30 minutes). The PDMS was then poured onto the master, care being taken not to introduce air bubbles, and baked at 80˚C in a convection oven for at

least 45 minutes. In some cases (Paper III) fluidic connections were cast into the PDMS at this stage instead of glueing them afterwards, see the next section. In this case about 1 cm of tubing (21) with the ends cut as flat as possible where stood on the master in the desired position before the PDMS was carefully poured around them.

Plasma bonding and gluing – putting together the finished device

Holes were punched through the PDMS using a sharpened steel tube (19) to allow access to the fluidics channels (if the tubes where not cast into the PDMS in the previous step). The surface of the patterned PDMS and the blank surface that was used to seal the channels (this is usually glass (22) but for the stretching experiments in Paper I was a blank slab of PDMS) were both treated with oxygen plasma @ 8mbar for 30 seconds (20). Finally connection tubes (21) of length ~1cm were glued over the access holes using a silicone adhesive (23).

Table 7A Material and equipment used in the replica moulding of PDMS structures.

		Description of equipment/material	Model/product name	Manufacturer
Casting PDMS	16	Silicone rubber Polydimethylsiloxane	Silgard 184	Dow Corning, Midland, MI, USA
	17	Vacuum chamber	-	-
	18	Convection oven (80˚C)	-	-

Table 8A Material and equipment used in assembly of PDMS fluidics devices.

		Description of equipment/material	Model/product name	Manufacturer
Final assembly of device	19	1mm steel tube	-	-
	20	Oxygen plasma oven	Plasma Preen II-862,	Plasmatic systems, Inc, North Brunswick, NJ, USA
	21	Silicone tubing	Outer diameter 5mm Inner diameter 3mm	- -
	22	Microscope slides	Microscope slides 76 x 26 mm	Menzel-Gläser
	23	Silcone adhesive	Elastosil®A07	Wacker Chemie AG, München, Germany

Appendix 4 Detailed Lab Setup

Paper I

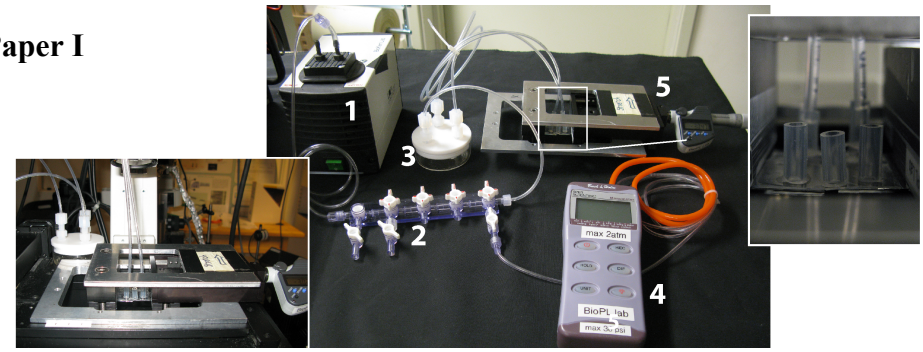

Figure A42 The experimental setup for the elastic DLD experiments reported in paper I. Pressure driven flow was created in the device using a vacuum pump (1). The pressure from the pump was controlled using a controlled leak valve (2) and stabilized using a glass bottle as a capacitance (3). The bottle served also to collect waste. Pressure was measured with a pressure gauge (4). The PDMS device was stretched using a custom built chuck (5). The small inset shows the device with fluidic connections mounted in the chuck. The large inset shows the stretching chuck and device mounted in an epifluorescence microscope.

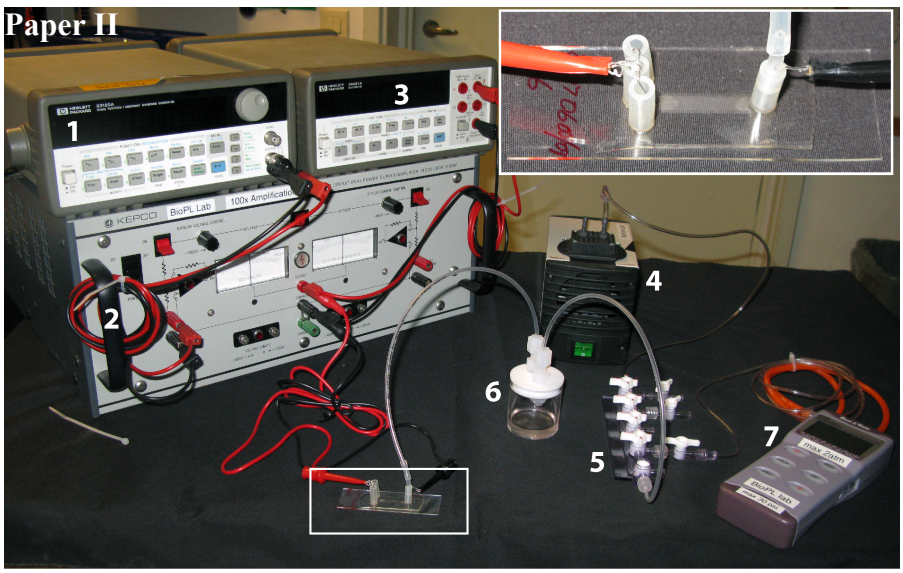

Figure A43 The experimental setup for the DEP DLD experiments performed in paper II. The AC voltage was generated with a function generator (1) with a maximum peak-to-peak voltage of 10 V. This signal was then amplified 100x (2) and the resulting voltage measured with a voltmeter (3) Pressure-driven flow was created in the device using a vacuum pump (4). The pressure from the pump was controlled using a controlled leak (5) and stabilized using a glass bottle as a capacitance (6). The bottle served also to collect waste. Pressure was measured with a pressure gauge (7). The inset shows the device with fluidic connections and platinum electrodes.

Papers III and IV

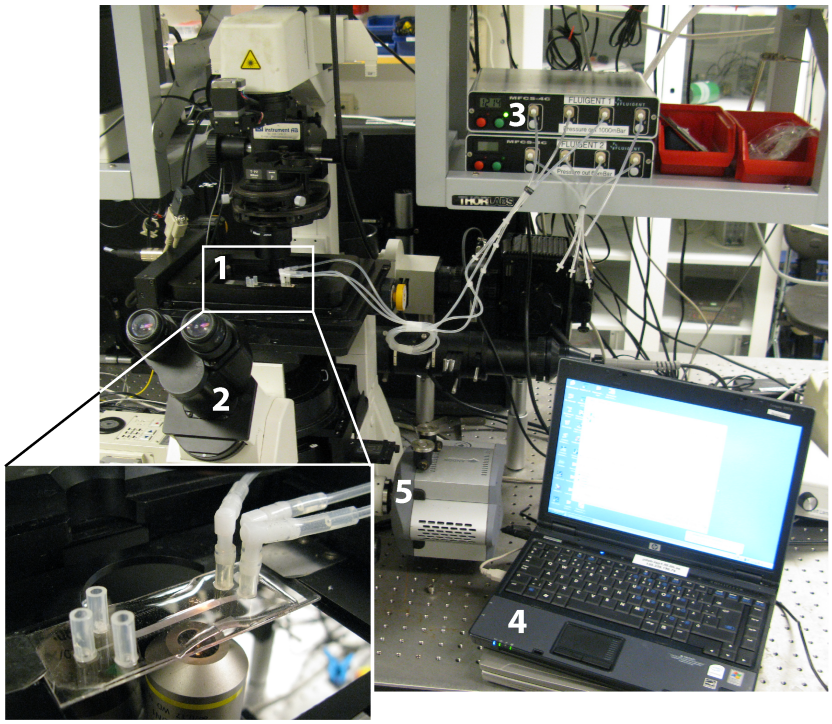

Figure A44 The experimental setup for the experiments performed in Papers III and IV. (1) The device mounted in the inverted microscope. In the inset the connections to the pressure controllers can be seen as well as three outlet reservoirs to collect the separated samples. (2) Nikon Eclipse TE2000-U inverted microscope (Nikon Corporation, Tokyo, Japan) with transmission and epifluorescence illumination. (3) MFCS-4C pressure controllers (Fluigent, Paris, France), 0-80 mbar and 0-1000 mbar. The accuracy of the controllers is ± 1% of the maximum pressure for both controllers meaning that the high-pressure controller is not suitable for use at pressures below ~100 mbar for which the low-pressure controller was used. (4) Laptop used to control pressure. (5) Camera used to capture images from microscope. The camera shown in the image is an Andor Ixon EMCCD camera (Andor Technology, Belfast, Northern Ireland) but an Luca (also from Andor) and a high-speed EoSens mini MC-1370 camera (Mikrotron GmbH, Unterschleissheim, Germany) where also used. Images where captured to a computer using IQ software (Andor Technology, Belfast, Northern Ireland).

References

1. *Helicobacter sp 01.jpg*. [cited 2011 october 10]; Available from: http://en.wikipedia.org/wiki/File:Helicobacter_sp_01.jpg.
2. *Campylobacter.jpg*. [cited 2011 october 10]; Available from: http://en.wikipedia.org/wiki/File:Campylobacter.jpg.
3. *Staphylococcus aureus VISA 2.jpg*. [cited 2011 october 10]; Available from: http://en.wikipedia.org/wiki/File:Staphylococcus_aureus_VISA_2.jpg.
4. *Cholera bacteria SEM.jpg*. [cited 2011 october 10]; Available from: http://en.wikipedia.org/wiki/File:Cholera_bacteria_SEM.jpg.
5. Li, A.L., H. Seipelt, C. Muller, Y.D. Shi, and G.M. Artmann, *Effects of salicylic acid derivatives on red blood cell membranes.* Pharmacology & Toxicology, 1999. **85**(5): p. 206-211.
6. Huang, L.R., E.C. Cox, R.H. Austin, and J.C. Sturm, *Continuous Particle Separation Through Deterministic Lateral Displacement.* Science, 2004. **304**(5673): p. 987-990.
7. Davis, J.A., D.W. Inglis, K.J. Morton, D.A. Lawrence, L.R. Huang, S.Y. Chou, J.C. Sturm, and R.H. Austin, *Deterministic hydrodynamics: Taking blood apart.* Proceedings of the National Academy of Sciences of the United States of America, 2006. **103**(40): p. 14779-14784.
8. Flejter, W.L., R. Huang, T.A. Barber, M.A. Schmidt, R.G. Tompkins, M. Toner, D.W. Bianchi, and R. Kapur, *A microfluidics approach for the isolation of nucleated red blood cells (NRBCs) from the peripheral blood of pregnant women.* Prenatal Diagnosis, 2008. **28**(10): p. 892-899.
9. Green, J.V., M. Radisic, and S.K. Murthy, *Deterministic Lateral Displacement as a Means to Enrich Large Cells for Tissue Engineering.* Analytical Chemistry, 2009. **81**(21): p. 9178-9182.
10. Holm, S.H., J.P. Beech, M.P. Barrett, and J.O. Tegenfeldt, *Separation of parasites from human blood using deterministic lateral displacement.* Lab on a Chip, 2011. **11**(7): p. 1326-1332.
11. Morton, K.J., K. Loutherback, D.W. Inglis, O.K. Tsui, J.C. Sturm, S.Y. Chou, and R.H. Austin, *Hydrodynamic Metamaterials: Microfabricated Arrays to Steer, Refract, and Focus Streams of Biomaterials.* Proceedings of the National Academy of Sciences of the United States of America, 2008. **105**(21): p. 7434-7438.

12. Inglis, D.W., N. Herman, and G. Vesey, *Highly accurate deterministic lateral displacement device and its application to purification of fungal spores.* Biomicrofluidics, 2010. **4**(2): p. -.
13. Inglis, D.W., M. Lord, and R.E. Nordon, *Scaling deterministic lateral displacement arrays for high throughput and dilution-free enrichment of leukocytes.* Journal of Micromechanics and Microengineering, 2011. **21**(5): p. -.
14. Inglis, D.W., *Microfluidic Devices for Cell Separation*, in *Electrical Engineering*2008, Princeton. p. 143.
15. Joensson, H.N., M. Uhlen, and H.A. Svahn, *Droplet size based separation by deterministic lateral displacement-separating droplets by cell-induced shrinking.* Lab on a Chip, 2011. **11**(7): p. 1305-1310.
16. Giddings, J.C., *Unified Separation Science*1991, New York: Wiley. xxiv, 320 p.
17. Cranston, H.A., C.W. Boylan, G.L. Carroll, S.P. Sutera, J.R. Williamson, I.Y. Gluzman, and D.J. Krogstad, *Plasmodium-Falciparum Maturation Abolishes Physiologic Red-Cell Deformability.* Science, 1984. **223**(4634): p. 400-403.
18. Nash, G.B., E. Obrien, E.C. Gordonsmith, and J.A. Dormandy, *Abnormalities in the Mechanical-Properties of Red Blood-Cells Caused by Plasmodium-Falciparum.* Blood, 1989. **74**(2): p. 855-861.
19. Suresh, S., *Biomechanics and biophysics of cancer cells.* Acta Biomaterialia, 2007. **3**(4): p. 413-438.
20. Gogos, C.A., G.A. Athanassiou, A.G. Moutzouri, and A.T. Skoutelis, *Red blood cell deformability in patients with human immunodeficiency virus infection.* European Journal of Clinical Microbiology & Infectious Diseases, 2010. **29**(7): p. 845-849.
21. Barabino, G.A., M.O. Platt, and D.K. Kaul, *Sickle Cell Biomechanics.* Annual Review of Biomedical Engineering, Vol 12, 2010. **12**: p. 345-367.
22. Turchetti, V., C. De Matteis, F. Leoncini, L. Trabalzini, M. Guerrini, and S. Forconi, *Variations of erythrocyte morphology in different pathologies.* Clinical Hemorheology and Microcirculation, 1997. **17**(3): p. 209-215.
23. Sheetz, M.P. and S.J. Singer, *Biological-Membranes as Bilayer Couples - Molecular Mechanism of Drug-Erythrocyte Interactions.* Proceedings of the National Academy of Sciences of the United States of America, 1974. **71**(11): p. 4457-4461.
24. Sheetz, M.P. and S.J. Singer, *Equilibrium and Kinetic Effects of Drugs on Shapes of Human Erythrocytes.* Journal of Cell Biology, 1976. **70**(1): p. 247-251.
25. Henkelman, S., M.J. Dijkstra-Tiekstra, J. de Wildt-Eggen, R. Graaff, G. Rakhorst, and W. van Oeveren, *Is red blood cell rheology*

preserved during routine blood bank storage? Transfusion, 2010. **50**(4): p. 941-948.
26. Hess, J.R., *Red cell storage.* Journal of Proteomics, 2010. **73**(3): p. 368-373.
27. Bolton, F.G., M.J. Street, and A.J. Pace, *Changes in Erythrocyte Volume and Shape in Pregnancy.* British Journal of Obstetrics and Gynaecology, 1982. **89**(12): p. 1018-1020.
28. Chan, S.Y.W., C. Wang, S.T.H. Chan, P.C. Ho, W.W.K. So, Y.F. Chan, and H.K. Ma, *Predictive Value of Sperm Morphology and Movement Characteristics in the Outcome of Invitro Fertilization of Human Oocytes.* Journal of in Vitro Fertilization and Embryo Transfer, 1989. **6**(3): p. 142-148.
29. Kelly, G.M., J.I. Kilpatrick, M.H. van Es, P.P. Weafer, and P.J. Prendergast, *Bone cell elasticity and morphology changes during the cell cycle.* Journal of Biomechanics, 2011. **44**: p. 1484-1490.
30. Chappuis, F., L. Loutan, P. Simarro, V. Lejon, and P. Buscher, *Options for field diagnosis of human African trypanosomiasis.* Clinical Microbiology Reviews, 2005. **18**(1): p. 133-+.
31. Chen, X. and D.F. Cui, *Microfluidic Devices for Sample Pretreatment and Applications.* Microsystem Technologies-Micro- and Nanosystems-Information Storage and Processing Systems, 2009. **15**(5): p. 667-676.
32. Boeck, G., *Current status of flow cytometry in cell and molecular biology.* International Review of Cytology - a Survey of Cell Biology, Vol 204, 2001. **204**: p. 239-298.
33. Pappas, D. and K. Wang, *Cellular Separations: A Review of New Challenges in Analytical Chemistry.* Analytica Chimica Acta, 2007. **601**(1): p. 26-35.
34. Terry, S.C., J.H. Jerman, and J.B. Angell, *Gas-Chromatographic Air Analyzer Fabricated on a Silicon-Wafer.* Ieee Transactions on Electron Devices, 1979. **26**(12): p. 1880-1886.
35. Manz, A., N. Graber, and H.M. Widmer, *Miniaturized Total Chemical-Analysis Systems - a Novel Concept for Chemical Sensing.* Sensors and Actuators B-Chemical, 1990. **1**(1-6): p. 244-248.
36. Mosadegh, B., T. Bersano-Begey, J.Y. Park, M.A. Burns, and S. Takayama, *Next-generation integrated microfluidic circuits.* Lab on a Chip, 2011. **11**(17): p. 2813-2818.
37. Dittrich, P.S. and A. Manz, *Lab-On-A-Chip: Microfluidics in Drug Discovery.* Nature Reviews Drug Discovery, 2006. **5**(3): p. 210-218.
38. Franke, T.A. and A. Wixforth, *Microfluidics for Miniaturized Laboratories on a Chip.* Chemphyschem, 2008. **9**(15): p. 2140-2156.
39. Erickson, D. and D.Q. Li, *Integrated Microfluidic Devices.* Analytica Chimica Acta, 2004. **507**(1): p. 11-26.

40. Verpoorte, E. and N.F. De Rooij, *Microfluidics Meets MEMS.* Proceedings of the Ieee, 2003. **91**(6): p. 930-953.
41. Mark, D., S. Haeberle, G. Roth, F. von Stetten, and R. Zengerle, *Microfluidic lab-on-a-chip platforms: requirements, characteristics and applications.* Chemical Society Reviews, 2010. **39**(3): p. 1153-1182.
42. Craighead, H., *Future Lab-On-A-Chip Technologies for Interrogating Individual Molecules.* Nature, 2006. **442**(7101): p. 387-393.
43. Squires, T.M. and S.R. Quake, *Microfluidics: Fluid Physics at the Nanoliter Scale.* Reviews of Modern Physics, 2005. **77**(3): p. 977-1026.
44. Beebe, D.J. and A.L. Paguirigan, *Microfluidics meet cell biology: bridging the gap by validation and application of microscale techniques for cell biological assays.* Bioessays, 2008. **30**(9): p. 811-821.
45. El-Ali, J., P.K. Sorger, and K.F. Jensen, *Cells on Chips.* Nature, 2006. **442**(7101): p. 403-411.
46. Andersson, H. and A. van den Berg, *Microfluidic Devices for Cellomics: A Review.* Sensors and Actuators B-Chemical, 2003. **92**(3): p. 315-325.
47. Bhagat, A.A.S., H. Bow, H.W. Hou, S.J. Tan, J. Han, and C.T. Lim, *Microfluidics for cell separation.* Medical & Biological Engineering & Computing, 2010. **48**(10): p. 999-1014.
48. Lenshof, A. and T. Laurell, *Continuous separation of cells and particles in microfluidic systems.* Chemical Society Reviews, 2010. **39**(3): p. 1203-1217.
49. Di Carlo, D., D.R. Gossett, W.M. Weaver, A.J. Mach, S.C. Hur, H.T.K. Tse, W. Lee, and H. Amini, *Label-free cell separation and sorting in microfluidic systems.* Analytical and Bioanalytical Chemistry, 2010. **397**(8): p. 3249-3267.
50. Chen, P., X. Feng, W. Du, and B.-F. Liu, *Microfluidic chips for cell sorting.* Frontiers in Bioscience, 2008. **13**: p. 2464-2483.
51. Kavanagh, D.M., M. Kersaudy-Kerhoas, R.S. Dhariwal, and M.P.Y. Desmulliez, *Current and emerging techniques of fetal cell separation from maternal blood.* Journal of Chromatography B-Analytical Technologies in the Biomedical and Life Sciences, 2010. **878**(22): p. 1905-1911.
52. Yi, C.Q., C.W. Li, S.L. Ji, and M.S. Yang, *Microfluidics technology for manipulation and analysis of biological cells.* Analytica Chimica Acta, 2006. **560**(1-2): p. 1-23.
53. Toner, M. and D. Irimia, *Blood-on-a-chip.* Annual Review of Biomedical Engineering, 2005. **7**: p. 77-103.
54. Sorger, P.K., *Microfluidics closes in on point-of-care assays.* Nature Biotechnology, 2008. **26**(12): p. 1345-1346.

55. Sia, S.K. and L.J. Kricka, *Microfluidics and point-of-care testing.* Lab on a Chip, 2008. **8**(12): p. 1982-1983.
56. Linder, V., *Microfluidics at the crossroad with point-of-care diagnostics.* Analyst, 2007. **132**(12): p. 1186-1192.
57. Yager, P., T. Edwards, E. Fu, K. Helton, K. Nelson, M.R. Tam, and B.H. Weigl, *Microfluidic Diagnostic Technologies for Global Public Health.* Nature, 2006. **442**(7101): p. 412-418.
58. others, S.a., *Taking technologies out of the lab and into environments where they can improve the health and quality of life of the poorest.* Nature Medicine, 2011.
59. Weigl, B., G. Domingo, P. LaBarre, and J. Gerlach, *Towards non- and minimally instrumented, microfluidics-based diagnostic devices.* Lab on a Chip, 2008. **8**(12): p. 1999-2014.
60. Pamme, N., *Continuous Flow Separations in Microfluidic Devices.* Lab on a Chip, 2007. **7**(12): p. 1644-1659.
61. Lumsden, W.H.R., C.D. Kimber, D.A. Evans, and S.J. Doig, *Trypanosoma-Brucei - Miniature Anion-Exchange Centrifugation Technique for Detection of Low Parasitemias - Adaptation for Field Use.* Transactions of the Royal Society of Tropical Medicine and Hygiene, 1979. **73**(3): p. 312-317.
62. Lumsden, W.H.R., C.D. Kimber, and M. Strange, *Trypanosoma-Brucei - Detection of Low Parasitemias in Mice by a Miniature Anion-Exchanger Centrifugation Technique.* Transactions of the Royal Society of Tropical Medicine and Hygiene, 1977. **71**(5): p. 421-424.
63. Tabrizian, M. and T.F. Didar, *Adhesion based detection, sorting and enrichment of cells in microfluidic Lab-on-Chip devices.* Lab on a Chip, 2010. **10**(22): p. 3043-3053.
64. Grutzkau, A. and A. Radbruch, *Small But Mighty: How the MACS (R)-Technology Based on Nanosized Superparamagnetic Particles has Helped to Analyze the Immune System Within the Last 20 Years.* Cytometry Part A, 2010. **77A**(7): p. 643-647.
65. Johnson, K.W., A. Dooner, and P.J. Quesenberry, *Fluorescence activated cell sorting: A window on the stem cell.* Current Pharmaceutical Biotechnology, 2007. **8**(3): p. 133-139.
66. Di Carlo, D., *Inertial microfluidics.* Lab on a Chip, 2009. **9**(21): p. 3038-3046.
67. Di Carlo, D., D. Irimia, R.G. Tompkins, and M. Toner, *Continuous inertial focusing, ordering, and separation of particles in microchannels.* Proceedings of the National Academy of Sciences of the United States of America, 2007. **104**(48): p. 18892-18897.
68. Gossett, D.R. and D. Di Carlo, *Particle Focusing Mechanisms in Curving Confined Flows.* Analytical Chemistry, 2009. **81**(20): p. 8459-8465.

69. Kuntaegowdanahalli, S.S., A.A.S. Bhagat, G. Kumar, and I. Papautsky, *Inertial microfluidics for continuous particle separation in spiral microchannels.* Lab on a Chip, 2009. **9**(20): p. 2973-2980.
70. Lee, W.C., A.A.S. Bhagat, S. Huang, K.J. Van Vliet, J. Han, and C.T. Lim, *High-throughput cell cycle synchronization using inertial forces in spiral microchannels.* Lab on a Chip, 2011. **11**(7): p. 1359-1367.
71. Mach, A.J. and D. Di Carlo, *Continuous Scalable Blood Filtration Device Using Inertial Microfluidics.* Biotechnology and Bioengineering, 2010. **107**(2): p. 302-311.
72. Wu, Z., B. Willing, J. Bjerketorp, J.K. Jansson, and K. Hjort, *Soft inertial microfluidics for high throughput separation of bacteria from human blood cells.* Lab on a Chip, 2009. **9**(9): p. 1193-1199.
73. Hur, S.C., N.K. Henderson-MacLennan, E.R.B. McCabe, and D. Di Carlo, *Deformability-based cell classification and enrichment using inertial microfluidics.* Lab on a Chip, 2011. **11**(5): p. 912-920.
74. Di Carlo, D., S.C. Hur, N.K. Henderson-MacLennan, and E.R.B. McCabe, *Deformability-based cell classification and enrichment using inertial microfluidics.* Lab on a Chip, 2011. **11**(5): p. 912-920.
75. Di Carlo, D., S.C. Hur, S.E. Choi, and S. Kwon, *Inertial focusing of non-spherical microparticles.* Applied Physics Letters, 2011. **99**(4).
76. Sollier, E., M. Masaeli, H. Amini, K. Camacho, N. Doshi, S. Mitragotri, and D. Di Carlo. *Effect of particle shape on inertial focusing*. in *The Fifhteenth International Conference on Miniaturized Systems for Chemistry and Life Sciences*. 2011. Seattle, Washington, USA.
77. Lay, C., C.Y. Teo, L. Zhu, X.L. Peh, H.M. Ji, B.R. Chew, R. Murthy, H.H. Feng, and W.T. Liu, *Enhanced Microfiltration Devices Configured with Hydrodynamic Trapping and a Rain Drop Bypass Filtering Architecture for Microbial Cells Detection.* Lab on a Chip, 2008. **8**(5): p. 830-833.
78. Ji, H.M., V. Samper, Y. Chen, C.K. Heng, T.M. Lim, and L. Yobas, *Silicon-Based Microfilters for Whole Blood Cell Separation.* Biomedical Microdevices, 2008. **10**(2): p. 251-257.
79. Brody, J.P., T.D. Osborn, F.K. Forster, and P. Yager, *A Planar Microfabricated Fluid Filter.* Sensors and Actuators a-Physical, 1996. **54**(1-3): p. 704-708.
80. Di Carlo, D., L.Y. Wu, and L.P. Lee, *Dynamic Single Cell Culture Array.* Lab on a Chip, 2006. **6**(11): p. 1445-1449.
81. Huebner, A., D. Bratton, G. Whyte, M. Yang, A.J. deMello, C. Abell, and F. Hollfelder, *Static Microdroplet Arrays: A Microfluidic Device for Droplet Trapping, Incubation and Release for Enzymatic and Cell-Based Assays.* Lab on a Chip, 2009. **9**(5): p. 692-698.

82. Nam, K.H. and D.T. Eddington, *Size-Based Separation of Microparticles in a Multilayered Microfluidic Device.* Journal of Microelectromechanical Systems, 2010. **19**(2): p. 375-383.
83. Brody, J., B. Austin, and M. Bitensky, *Red-Blood-Cell Flow-through a Microfabricated Structure.* Biophysical Journal, 1994. **66**(2): p. A85-A85.
84. Brody, J.P., Y.Q. Han, R.H. Austin, and M. Bitensky, *Deformation and Flow of Red-Blood-Cells in a Synthetic Lattice - Evidence for an Active Cytoskeleton.* Biophysical Journal, 1995. **68**(6): p. 2224-2232.
85. Bow, H., I.V. Pivkin, M. Diez-Silva, S.J. Goldfless, M. Dao, J.C. Niles, S. Suresh, and J. Han, *A microfabricated deformability-based flow cytometer with application to malaria.* Lab on a Chip, 2011. **11**(6): p. 1065.
86. Yamada, M., M. Nakashima, and M. Seki, *Pinched Flow Fractionation: Continuous Size Separation of Particles Utilizing a Laminar Flow Profile in a Pinched Microchannel.* Analytical Chemistry, 2004. **76**(18): p. 5465-5471.
87. Yamada, M., M. Nakashima, Y. Sai, M. Yasuda, and M. Seki, *Pinched flow fractionation for rapid and continuous particle separation in microfluidic devices*, in *Micro Total Analysis Systems 2004, Vol 1*, T.N.J.J.K.H.D.J.K.J.P. Laurell, Editor 2005. p. 414-416.
88. Larsen, A.V., L. Poulsen, H. Birgens, M. Dufva, and A. Kristensen, *Pinched flow fractionation devices for detection of single nucleotide polymorphisms.* Lab on a Chip, 2008. **8**(5): p. 818-821.
89. Lee, K.H., S.B. Kim, K.S. Lee, and H.J. Sung, *Enhancement by optical force of separation in pinched flow fractionation.* Lab on a Chip, 2011. **11**(2): p. 354-357.
90. Morijiri, T., S. Sunahiro, M. Senaha, M. Yamada, and M. Seki, *Sedimentation pinched-flow fractionation for size- and density-based particle sorting in microchannels.* Microfluidics and Nanofluidics, 2011. **11**(1): p. 105-110.
91. Bhagat, A.A.S., H.W. Hou, L.D. Li, C.T. Lim, and J. Han, *Pinched flow coupled shear-modulated inertial microfluidics for high-throughput rare blood cell separation.* Lab on a Chip, 2011. **11**(11): p. 1870-1878.
92. Sugaya, S., M. Yamada, and M. Seki, *Observation of nonspherical particle behaviors for continuous shape-based separation using hydrodynamic filtration.* Biomicrofluidics, 2011. **5**(2).
93. Shevkoplyas, S.S., T. Yoshida, L.L. Munn, and M.W. Bitensky, *Biomimetic autoseparation of leukocytes from whole blood in a microfluidic device.* Analytical Chemistry, 2005. **77**(3): p. 933-937.
94. Han, J.Y., H.W. Hou, A.A.S. Bhagat, A.G.L. Chong, P. Mao, K.S.W. Tan, and C.T. Lim, *Deformability based cell margination-A simple*

microfluidic design for malaria-infected erythrocyte separation. Lab on a Chip, 2010. **10**(19): p. 2605-2613.
95. Yang, S., A. Undar, and J.D. Zahn, *A microfluidic device for continuous, real time blood plasma separation.* Lab on a Chip, 2006. **6**(7): p. 871-880.
96. Augustsson, P., J. Persson, S. Ekstrom, M. Ohlin, and T. Laurell, *Decomplexing biofluids using microchip based acoustophoresis.* Lab on a Chip, 2009. **9**(6): p. 810-818.
97. Laurell, T., F. Petersson, L. Aberg, and A.M. Sward-Nilsson, *Free flow acoustophoresis: Microfluidic-based mode of particle and cell separation.* Analytical Chemistry, 2007. **79**(14): p. 5117-5123.
98. Suwa, M.S., M. and H. Watarai, *Magnetoanalysis of micro/nanoparticles: A review.* Analytica Chimica Acta, 2011. **690**(2): p. 137-147.
99. Pethig, R., *Review Article-Dielectrophoresis: Status of the theory, technology, and applications.* Biomicrofluidics, 2010. **4**(2).
100. Nguyen, N.-T. and S.T. Wereley, *Fundamentals and Applications of Microfluidics*. 2nd ed. Artech House integrated microsystems series2006, Boston: Artech House. xiii, 497 p.
101. Bruus, H., *Theoretical Microfluidics*. Oxford master series in condensed matter physics 2007: Oxford university press. p. 364.
102. Hauke, G., *An Introduction to Fluid Mechanics and Transport Phenomena*2008, New York: Springer. p. 296.
103. Purcell, E.M., *Life at Low Reynolds-Number.* American Journal of Physics, 1977. **45**(1): p. 3-11.
104. Stone, H.A., A.D. Stroock, and A. Ajdari, *Engineering Flows in Small Devices: Microfluidics Toward a Lab-On-A-Chip.* Annual Review of Fluid Mechanics, 2004. **36**: p. 381-411.
105. Weigl, B.H., R.L. Bardell, and C.R. Cabrera, *Lab-On-A-Chip for Drug Development.* Advanced Drug Delivery Reviews, 2003. **55**(3): p. 349-377.
106. Whitesides, G.M., *The origins and the future of microfluidics.* Nature, 2006. **442**(7101): p. 368-373.
107. Huang, P. and K.S. Breuer, *Direct measurement of slip length in electrolyte solutions.* Physics of Fluids, 2007. **19**(2).
108. Heller, M. and H. Bruus, *A theoretical analysis of the resolution due to diffusion and size dispersion of particles in deterministic lateral displacement devices.* Journal of Micromechanics and Microengineering, 2008. **18**(7): p. -.
109. Long, B.R., M. Heller, J.P. Beech, H. Linke, H. Bruus, and J.O. Tegenfeldt, *Multidirectional sorting modes in deterministic lateral displacement devices.* Phys Rev E Stat Nonlin Soft Matter Phys, 2008. **78**(4 Pt 2): p. 046304.

110. Pohl, H.A., *Dielectrophoresis, a New Technique for Studying Cells and Organelles.* Bulletin of the American Physical Society, 1970. **15**(11): p. 1362-&.
111. Pohl, H.A., *Biological Dielectrophoresis.* Bulletin of the American Physical Society, 1973. **18**(3): p. 320-320.
112. Pohl, H.A. and J.S. Crane, *Dielectrophoresis of Cells.* Biophysical Journal, 1971. **11**(9): p. 711-727.
113. Pohl, H.A. and I. Hawk, *Separation of Living and Dead Cells by Dielectrophoresis.* Science, 1966. **152**(3722): p. 647-649.
114. Morgan, H. and N. Green, *AC Electrokinetics: Colloids and Nanoparticles*. Microtechnologies and microsystems series, ed. P.R. Pethig2003: Research Studies Press Ltd.
115. Jeffery, G.B., *The motion of ellipsoidal particles in a viscous fluid.* Proceedings of the Royal Society of London Series a-Containing Papers of a Mathematical and Physical Character, 1922. **102**(715): p. 161-179.
116. Goldsmit.Hl and J. Marlow, *Flow Behavior of Erythrocytes .1. Rotation and Deformation in Dilute Suspensions.* Proceedings of the Royal Society of London Series B-Biological Sciences, 1972. **182**(1068): p. 351-&.
117. Tsukada, K., E. Sekizuka, C. Oshio, and H. Minamitani, *Direct measurement of erythrocyte deformability in diabetes mellitus with a transparent microchannel capillary model and high-speed video camera system.* Microvascular Research, 2001. **61**(3): p. 231-239.
118. Fedosov, D.A., B. Caswell, and G.E. Karniadakis, *A Multiscale Red Blood Cell Model with Accurate Mechanics, Rheology, and Dynamics.* Biophysical Journal, 2010. **98**(10): p. 2215-2225.
119. Noguchi, H. and G. Gompper, *Shape transitions of fluid vesicles and red blood cells in capillary flows.* Proceedings of the National Academy of Sciences of the United States of America, 2005. **102**(40): p. 14159-14164.
120. Loutherback, K., J. Puchalla, R.H. Austin, and J.C. Sturm, *Deterministic Microfluidic Ratchet.* Physical Review Letters, 2009. **102**(4): p. 145301.
121. Balvin, M., E. Sohn, T. Iracki, G. Drazer, and J. Frechette, *Directional Locking and the Role of Irreversible Interactions in Deterministic Hydrodynamics Separations in Microfluidic Devices.* Physical Review Letters, 2009. **103**(7): p. -.
122. Davis, J.A., *Microfluidic Separation of Blood Components through Deterministic Lateral Displacement*, in *Electrical Engineering*2008, Princeton: Princeton. p. 152.
123. Martensson, T., P. Carlberg, M. Borgstrom, L. Montelius, W. Seifert, and L. Samuelson, *Nanowire arrays defined by nanoimprint lithography.* Nano Letters, 2004. **4**(4): p. 699-702.

124. Loutherback, K., K.S. Chou, J. Newman, J. Puchalla, R.H. Austin, and J.C. Sturm, *Improved performance of deterministic lateral displacement arrays with triangular posts.* Microfluidics and Nanofluidics, 2010. **9**(6): p. 1143-1149.
125. Inglis, D.W., *Efficient microfluidic particle separation arrays.* Applied Physics Letters, 2009. **94**(1): p. -.
126. Frechette, J. and G. Drazer, *Directional locking and deterministic separation in periodic arrays.* Journal of Fluid Mechanics, 2009. **627**: p. 379-401.
127. Quek, R., D.V. Le, and K.H. Chiam, *Separation of deformable particles in deterministic lateral displacement devices.* Physical Review E, 2011. **83**(5): p. -.
128. Choi, S.E., J.M. Karp, and R. Karnik. *Continuous cell sorting by deterministic cell rolling*. in *The 15th International Conference on Miniaturized Systems for Chemistry and Life Sciences*. 2011. Seattle, Washington, USA.
129. Ceriotti, L., N.F. de Rooij, and E. Verpoorte, *An integrated fritless column for on-chip capillary electrochromatography with conventional stationary phases.* Analytical Chemistry, 2002. **74**(3): p. 639-647.
130. Inglis, D.W., J.A. Davis, T.J. Zieziulewicz, D.A. Lawrence, R.H. Austin, and J.C. Sturm, *Determining blood cell size using microfluidic hydrodynamics.* Journal of Immunological Methods, 2008. **329**(1-2): p. 151-156.
131. Morton, K.J., K. Loutherback, D.W. Inglis, O.K. Tsui, J.C. Sturm, S.Y. Chou, and R.H. Austin, *Crossing Microfluidic Streamlines to Lyse, Label and Wash Cells.* lab chip, 2008. **8**(9): p. 1448–1453.
132. Mair, D.A., E. Geiger, A.P. Pisano, J.M.J. Frechet, and F. Svec, *Injection molded microfluidic chips featuring integrated interconnects.* Lab on a Chip, 2006. **6**(10): p. 1346-1354.
133. Utko, P., F. Persson, A. Kristensen, and N.B. Larsen, *Injection molded nanofluidic chips: Fabrication method and functional tests using single-molecule DNA experiments.* Lab on a Chip, 2011. **11**(2): p. 303-308.
134. Vig, A.L., T. Makela, P. Majander, V. Lambertini, J. Ahopelto, and A. Kristensen, *Roll-to-roll fabricated lab-on-a-chip devices.* Journal of Micromechanics and Microengineering, 2011. **21**(3).
135. Xia, Y.N. and G.M. Whitesides, *Soft Lithography.* Annual Review of Materials Science, 1998. **28**: p. 153-184.
136. McDonald, J.C., D.C. Duffy, J.R. Anderson, D.T. Chiu, H.K. Wu, O.J.A. Schueller, and G.M. Whitesides, *Fabrication of Microfluidic Systems in Poly(dimethylsiloxane).* Electrophoresis, 2000. **21**(1): p. 27-40.

137. Whitesides, G.M., E. Ostuni, S. Takayama, X.Y. Jiang, and D.E. Ingber, *Soft Lithography in Biology and Biochemistry.* Annual Review of Biomedical Engineering, 2001. **3**: p. 335-373.
138. McDonald, J.C. and G.M. Whitesides, *Poly(dimethylsiloxane) as a Material for Fabricating Microfluidic Devices.* Accounts of Chemical Research, 2002. **35**(7): p. 491-499.
139. Sia, S.K. and G.M. Whitesides, *Microfluidic Devices Fabricated in Poly(dimethylsiloxane) for Biological Studies.* Electrophoresis, 2003. **24**(21): p. 3563-3576.
140. Quake, S.R. and A. Scherer, *From Micro- to Nanofabrication with Soft Materials.* Science, 2000. **290**(5496): p. 1536-1540.
141. Michel, B., et al., *Printing Meets Lithography: Soft Approaches to High-Resolution Printing.* Ibm Journal of Research and Development, 2001. **45**(5): p. 697-719.
142. Yu, H.B., G.Y. Zhou, C.F. Siong, S.H. Wang, and F.W. Lee, *Novel Polydimethylsiloxane (PDMS) Based Microchannel Fabrication Method for Lab-On-A-Chip Application.* Sensors and Actuators B-Chemical, 2009. **137**(2): p. 754-761.
143. Unger, M.A., H.P. Chou, T. Thorsen, A. Scherer, and S.R. Quake, *Monolithic Microfabricated Valves and Pumps by Multilayer Soft Lithography.* Science, 2000. **288**(5463): p. 113-116.
144. Huh, D., K.L. Mills, X.Y. Zhu, M.A. Burns, M.D. Thouless, and S. Takayama, *Tuneable elastomeric nanochannels for nanofluidic manipulation.* Nature Materials, 2007. **6**(6): p. 424-428.
145. Lotters, J.C., W. Olthuis, P.H. Veltink, and P. Bergveld. *Polydimethylsiloxane as an Elastic Material Applied in a Capacitive Accelerometer*. in *6th European Workshop on Micromechanics (MME 95)*. 1995. Copenhagen, Denmark.
146. Li, Z.Y., Z.Y. Zhang, A. Scherer, and D. Psaltis, *Mechanically Tunable Optofluidic Distributed Feedback Dye Laser.* Optics Express, 2006. **14**(22): p. 10494-10499.
147. Park, W. and J.B. Lee, *Mechanically Tunable Photonic Crystal Structure.* Applied Physics Letters, 2004. **85**(21): p. 4845-4847.
148. Werber, A. and H. Zappe, *Tunable Pneumatic Microoptics.* Journal of Microelectromechanical Systems, 2008. **17**(5): p. 1218-1227.
149. Gonzalez, M., F. Axisa, F. Bossuyt, Y.Y. Hsu, B. Vandevelde, and J. Vanfleteren, *Design and Performance of Metal Conductors for Stretchable Electronic Circuits.* Circuit World, 2009. **35**(1): p. 22-29.
150. Jones, J., S.P. Lacour, and S. Wagner, *Interconnects for Elastically Stretchable and Deformable Electronic Surfaces.* Materials, Technology and Reliability of Advanced Interconnects-2005, 2005. **863**: p. 399-404.
151. Park, J., J. Ryu, S.K. Choi, E. Seo, J.M. Cha, S. Ryu, J. Kim, B. Kim, and S.H. Lee, *Real-Time Measurement of the Contractile*

Forces of Self-Organized Cardiomyocytes on Hybrid Biopolymer Microcantilevers. Analytical Chemistry, 2005. **77**(20): p. 6571-6580.
152. Zhao, Y. and X. Zhang. *In Situ Force Probing for Cardiac Myocyte Using PDMS Pillar Array*. in *8th International Conference on Miniaturized Systems for Chemistry and Life Sciences*. 2004. Malmo, SWEDEN.
153. Cao, Y., J. Chen, M.O. Adeoye, and W.O. Soboyejo, *Investigation of the Spreading and Adhesion of Human Osteosarcoma Cells on Smooth and Micro-Grooved Polydimethylsiloxane Surfaces.* Materials Science & Engineering C-Biomimetic and Supramolecular Systems, 2009. **29**(1): p. 119-125.
154. Kim, Y.C., S.J. Park, and J.K. Park, *Biomechanical Analysis of Cancerous and Normal Cells Based on Bulge Generation in a Microfluidic Device.* Analyst, 2008. **133**(10): p. 1432-1439.
155. Mehta, G., J. Lee, W. Cha, Y.C. Tung, J.J. Linderman, and S. Takayama, *Hard Top Soft Bottom Microfluidic Devices for Cell Culture and Chemical Analysis.* Analytical Chemistry, 2009. **81**(10): p. 3714-3722.
156. Selby, J.C. and M.A. Shannon, *Inflation of a Circular Elastomeric Membrane into a Horizontally Semi-Infinite Liquid Reservoir of Finite Vertical Depth: Quasi-Static Deformation Model.* International Journal of Engineering Science, 2009. **47**(5-6): p. 700-717.
157. Hardy, B.S., K. Uechi, J. Zhen, and H.P. Kavehpour, *The deformation of flexible PDMS microchannels under a pressure driven flow.* Lab on a Chip, 2009. **9**(7): p. 935-938.
158. Inglis, D.W., *A method for reducing pressure-induced deformation in silicone microfluidics.* Biomicrofluidics, 2010. **4**(2).
159. Liu, V.A., W.E. Jastromb, and S.N. Bhatia, *Engineering protein and cell adhesivity using PEO-terminated triblock polymers.* Journal of Biomedical Materials Research, 2002. **60**(1): p. 126-134.
160. Gascoyne, P.R.C. and J. Vykoukal, *Particle Separation by Dielectrophoresis.* Electrophoresis, 2002. **23**(13): p. 1973-1983.
161. Chou, C.F., J.O. Tegenfeldt, O. Bakajin, S.S. Chan, E.C. Cox, N. Darnton, T. Duke, and R.H. Austin, *Electrodeless Dielectrophoresis of Single- and Double-Stranded DNA.* Biophysical Journal, 2002. **83**(4): p. 2170-2179.
162. Gascoyne, P.R.C., Y. Huang, R. Pethig, J. Vykoukal, and F.F. Becker, *Dielectrophoretic Separation of Mammalian-Cells Studied by Computerized Image-Analysis.* Measurement Science & Technology, 1992. **3**(5): p. 439-445.
163. Becker, F.F., X.B. Wang, Y. Huang, R. Pethig, J. Vykoukal, and P.R.C. Gascoyne, *Separation Of Human Breast-Cancer Cells From Blood By Differential Dielectric Affinity.* Proceedings of the National Academy of Sciences of the United States of America, 1995. **92**(3): p. 860-864.

164. Gascoyne, P.R.C., Y. Huang, X.J. Wang, J. Yang, G. DeGasperis, and X.B. Wang, *Cell Separation by Conventional Dielectrophoresis Combined with Field-Flow-Fractionation.* Biophysical Journal, 1996. **70**(2): p. Tu412-Tu412.
165. Huang, Y., X.B. Wang, F.F. Becker, and P.R.C. Gascoyne, *Introducing Dielectrophoresis as a New Force Field for Field-Flow Fractionation.* Biophysical Journal, 1997. **73**(2): p. 1118-1129.
166. Fuhr, G., R. Hagedorn, T. Muller, W. Benecke, B. Wagner, and J. Gimsa, *Asynchronous Traveling-Wave Induced Linear Motion Of Living Cells.* Studia Biophysica, 1991. **140**(2): p. 79-102.
167. Huang, Y., X.B. Wang, J.A. Tame, and R. Pethig, *Electrokinetic Behavior of Colloidal Particles in Travelling Electric-Fields - Studies Using Yeast Cells.* Journal of Physics D-Applied Physics, 1993. **26**(9): p. 1528-1535.
168. Fiedler, S., S.G. Shirley, T. Schnelle, and G. Fuhr, *Dielectrophoretic Sorting of Particles and Cells in a Microsystem.* Analytical Chemistry, 1998. **70**(9): p. 1909-1915.
169. Li, Y.L., C. Dalton, H.J. Crabtree, G. Nilsson, and K.V.I.S. Kaler, *Continuous Dielectrophoretic Cell Separation Microfluidic Device.* Lab on a Chip, 2007. **7**(2): p. 239-248.
170. Holmes, D., H. Morgan, and N.G. Green, *High Throughput Particle Analysis: Combining Dielectrophoretic Particle Focussing with Confocal Optical Detection.* Biosensors & Bioelectronics, 2006. **21**(8): p. 1621-1630.
171. Hu, X.Y., P.H. Bessette, J.R. Qian, C.D. Meinhart, P.S. Daugherty, and H.T. Soh, *Marker-specific sorting of rare cells using dielectrophoresis.* Proceedings of the National Academy of Sciences of the United States of America, 2005. **102**(44): p. 15757-15761.
172. Yu, C.H., J. Vykoukal, D.M. Vykoukal, J.A. Schwartz, L. Shi, and P.R.C. Gascoyne, *A Three-Dimensional Dielectrophoretic Particle Focusing Channel for Microcytometry Applications.* Journal of Microelectromechanical Systems, 2005. **14**(3): p. 480-487.
173. Demierre, N., T. Braschler, P. Linderholm, U. Seger, H. van Lintel, and P. Renaud, *Characterization and Optimization of Liquid Electrodes for Lateral Dielectrophoresis.* Lab on a Chip, 2007. **7**(3): p. 355-365.
174. Barrett, M.P., R.J.S. Burchmore, A. Stich, J.O. Lazzari, A.C. Frasch, J.J. Cazzulo, and S. Krishna, *The trypanosomiases.* Lancet, 2003. **362**(9394): p. 1469-1480.
175. Chappuis, F., L. Loutan, P. Simarro, V. Lejon, and P. Buscher, *Options for Field Diagnosis of Human African Trypanosomiasis.* Clin. Microbiol. Rev., 2005. **18**(1): p. 133-146.
176. Barrett, M.P., D.W. Boykin, R. Brun, and R.R. Tidwell, *Human African trypanosomiasis: pharmacological re-engagement with a*

neglected disease. British Journal of Pharmacology, 2007. **152**(8): p. 1155-1171.
177. Lutumba, P., J. Robays, C. Miaka, V. Kande, D. Mumba, P. Büscher, B. Dujardin, and M. Boelaert, *Validité coûte, et faisabilité de la mAECT et CTC comme tests de confirmation dans la détection de la Trypanosomiase Humaine Africaine.* Tropical Medicine & International Health, 2006. **11**(4): p. 470-478.
178. Paulitschke, M. and G.B. Nash, *Micropipette Methods for Analyzing Blood-Cell Rheology and their Application to Clinical Research.* Clinical Hemorheology, 1993. **13**(4): p. 407-434.
179. Mitchison, J.M. and M.M. Swann, *The Mechanical Properties of the Cell Surface .1. The Cell Elastimeter.* Journal of Experimental Biology, 1954. **31**(3): p. 443-&.
180. Bremmell, K.E., A. Evans, and C.A. Prestidge, *Deformation and nano-rheology of red blood cells: An AFM investigation.* Colloids and Surfaces B-Biointerfaces, 2006. **50**(1): p. 43-48.
181. Sun, Y., J. Chen, M. Abdelgawad, L.M. Yu, N. Shakiba, W.Y. Chien, Z. Lu, W.R. Geddie, and M.A.S. Jewett, *Electrodeformation for single cell mechanical characterization.* Journal of Micromechanics and Microengineering, 2011. **21**(5).
182. Wang, N. and D.E. Ingber, *Probing transmembrane mechanical coupling and cytomechanics using magnetic twisting cytometry.* Biochemistry and Cell Biology-Biochimie Et Biologie Cellulaire, 1995. **73**(7-8): p. 327-335.
183. Sleep, J., D. Wilson, R. Simmons, and W. Gratzer, *Elasticity of the red cell membrane and its relation to hemolytic disorders: An optical tweezers study.* Biophysical Journal, 1999. **77**(6): p. 3085-3095.
184. Guck, J., J.A. Chiang, and J. Kas, *The optical stretcher u a novel tool to characterize the cytoskeleton.* Molecular Biology of the Cell, 1998. **9**: p. 105A-105A.
185. Teitel, P., *Basic Principles of Filterability Test (Ft) and Analysis of Erythrocyte Flow Behavior.* Blood Cells, 1977. **3**(1): p. 55-70.
186. Jones, J.G., R.A. Adams, and S.A. Evans, *Bulk Filtration through Micropore Membranes for Analyzing Blood-Cell Rheology in Clinical Research.* Clinical Hemorheology, 1994. **14**(2): p. 149-169.
187. Piagnerelli, M., K.Z. Boudjeltia, D. Brohee, A. Vereerstraeten, P. Piro, J.L. Vincent, and M. Vanhaeverbeek, *Assessment of erythrocyte shape by flow cytometry techniques.* Journal of Clinical Pathology, 2007. **60**(5): p. 549-554.
188. Streekstra, G.J., J.G.G. Dobbe, and A.G. Hoekstra, *Quantification of the fraction poorly deformable red blood cells using ektacytometry.* Optics Express, 2010. **18**(13): p. 14173-14182.

189. Quinto-Su P A, K.C., Preiser P R, Ohl C-D, *Red blood cell rheology using single controlled laser-induced cavitation bubbles.* Lab Chip, 2011. **11**: p. 672-678.
190. Tomaiuolo, G., M. Simeone, V. Martinelli, B. Rotoli, and S. Guido, *Red blood cell deformation in microconfined flow.* Soft Matter, 2009. **5**(19): p. 3736-3740.
191. Dobbe, J.G.G., M.R. Hardeman, G.J. Streekstra, J. Strackee, C. Ince, and C.A. Grimbergen, *Analyzing red blood cell-deformability distributions.* Blood Cells Molecules and Diseases, 2002. **28**(3): p. 373-384.
192. Mokken, F.C., M. Kedaria, C.P. Henny, M.R. Hardeman, and A.W. Gelb, *The Clinical Importance of Erythrocyte Deformability, a Hemorrheological Parameter.* Annals of Hematology, 1992. **64**(3): p. 113-122.
193. Gedde, M.M., E.Y. Yang, and W.H. Huestis, *Shape Response of Human Erythrocytes to Altered Cell Ph.* Blood, 1995. **86**(4): p. 1595-1599.
194. Gedde, M.M., E.Y. Yang, and W.H. Huestis, *Resolution of the paradox of red cell shape changes in low and high pH.* Biochimica Et Biophysica Acta-Biomembranes, 1999. **1417**(2): p. 246-253.
195. Lim, H.W.G., M. Wortis, and R. Mukhopadhyay, *Stomatocyte-discocyte-echinocyte sequence of the human red blood cell: Evidence for the bilayer-couple hypothesis from membrane mechanics.* Proceedings of the National Academy of Sciences of the United States of America, 2002. **99**(26): p. 16766-16769.
196. Singer, S.J. and G.L. Nicolson, *Fluid Mosaic Model of Structure of Cell-Membranes.* Science, 1972. **175**(4023): p. 720-&.
197. Downey, G.P., D.E. Doherty, B. Schwab, E.L. Elson, P.M. Henson, and G.S. Worthen, *Retention of Leukocytes in Capillaries - Role of Cell-Size and Deformability.* Journal of Applied Physiology, 1990. **69**(5): p. 1767-1778.
198. Rimsza, L.M., M.C. Sola-Visner, R.D. Christensen, and A.D. Hutson, *Megakaryocyte size and concentration in the bone marrow of thrombocytopenic and nonthrombocytopenic neonates.* Pediatric Research, 2007. **61**(4): p. 479-484.
199. Frojmovic, M.M. and R. Panjwani, *Geometry of Normal Mammalian Platelets by Quantitative Microscopic Studies.* Biophysical Journal, 1976. **16**(9): p. 1071-1089.
200. Lim, C.T., A.A.S. Bhagat, H.W. Hou, L.D. Li, and J.Y. Han, *Pinched flow coupled shear-modulated inertial microfluidics for high-throughput rare blood cell separation.* Lab on a Chip, 2011. **11**(11): p. 1870-1878.
201. Weinman, D., *Trypanosoma-Cyclops N-Sp - Pigmented Trypanosome from Malaysian Primates Macaca-Nemestrina and*

M-Ira. Transactions of the Royal Society of Tropical Medicine and Hygiene, 1972. **66**(4): p. 628-&.
202. Thiel, A., A. Scheffold, and A. Radbruch, *Immunomagnetic cell sorting - pushing the limits.* Immunotechnology, 1998. **4**(2): p. 89-96.
203. Coulter, W.H., *Means for counting particles suspended in fluid*, 1953.
204. Büscher, P., D. Mumba Ngoyi, J. Kabor√©, V. Lejon, J. Robays, V. Jamonneau, N. Bebronne, W. Van der Veken, and S. Bi√©ler, *Improved Models of Mini Anion Exchange Centrifugation Technique (mAECT) and Modified Single Centrifugation (MSC) for Sleeping Sickness Diagnosis and Staging.* PLoS Negl Trop Dis, 2009. **3**(11): p. e471.
205. Ehrlich, D.J., B.K. McKenna, J.G. Evans, and M.C. Cheung, *A parallel microfluidic flow cytometer for high-content screening.* Nature Methods, 2011. **8**(5): p. 401-U41.
206. Ehrlich, D.J., B.K. Mckenna, A.A. Selim, and F.R. Bringhurst, *384-Channel parallel microfluidic cytometer for rare-cell screening.* Lab on a Chip, 2009. **9**(2): p. 305-310.
207. Laurell, T., F. Petersson, A. Nilsson, C. Holm, and H. Jonsson, *Continuous separation of lipid particles from erythrocytes by means of laminar flow and acoustic standing wave forces.* Lab on a Chip, 2005. **5**(1): p. 20-22.
208. Korohoda, W. and A. Wilk, *Cell electrophoresis - A method for cell separation and research into cell surface properties.* Cellular & Molecular Biology Letters, 2008. **13**(2): p. 312-326.
209. Mauritz, J.M.A., T. Tiffert, R. Seear, F. Lautenschlager, A. Esposito, V.L. Lew, J. Guck, and C.F. Kaminski, *Detection of Plasmodium falciparum-infected red blood cells by optical stretching.* Journal of Biomedical Optics, 2010. **15**(3).
210. MacDonald, M.P., G.C. Spalding, and K. Dholakia, *Microfluidic sorting in an optical lattice.* Nature, 2003. **426**(6965): p. 421-424.
211. Zheng, S., H. Lin, J.Q. Liu, M. Balic, R. Datar, R.J. Cote, and Y.C. Tai, *Membrane microfilter device for selective capture, electrolysis and genomic analysis of human circulating tumor cells.* Journal of Chromatography A, 2007. **1162**(2): p. 154-161.
212. Lee, G.B., H.W. Wu, X.Z. Lin, and S.M. Hwang, *A microfluidic device for separation of amniotic fluid mesenchymal stem cells utilizing louver-array structures.* Biomedical Microdevices, 2009. **11**(6): p. 1297-1307.
213. Seki, M., J. Takagi, M. Yamada, and M. Yasuda, *Continuous particle separation in a microchannel having asymmetrically arranged multiple branches.* Lab on a Chip, 2005. **5**(7): p. 778-784.
214. Vig, A.L. and A. Kristensen, *Separation enhancement in pinched flow fractionation.* Applied Physics Letters, 2008. **93**(20).

215. Kristensen, A., A.V. Larsen, L. Poulsen, H. Birgens, and M. Dufva, *Pinched flow fractionation devices for detection of single nucleotide polymorphisms.* Lab on a Chip, 2008. **8**(5): p. 818-821.
216. Zheng, S.Y., J.Q. Liu, and Y.C. Tai, *Streamline-based microfluidic devices for erythrocytes and leukocytes separation.* Journal of Microelectromechanical Systems, 2008. **17**(4): p. 1029-1038.
217. Beech, J.P., P. Jonsson, and J.O. Tegenfeldt, *Tipping the balance of deterministic lateral displacement devices using dielectrophoresis.* Lab on a Chip, 2009. **9**(18): p. 2698-2706.
218. Wu, Z.G., B. Willing, J. Bjerketorp, J.K. Jansson, and K. Hjort, *Soft inertial microfluidics for high throughput separation of bacteria from human blood cells.* Lab on a Chip, 2009. **9**(9): p. 1193-1199.
219. Han, J., W.C. Lee, A.A.S. Bhagat, S. Huang, K.J. Van Vliet, and C.T. Lim, *High-throughput cell cycle synchronization using inertial forces in spiral microchannels.* Lab on a Chip, 2011. **11**(7): p. 1359-1367.
220. Beck, M., M. Graczyk, I. Maximov, E.L. Sarwe, T.G.I. Ling, M. Keil, and L. Montelius, *Improving stamps for 10 nm level wafer scale nanoimprint lithography.* Microelectronic Engineering, 2002. **61-2**: p. 441-448.